The RNA helicase UPF1 associates with mRNAs co-transcriptionally and is required in nuclear processes of gene expression

Anand K. Singh[1], Subhendu Roy Choudhury[1], Sandip De[1¶], Jie Zhang[2], Stephen Kissane[1], Vibha Dwivedi[1], Preethi Ramanathan[1], Luisa Orsini[1], Daniel Hebenstreit[2] and Saverio Brogna[1*]

1. School of Biosciences, University of Birmingham, Edgbaston, Birmingham, B15 2TT, UK
2. Life Sciences, University of Warwick, Coventry, CV4 7AL, UK

¶. Present address: *Division of Developmental Biology, Eunice Kennedy Shriver National Institute of Child Health and Human Development, National Institutes of Health, Bethesda, MD 20892, USA*

Summary

UPF1 is an RNA helicase that is required for efficient nonsense-mediated mRNA decay (NMD) in eukaryotes, and the predominant view is that UPF1 mainly operates on the 3'UTRs of mRNAs that are directed for NMD in the cytoplasm. Here we offer evidence, obtained from *Drosophila*, that UPF1 constantly moves between the nucleus and cytoplasm and that it has multiple functions in the nucleus. It is associated, genome-wide, with nascent RNAs at most of the active Pol II transcription sites and at some Pol III-transcribed genes, as demonstrated microscopically on the polytene chromosomes of salivary gland and by ChIP-seq analysis in S2 cells. Intron recognition seems to interfere with association and translocation of UPF1 on nascent pre-mRNA transcripts, and cells depleted of UPF1 show defects in several processes essential to correct gene expression – including Pol II pausing, the release of mRNAs from transcription sites, and mRNA export from the nucleus.

*Corresponding author: s.brogna@bham.ac.uk

Running title: UPF1 also acts on nuclear RNAs

Key words: UPF1, NMD, transcription, splicing, mRNA export, RNA helicases, polytene chromosomes, *Drosophila*

Introduction

UPF1 (UP-Frameshift-1) is a universally conserved eukaryotic protein that was first identified in a *Saccharomyces cerevisiae* genetic screen for mutations that enhance up-frameshift tRNA suppression (Culbertson et al., 1980; Leeds et al., 1992), and gained other names – including *NAM7* (*S. cerevisiae*) and *SMG2* (*Caenorhabditis elegans*) – from other genetic screens (Altamura et al., 1992; Hodgkin et al., 1989; Pulak and Anderson, 1993). Cells that lack active UPF1, accumulate mRNAs with nonsense, frameshift or other mutant alleles that introduce a premature translation termination codon (PTC) (Leeds *et al.*, 1991; Pulak and Anderson, 1993).

These observations are generally interpreted as evidence that UPF1 and related proteins are primarily required for nonsense-mediated mRNA decay (NMD), a conserved mRNA surveillance mechanism of eukaryotes that detects and destroys mRNAs at which translation terminates prematurely (Fatscher *et al*., 2015; He and Jacobson, 2015; Karousis *et al*., 2016; Kurosaki and Maquat, 2016). NMD is mainly regarded as a quality control mechanism that prevents cells from wastefully making truncated (and potentially toxic) proteins and that regulates the selective expression of specific mRNA isoforms during cell homeostasis and differentiation (Goetz and Wilkinson, 2017; Lykke-Andersen and Jensen, 2015).

Standard NMD models postulate that UPF1 monitors translation termination on ribosomes by interacting with a peptide release factor (eRF1 or eRF3). However, recent reports on mammalian translation systems have suggested, in contrast to earlier reports on other organisms (Czaplinski *et al*., 1998; Ivanov *et al.*, 2008; Kashima *et al.*, 2006; Keeling *et al.*, 2004; Singh *et al.*, 2008; Wang *et al.*, 2001), that UPF1 does not bind to either of these. They suggested, instead, that UPF3B may contact release factors, slow the termination of translation and facilitate post-termination release of ribosomes – and so fulfil the termination monitoring role that has been assigned to UPF1 (Gao and Wilkinson, 2017; Muhlemann and Karousis, 2017; Neu-Yilik *et al.*, 2017).

UPF1 is an ATP-driven helicase that unwinds RNA secondary structures and so can displace RNA-bound proteins (Bhattacharya *et al.*, 2000; Chakrabarti *et al.*, 2011; Czaplinski *et al.*, 1995; Fiorini *et al.*, 2015). Its helicase activity is required for NMD, but how this helps to target particular transcripts for NMD is not clear (Brogna *et al.*, 2016; Brogna and Wen, 2009). UPF1 is predominantly associated with 3'UTRs of cytoplasmic mRNAs and it might be selectively recruited to or activated on NMD targets with abnormally long 3'UTRs (Karousis et al., 2016; Kurosaki and Maquat, 2016). However, UPF1 appears to bind mRNAs fairly indiscriminately, whatever the position of their stop codon or PTC and whether or not they include NMD-inducing features such as an abnormally long 3'UTR or an exon junction downstream of the stop codon (Hogg and Goff, 2010; Hurt *et al.*, 2013; Zund *et al.*, 2013).

UPF1 is most abundant in the cytoplasm and its roles discussed above depend on ribosomal translation and occur on cytoplasmic mRNAs. However, nuclear functions have also been reported. UPF1 traffics in and out of the nucleus, it interacts with chromatin, it co-purifies with the catalytic subunits of DNA polymerase δ, and UPF1 depletion impairs DNA replication and telomere maintenance (Ajamian et al., 2015; Azzalin and Lingner, 2006; Azzalin et al., 2007; Carastro et al., 2002; Chawla et al., 2011; Mendell et al., 2002). Moreover, there is evidence that UPF1 might contribute directly to nuclear RNA processing and nuclear export of HIV-1 genomic RNAs in HeLa cells (Ajamian et al., 2015; Brogna et al., 2016; de Turris et al., 2011; Flury et al., 2014; Varsally and Brogna, 2012).

In the present study we show that UPF1 is involved in the formation and nuclear processing of mRNAs in *Drosophila*. First, UPF1 is a mobile protein that constantly shuttles between the nucleus and cytoplasm, and its distribution in the cell, with more in the cytoplasm than the nucleus, approximately reflects that of mRNA. UPF1 associates with nascent transcripts on chromosomes – mostly with Pol II transcripts, but also with some Pol III-transcribed genes – and more of the transcript-associated UPF1 is bound with exons than with introns, suggesting that 5' splice sites might act as a roadblock to the 5'-to-3' transit of UPF1 along the pre-mRNA. Additionally, UPF1

is needed for the efficient release of polyadenylated mRNA from chromosomal transcription sites and for its export from nuclei. These observations show that UPF1 starts scanning pre-mRNA transcripts whilst they are still being assembled in ribonucleoprotein (RNP) complexes on chromosomes and suggest that it fulfils previously unrecognised role(s) in facilitating nuclear processes of gene expression and mRNA export. The broad and dynamic association of UPF1 with mRNAs might also be the reason why none of the prevailing models satisfactorily explains how UPF1 could target specific transcript to NMD.

Results

Drosophila anti-UPF1 antibodies

To explore the functions of UPF1, we generated three monoclonal anti-peptide antibodies that target regions of *Drosophila* UPF1 outside the RNA helicase domain: one epitope in the N-terminal flanking regions (antibody 1C13 against Pep2), and two near the C-terminus (Ab 7D17 *vs.* Pep11; and Ab 7B12 *vs.* Pep12) (see Figure S1 and Supplementary Table S1). Each antibody detected UPF1 as a single band by Western blotting of *Drosophila* S2 cell extracts, with minimal cross-reactivity with other proteins, and also detected a second, larger band of the expected molecular mass in extracts from S2 cells that over-express UPF1-GFP (Figure 1A-1C; Figure S1). Unless otherwise indicated, antibody 7B12 was used in the experiments described below. As expected, *UPF1* RNAi specifically reduced the amount of UPF1 in S2 cells (Figure 1B) without affecting the levels of several other proteins we tested as controls (Figure 1B).

UPF1 rapidly shuttles between nucleus and cytoplasm

We examined the subcellular localization of immunostained UPF1 in *Drosophila* salivary glands, which are made up of large secretory cells with polytene nuclei. UPF1 was most abundant in the cytoplasm and perinuclear region, and there was also distinct but less intense nuclear staining, mainly around the chromosomes (Figure 1D). Following cell fractionation of S2 cells, α-tubulin and RNA Pol II were, as expected, restricted to the cytoplasmic and nuclear fractions, respectively – and a small proportion of the UPF1 co-purified with nuclei whilst most was in the cytoplasmic fraction (Figure 1C).

Both cytoplasmic and nuclear UPF1 were also present in other larval tissues, with varying relative immunostaining intensities. Perinuclear and intra-nuclear UPF1 were more abundant in Malpighian tubules and gut (Figure S2). In enterocytes (EC), staining was similar in the cytoplasm and within the nucleus, and the most intense UPF1 signal was perinuclear (Figure S2B).

In salivary glands expressing UPF1-GFP (Figure S3A) the perinuclear signals co-localised with binding of wheat germ agglutinin (WGA) – a lectin that predominantly interacts with O-GlcNAc-modified nuclear pore proteins (Mizuguchi-Hata *et al.*, 2013) – and this UPF1-GFP may be associated with components of the nuclear pore complex, as has been proposed for *S. cerevisiae* UPF1 (Nazarenus *et al.*, 2005). It is noteworthy, unexplained though, that *UPF1* RNAi reduced the perinuclear WGA binding in salivary glands (Figure 3SB); cells were also smaller, as would be predicted from its requirement in cell growth during *Drosophila* development (Metzstein and Krasnow, 2006).

Since UPF1 is present both in cytoplasm and nuclei, with the relative quantities varying between cell-types, we wondered how rapidly UPF1 shuttles between cell compartments. Such trafficking has been reported in HeLa cells, with UPF1 accumulating in the nuclei following treatment with leptomycin B (LMB) (Ajamian et al., 2015; Mendell et al., 2002); this drug selectively inhibits CRM1-mediated protein export from the nucleus in most eukaryotes (Fukuda *et al.*, 1997).

We therefore explored the intracellular localization and dynamics of UPF1 in *Drosophila* salivary glands. Immunostained endogenous UPF1 and UPF1-GFP showed similar intracellular distributions, with an intense cytoplasmic signal and a weaker but still obvious signal in the regions occupied by chromosomes (Figure S4A: the cytoplasmic texture of the salivary cells in these confocal images reflects the fact that they are packed with secretory vesicles at this stage of larval development). In glands treated with LMB for 60 minutes most of the UPF1-GFP was within the nucleus but largely excluded from the nucleolus (Figure S4A, right panels), suggesting that UPF1 exit from the nucleus utilises a CRM1-dependent mechanism. This UPF1 redistribution was rapid in living glands: UPF1 was accumulating in the nucleus by the earliest time we could collect images (within ~5-6 min), and much of the cell's UPF1 was in the nucleus within half an hour (Figure S4B).

Heat-shock caused a similar redistribution of much of UPF1 from cytoplasm to nucleus, and this was partially reversed when the tissue was returned to its initial

temperature (Figure S4C).

We next used two live cell imaging techniques – Fluorescence Loss in Photo-bleaching (FLIP) and Fluorescence Recovery after Photo-bleaching (FRAP) (Singh and Lakhotia, 2015) – to examine the mobility of UPF1-GFP in salivary gland cells. FLIP revealed that sustained photobleaching of a small area of the cytoplasm led, within the continuously illuminated area, to an initial rapid decrease in UPF1-GFP fluorescence followed by a continued slower reduction. Fluorescence also declined steadily both elsewhere in the cytoplasm, and, more slowly, within the nucleus (Figure 1E). These observations demonstrate ongoing diffusion of UPF1 throughout the cytoplasm, and that nuclear UPF1 can leave the nucleus and enter the photodepletable cytoplasmic UPF1 pool at a fairly steady rate.

The FRAP studies monitored the speed with which unbleached UPF1-GFP diffuses into and repopulates a photobleached region of the cytoplasm or nucleus. Almost all of the UPF1 in each cell compartment was rapidly mobile, and the halftime for repopulation of each bleached area was only a few seconds (Figure 1F).

These observations indicate that UPF1 is freely mobile within cell compartments and that it constantly moves in and out of the nucleus by mechanisms that include the CRM1-dependent nuclear protein export pathway.

UPF1 associates with transcribing regions of the chromosomes

To gain insight into the role(s) of UPF1 in the nucleus, we used immunostaining to examine whether it associates with the polytene chromosomes of *Drosophila* salivary glands. These well-characterised giant interphase chromosomes are formed after multiple rounds of endoreplication without chromosomal segregation, and they provide a powerful system in which to visualise transcription and pre-mRNA processing at individual gene loci.

UPF1 was present predominantly at interbands and puffs: cytologically distinct chromosome regions in which the chromatin is less condensed and that correspond to transcriptionally active sites (Figure 2A). The immunofluorescence signal appears to

be specific, as: a) UPF1-RNAi drastically depletes the endogenous UPF1 chromosomal signal (Figures S5A and S5B); and b) transgenically over-expressed UPF1-GFP, detected either by its fluorescence or with an anti-GFP antibody, shows a similar banding pattern at the chromosomes (Figure S5C).

We then undertook double immunostaining of chromosomes for UPF1 and for Ser2 Pol II – the form of Pol II that transcribes through the main body of genes which is characterised by having the C-terminal domain (CTD) of its largest subunit Ser2-phosphorylated (Boehm *et al.*, 2003). Much of the UPF1 co-localized with Ser2 Pol II, as would be expected from this type of banding pattern (Figure S6A).

The association of UPF1 with the chromosomes depends on transcription. This is illustrated by the changes in UPF1 immunostaining that followed heat-shock, which induces transcription at specific cytological puffs encoding heat-shock proteins and of hsrω lncRNAs at locus 93D (Lakhotia *et al*., 2012). This revealed a pattern of UPF1 association at heat shock puffs and of detachment from most other transcription sites (Figure 2B). UPF1 was recruited to activated heat-shock genes that contained (33B, 63B, 64F, 67B, 70A and 93D) or lacked (87A, 87C and 95D) introns (Figure 2B).

These observations suggested that UPF1 associates with genes that are being transcribed. UPF1 was also recruited to other genes following transcription activation, such as an ecdysone-inducible transgene (S136 at chromosomal position 63B) at normal temperature (Choudhury *et al.*, 2016). No UPF1 was found at this locus while it is inactive, but when ecdysone activated the transgene it produced a cytologically distinguishable transcription puff with which UPF1 was associated (Figure 2C).

UPF1 mainly associates with Pol II sites that are undergoing transcription and depends on the nascent transcript

We examined the association of UPF1 and of Ser2 Pol II with multiple gene loci by chromatin immunoprecipitation (ChIP) of S2 cell extracts, followed by high-throughput DNA sequencing (ChIP-Seq). UPF1 was associated with many transcriptionally active genes, most of which are Pol II transcription sites. Figure 3A

shows enrichment profiles of UPF1 and of Ser2 Pol II across a representative chromosome region. *Actin5C* provided a striking example of correspondence between the ChIP-seq and polytene immunostaining results: it was one of the most UPF1-enriched genes in the ChIP-seq data (Table S2, Figure S9 shows the UPF1 ChIP-seq profile of *Actin5C*) and displayed one of the brightest UPF1 chromosomal signals at the gene locus corresponding to interband 5C on the X chromosome (Figure 2A). The ChIP-seq data also show UPF1 association with a few Pol III genes (Table S2, to be discussed later).

The enrichment profile of UPF1 at Pol II loci closely followed that of Ser2 Pol II, and UPF1 enrichment was greatest at highly expressed genes (Figure 3A; and Figure S8A and S9 show additional examples of UPF1-enriched genes). There was a close correlation between UPF1 and Ser2 Pol II ChIP-seq signals, and also between these and mRNA levels (Figure 3B and 3C). Real-time PCR was used to validate the ChIP-seq data at several genes, both in S2 cells and salivary glands (Figure S7; and other examples are shown below). UPF1-RNAi drastically reduced the UPF1 enrichment at transcription sites, both confirming the specificity of the antibody and validating the ChIP protocol (Fig S7C).

A metagene analysis of the ChIP-seq data shows that UPF1 is associated with genes, and particularly with highly expressed genes (blue trace), throughout their transcription units (Figure 3D) whereas Ser2 Pol II typically shows higher loading around transcription start sites (TSS) – as previously reported in *Drosophila* and other organisms (Adelman and Lis, 2012; Muse et al., 2007). Typically, therefore, most gene-associated UPF1 was further downstream than the TSS-proximal Ser2 Pol II peak, especially at highly expressed genes (Figure 3E: striking examples of this pattern are the *Su(z)2* and *Psc* genes (Figure 3A) and the *α-Tub84B* gene (Figure S8A).

A comparison of the UPF1 loading of genes with different Ser2 Pol II loading profiles suggests that UPF1 association depends on transcription elongation: UPF1 did not associate with genes at which Ser2 Pol II was associated only with the TSS pausing site and which were not being actively transcribed (*e.g. Adam TS-A*, panel 5 in Figure

S8A).

The association of UPF1 with Pol II transcription sites is partially sensitive to RNase treatment, suggesting that UPF1 loads onto nascent RNA. This was apparent both for immunostained UPF1 on polytene chromosomes (Figure S6B and C) and when assayed by ChIP at specific genes by qPCR in S2 cells (Figure S7D). UPF1 association was, though, less sensitive to RNase treatment than that of the RNA binding protein hnRNPA1 (Figure S6B-C), which is almost all detached following the same RNase treatment. Some of UPF1 co-purifies with Ser2 Pol II in a standard immunoprecipitation of S2 cell nuclear extracts, the interaction is similarly sensitive to RNase treatment though (Figure S7E): less than that of hnRNPA1, but comparable to that of eIF4AIII, one of the exon junction complex (EJC) proteins that are loaded onto nascent RNAs (Choudhury et al., 2016).

We also examined the effect on salivary glands of 5,6-dichloro-1-beta-D-ribofuranosylbenzimidazole (DRB), a drug that blocks Pol II transcription by inhibiting Ser2 phosphorylation (Bensaude, 2011). In the presence of DRB, unphosphorylated Pol II (Pol II) initiates transcription but does not engage in productive elongation as this would require Ser2-phosphorylated Pol II (Ser2 Pol II) (Adelman and Lis, 2012). DRB treatment left interbands and puffs cytologically unaffected, as expected, but it markedly reduced the amount of UPF1 associated with gene loci (Figure S6D-E), providing further evidence that transcript elongation into the body of the gene is needed for this association to occur. DRB also reduced the association of UPF1 and Ser2 Pol II with genes, such as the highly expressed *RpL23A*, in S2 cells (Figure 3F).

UPF1 at Pol III transcription sites

UPF1 was found mainly at Pol II transcription sites, most of which are protein-coding genes, but our ChIP-seq data also revealed it at a minority of Pol III genes. The latter included 7SK and both paralogous genes of 7SL snRNAs (Figure S8B) – but not, for example, the much more numerous Pol III-transcribed tRNA genes (Figure S8C, Table S2).

Intron recognition interferes with UPF1 association with nascent transcripts

UPF1 was recruited both to intron-containing and intronless genes that were undergoing transcription (Figure S9A, and see also the earlier discussion of heat-shock gene activation), so recruitment did not depend on pre-mRNA splicing. Within intron-containing genes, however, more UPF1 was associated with exons than with introns – as can be seen in the ChIP-seq profiles of highly UPF1-enriched genes such as *Xrp1* (Figure 4A; and Figure S9 shows other examples of genes displaying this pattern).

This exon-biased UPF1 enrichment was confirmed by real time PCR in multiple ChIP experiments (Figure 4B); and it is genome-wide, as demonstrated by comparing UPF1 association with introns and with their flanking exons in the ChIP-seq data from many genes (Figure 4C, UPF1 enrichment is significantly higher for both the left (P = 6.737e-8) and the right flanking exon (2.391e-9); for details of how we corrected for possible bias in chromatin fragmentation or sequencing coverage, see Methods). This pattern is made visually apparent by plotting normalized enrichment in exons and introns, each scaled as a percentage of their full length (Figure 4D), and by comparing the density plots of normalised UPF1 enrichment values in introns and flanking exons, which show more values that are enriched in exons than introns (Fig 4E, compare red and yellow lines *vs.* the blue line in the right half of the graph).

The lower frequency with which UPF1 associated with introns suggested that some features of unspliced transcripts must interfere with the UPF1 interaction. We hypothesised that 5' splice sites (5'ss) at the starts of introns, where the initial U1 snRNP spliceosome complex would bind, might act as road-blocks to UPF1 translocation along nascent pre-mRNAs and that removal of U1 might allow UPF1 to move on through the intron (Figure 4G). We therefore used ChIP in S2 cells to compare the enrichment of UPF1 at exons and introns in the *Xrp1* gene in cells that had been depleted either of the U1 snRNP protein U1-70K or of Y14 or eIF4III (two of the EJC proteins that bind the nascent pre-mRNA but are not likely to play a direct splicing role in *Drosophila*; see (Choudhury et al., 2016)). The normal bias towards

UPF1-exon association in *Xrp1* transcripts was abolished in the U1-70K-depleted cells but persisted in cells depleted of eIF4AIII or Y14 (Figure 4F).

Moreover, genes with the most marked exon-biased UPF1 enrichment, such as *Xrp1*, are efficiently co-transcriptionally spliced (see the Nascent RNA-seq profile in Figure 4A), whereas genes with no detectable exon-biased UPF1 enrichment, such as *CG5059*, are poorly co-transcriptionally spliced (Figure S9C) and are typically expressed at low levels, as reported (Khodor et al., 2011). It seems therefore, that intron recognition interferes with the association of UPF1 with the unspliced nascent transcript.

Pol II tends to stall near Transcription Start Sites (TSSs) in UPF1-depleted cells

We next determined whether the availability of UPF1 influences the relative amounts of unphosphorylated Pol II and Ser2 Pol II that associate with genes in S2 cells.

Both unphosphorylated and, to a lesser extent, Ser2-phosphorylated Pol II were most frequently associated with the start of genes (Figure 5A-5D). Its loading peaked 20 to 60 nucleotides downstream of the TSS (as shown in the expanded depiction in Figure 5B that is based on many more genes), at a position that corresponds to the average distance from TSSs to Pol II pausing sites (Adelman and Lis, 2012). Significantly more unphosphorylated Pol II accumulated there in cells depleted of UPF1 ($P = 0.011$; light blue line in Figure 5B, based on quantifying the aggregate Pol II signal over a +/- 100bp span at each of 25440 TSSs): many TSSs showed a 1.2-fold or greater increase in the UPF1-depleted cells (Table S3). Conversely, the amount of Ser2 Pol II associated with these TSSs was unchanged or marginally reduced in UPF1-depleted cells (Figure 5C-5D).

The increase in unphosphorylated Pol II loading downstream of the TSS in UPF1-depleted cells, alongside fairly constant Ser2 Pol II loading, is illustrated here by *Xrp1* and *RpS3A* (Figure 5E), two genes that are highly transcribed and show strong UPF1 association (Figure 4A, Table S2).

We also assessed transcription by monitoring the repopulation of genes by newly phosphorylated Ser2 Pol II following the withdrawal of DRB treatment. As expected, DRB treatment of S2 cells led to a drastic depletion of Ser2 Pol II and accumulation of unphosphorylated Pol II in cell extracts (Figure 5F, compare Control lanes 9 and 10 with DRB-treated lanes 1 and 2). Ser2 Pol II levels began to recover soon after DRB removal, and were similar to those of untreated control cells within 10 minutes (Figure 5F, compare lanes 7-8 with control lanes 9-10). However, this recovery seemed slower in the UPF1-depleted cells (Figure 5F, compare lanes 3 *vs*. 4 and 5 *vs*. 6). A similarly blunted recovery of gene-associated Ser2 Pol II in UPF1-depleted cells was detected by ChIP at the two gene loci (*Socs36E* and *Xrp1*) that were assayed by real-time PCR (Figure 5G).

Comparable genome-wide observations were made using polytene chromosome spreads. There were no obvious changes in Ser2 Pol II distribution when UPF1 was simply depleted (Figure S10A). When, though, UPF1 was depleted and the glands were also DRB treated, there was then a delay in the recovery of the Ser2 Pol II signal when DRB was removed (Figures S10B, S10C).

Cumulatively, these observations suggest that UPF1 might, by associating with nascent transcripts, influence the phosphorylation of Pol II and hence the transcription of some genes.

UPF1 depletion leads to nuclear mRNA retention

We also assessed whether depleting UPF1 in the salivary gland cells of 3rd instar larvae would have any effect on mRNA release from transcription sites and its subsequent processing and export from the nucleus.

First we examined the overall cellular distribution of poly(A) RNA – which is referred to from here on simply as poly(A) – by oligo(dT) FISH (fluorescence *in situ* hybridization): this should detect mRNA that has been transcribed, spliced, released from Pol II and polyadenylated. In wild-type cells poly(A) was abundant and fairly evenly distributed throughout the cytoplasm, as would be expected for mature mRNA,

and there was little in the nuclei (Figure 6A). By contrast, the nuclei of UPF1-depleted cells retained a substantial amount of poly(A), and the cells appeared to contain less cytoplasmic poly(A) than wild-type cells. Much of the nuclear-retained poly(A) in the UPF1-depleted cells formed large cluster(s) in inter-chromosomal spaces (Figure 6A) that seemed neither to be linked to or in the proximity of any specific chromosomal region(s) or defined transcription site(s).

An appreciable amount of poly(A) signal, which was not within clusters, was clearly at the chromosomes though, in the UPF1-depleted cells (Figure 6A, panels III and VI). We therefore used oligo(dT) FISH on polytene chromosome spreads to compare wild-type and UPF1-depleted cells and to assess whether there is retention of poly(A) near transcription sites. There was little poly(A) associated with most of the wild-type chromosomes. However, a few interbands – such as 2C at the distal end of the X chromosome (Figure 6B) – showed clear poly(A) signals (Figure 6B, left panel), suggesting that some completed mRNAs that have been cleaved and polyadenylated remain associated, at least briefly, with transcription sites. Additionally, since UPF1 was obviously not associated with 2C (see Figure 2A), the poly(A) accumulation at 2C in wild-type cells may be a consequence of UPF1 not being normally associated with this transcription site.

Both the number of transcriptional sites showing poly(A) accumulation and the amount of poly(A)RNA associated with these sites were strikingly increased in UPF1-depleted cells (Figure 6B, right panel). For example, there was no visible poly(A) accumulation at site 5C, which corresponds to the highly transcribed *Actin5C* gene, in wild-type, but this band was obviously fluorescent in UPF1-depleted cells. Another example was site 2B – where constitutively expressed *sta* and *rush* are probably the most active genes at this larval stage – which showed a faint poly(A) signal in wild-type glands and a strong signal in UPF1-depleted cells. UPF1 was clearly associated with these transcription sites (2B and 5C) on polytene chromosomes (Fig 2A) and in S2 cells (as detected by ChIP: see Table S2 and Figure S9 for the UPF1 profile of *Actin5C*).

Cumulatively, these data make it clear that UPF1 plays important role(s) both in the release of mRNAs from transcription sites and in their transport out of the nucleus (Figure 6C shows a cartoon of a transcription site of either a wild-type or UPF1 depleted cell with or without mRNA retention).

Discussion

The RNA helicase UPF1 is usually most abundant in the cytoplasm and is mainly discussed in relation to NMD, leading to the common assumption that it acts mainly on mRNPs that have been exported from the nucleus. In contrast, we present evidence that UPF1 moves constantly within and between cell compartments, that it interacts with mRNA both in the nucleus and the cytoplasm, and that it starts its mRNA association(s) at transcription sites, cotranscriptionally and before pre-mRNA processing is complete.

Within the nucleus we found UPF1 associated with many actively transcribing Pol II sites, to which it seems mainly to be recruited by an interaction with nascent pre-mRNA. More of this transcript-tethered UPF1 is associated with exons than with the introns that separate them. However, this distinction is lost in cells depleted of the spliceosome component U1 snRNP, suggesting that when U1 snRNP is bound to the 5'ss of an intron at the initial stage of splicing, it may hinder UPF1 translocation along the pre-mRNA and cause it to dissociate. It is conceivable that this scanning of pre-mRNAs by UPF1 might influence splice site recognition and pre-mRNA splicing in a manner consistent with reported observations that UPF1 depletion provokes changes in the relative concentrations of many alternatively spliced transcripts in S2 cells (Brooks *et al.*, 2015) – and with the model offered in Figure 4G.

Simple affinity of UPF1 for RNA is not likely to be the primary reason why UPF1 associates with some nascent transcripts, for several reasons: UPF1 does not associate with some highly transcribed Pol II genes, such as spliceosomal snRNAs; nor with snRNA U6 or other highly active Pol III genes; nor with rRNA genes transcribed by Pol I; there would be no differential affinity for introns *vs*. exons within a transcript; and UPF1 appears to be excluded from the nucleolus, including its RNA-packed centre where rRNA genes are transcribed (McLeod *et al*., 2014). What features of some nascent transcripts, most often of Pol II-transcribed genes, dictate that UPF1 becomes associated with them, and for what purpose, remain to be determined. One obvious candidate would be the 7-methylguanosine (m7G) cap that is added

co-transcriptionally to the 5'end of pre-mRNAs but not to Pol I and Pol III transcripts (Ghosh and Lima, 2010). Since the m7G caps added to snRNAs and other small non-mRNA Pol II transcripts are further modified though by hypermethylation to generate 2, 2,7-trimethylguanosine (m(3)G) structures (Mouaikel et al., 2002), it might explain why these classes of transcripts are not UPF1-associated.

The association of UPF1 with nascent transcripts seems to be dynamic, and its putative 5'-to-3' scanning along RNA seems likely to be fast and, at least on intron-containing pre-mRNA, discontinuous. This pattern also suggests that when it encounters a steric block that cannot be removed UPF1 must be capable of quickly dissociating and re-loading elsewhere on the transcript. *In vitro*, UPF1 can translocate along RNAs over long distances – but only at a maximum scanning velocity of ~80 base/min (Fiorini *et al.*, 2015), which is much slower than the 2-3 kb/min of Pol II (Fiorini *et al*., 2015; Fukaya *et al*., 2017); possibly UPF1 translocates faster *in vivo*. We did not detect any major impairment of Pol II transcription in UPF1-depleted cells, but Pol II pausing downstream of the TSS was more apparent at some genes – for example, at *Xrp1*, a strikingly UPF1-associated gene. And transcription appears to recover more slowly from DRB inhibition in UPF1-depleted cells.

The most striking effects of UPF1 depletion were retention of poly(A) RNA at transcription sites and then its failure to be exported effectively from the nucleus. Completed mRNA transcripts that have been cleaved and polyadenylated are normally expected to be speedily released from transcription sites, but our data show that this is not always the case. We have both: a) identified some sites on polytene chromosomes that apparently accumulate poly(A) RNA even in wild-type glands; and b) shown that most of the active Pol II genes accumulate poly(A) RNA in UPF1-depleted glands. Poly(A) RNA accumulation in UPF1-depleted cells is most marked at genes with which UPF1 associates strongly in wild-type, such as *Actin5C* (as shown both microscopically and by ChIP-seq). Conversely, those few transcription sites at which poly(A) accumulates even in wild-type cells, may not normally be associated with UPF1, a striking example is transcription site 2C on the polytene chromosomes, which

showed the most apparent poly(A) accumulation but no obvious UPF1 association .

Evidence of retention of poly(A) and specific mRNAs in discrete nuclear foci or "dots" has previously been reported in cells defective in RNA processing, initially in mRNA export and processing mutants in yeast (Jensen *et al*., 2001). But whether these foci corresponded to intranuclear mRNP aggregates at sites adjacent to rather than at transcription sites is not clear – and so far these nuclear poly(A) foci have only been reported in cells in which one of several RNA processing reactions are impaired (Abruzzi *et al*., 2006; Paul and Montpetit, 2016). Whether the previously described "dots" correspond to the poly(A) clusters that accumulate in the inter-chromosomal spaces of UPF1-depleted nuclei and/or to accumulations of poly(A) at transcription sites, which we identified here, remains to be determined.

In summary, our results indicate that UPF1 plays some important genome-wide role(s) in nuclear processes of mRNA formation and in their release from transcription sites and export to the cytoplasm, at least in *Drosophila*.

Materials and Methods

Antibodies

These antibodies were used for immunostaining: mouse anti-UPF1 (described in this paper 7B12, typically diluted 1:100), mouse IgM anti-Ser2 Pol II (H5, Covance AB_10143905, 1:500), mouse anti-hnRNPA1 (Hrb87F, P11, 1:50)(Hovemann et al., 1991), mouse anti-GFP (B-2, Santa Cruz, SC-9996, 1:200), Tetramethylrhodamine Conjugate Wheat Germ Agglutinin (Thermo Fisher, W7024, 10µg/mL). The antibodies were used in Western blotting: mouse anti-UPF1 (7B12, 1:1000), mouse anti-α-tubulin (Sigma- Aldrich, T5168, 1:2500), rat anti-Ser2 Pol II (3E10, Merck Millipore, 04-1571, 1:5000), mouse anti-Rpb1 (7G5, 1:5000)(Conic et al., 2018); mouse anti-hnRNPA1 (1:200), rabbit anti-eIF4AIII (1:1000), rabbit anti-Y14 (1:1000); the last two antibodies were described previously (Choudhury et al., 2016). The antibodies used in ChIP are mouse anti-UPF1 (7B12, see below, 5-10 µg), rabbit anti-Ser2 Pol II (Abcam, ab5095, 5 µg), mouse anti-Pol II (8WG16, Abcam, ab817, 5µg) and mouse anti-GFP (B-2, Santa Cruz, 5 µg)..

Drosophila Stocks

Flies were reared in standard corn meal fly food media at 24°C. The yw strain was used as wild type. *UAS-UPF1-RNAi* (43144) and *UAS-GFP-UPF1* (24623) were obtained from the Bloomington stock centre. The *forkhead* (*Fkh*) Gal4 has a salivary gland specific expression from early stage of development (Henderson and Andrew, 2000). The transgenes expressing the *lacO*-tagged and ecdysone inducible S136 construct was described before (Choudhury et al., 2016).

Cell culture and RNA interference

S2 cells were cultured in Insect–XPRESS media (Lonza) supplemented with 10% Fetal Bovine Serum (FBS) and 1% Penicillin-Streptomycin-Glutamine mix (P/S/G, Invitrogen) at 27°C. To make the RNAi constructs for UPF1, eIF4AIII, Y14 and snRNPU1-70k mRNA, the specific sequences were PCR amplified from S2 cell genomic DNA by using corresponding primer pairs (Table S4). Along with the desired

gene sequence, all these primer pairs carried the T7 promoter sequence (in bold) at their 5' end (5'-T**TAATACGACTCACTATAG**GGGAGA-3'). The amplified PCR fragments were purified using Monarch® PCR and DNA Cleanup Kit (T1030S, NEB) and dsRNA was synthesized using the T7 RiboMAX express RNAi system (P1700, Promega). To induce RNAi, a six-well culture dish was seeded with 10^6 cells/well in serum-free media and mixed with 15 µg of dsRNA/well. Following 1 hr incubation at RT, 2 mL of complete media was added to each well and the cells were incubated for the next three days to knockdown the corresponding RNA and then harvested. The RNAi efficiency of UPF1, eIF4AIII and Y14 was measured by Western blotting while snRNPU1-70k was measured by real time PCR.

Generation of monoclonal antibodies against Drosophila UPF1

Antigens design, preparation, mice immunization and hybridoma generation were carried out by Abmart (Shanghai). Twelve peptide sequences predicted to be highly immunogenic were selected from *D. melanogaster* UPF1 (Table 1) and cloned in-frame in an expression vector to produce a recombinant protein incorporating all 12 antigens which were used as the immonogen (Abmart, SEAL^{TM} technology). Hybridoma clones were generated and used to induce 18 ascites, which were then screened by Western blotting of S2 cell protein extracts. Out of these, three that showed a single band of the expected size and minimal cross-reactivity were selected and more of the monoclonal antibodies subsequently purified from the corresponding hybridoma cell culture *in vitro*. Unless otherwise specified, 7B12 was used as the anti-UPF1 antibody throughout this study.

Larval tissue immunostaining

Whole-mount immunostaining was performed as previously described (Choudhury et al., 2016). In brief, the internal organs of 3rd instar larvae were dissected in 1X PBS (13 mM NaCl, 0.7 mM Na2HPO4, 0.3 mM NaH2PO4, pH 7.4) and fixed in 4% formaldehyde for 20 minutes at RT. Tissues were washed in 1XPBS followed by 1% Triton X-100 treatment for 20 minutes. Tissues were washed and incubated in blocking solution (10% Fetal Bovine Serum (FBS), 0.05% Sodium Azide in 1X PBS)

for 2 hrs at RT and then incubated in primary antibodies at 4^0C overnight. Tissues were washed and further incubated with appropriate fluorescent-tagged secondary antibodies for 2 hrs typically. After washing, tissues were incubated in DAPI (4–6-diamidino-2-phenylindole, Sigma-Aldrich, 1 µg/mL) for 10 minutes and mounted in PromoFluor Antifade Reagent (PK-PF-AFR1, PromoKine) mounting medium and examined using a Leica TCS SP2-AOBS confocal microscope.

LMB, DRB and larvae heat shock treatment

Wandering 3rd instar larvae were dissected in M3 media and tissues incubated with or without Leptomycin B (LMB, 50 nM) for 1 hr at RT. To examine the real-time effect of LMB treatment in the living cell, salivary glands were dissected in M3 media and incubated with a hanging drop of 50 nM LMB in M3 media in a cavity slide (Singh and Lakhotia, 2015). The fluorescence signal was acquired at 5-minute intervals with a Leica TCS SP2-AOBS confocal microscope. For ecdysone treatment, salivary glands were dissected in M3 media and incubated in 20-hydroxyecdysone (Sigma-Aldrich, H5142, 1µM) for 1 hr at RT. For RNase treatment, salivary glands were dissected in M3 media and incubated in 0.1% Triton X-100 for 2 minutes prior to adding RNase A (Invitrogen, 100µg/mL) a further 1 hr incubation at RT. To examine the effect of 5, 6-Dichlorobenzimidazole 1-β-D-ribofuranoside (DRB) treatment, salivary glands were dissected in M3 media and incubated with DRB (Sigma-Aldrich, 125µM) for 1 hr at RT. For heat shock response, larvae were placed in a pre-warmed microfuge tube lined with moist tissue paper and incubated in water-bath maintained at 37 ± 1^0C for 1 hr.

Live cell imaging (FRAP and FLIP)

Fluorescence recovery after photobleaching (FRAP) and fluorescence loss in photobleaching (FLIP) methods have been previously described (Klonis et al., 2002). Salivary glands expressing UPF1-GFP were dissected from 3rd instar larvae and mounted as a hanging drop in M3 media. For the FRAP the region of interest (ROI, a circle of fixed diameter) was rapidly photobleached with 100 iterations of 100% power Argon laser (488 nm) exposure. Subsequent recovery of fluorescence in the

photobleached region was examined at defined time intervals. As a control, fixed cells were examined to confirm irreversible photobleaching. FRAP experiments were carried out on salivary glands at room temperature. The fluorescence signal in ROI was normalized and data analysed following published methods (Phair and Misteli, 2000; Singh and Lakhotia, 2015). FLIP experiments were done as previously described (Phair and Misteli, 2000). Following an acquisition of five control images, GFP fluorescence in ROI1 was continuously photobleached with Argon laser (488 nm) at 100 % power by 50 iterations. The loss in fluorescence in another region of interest, the ROI2 was measured for the same length of time. Fluorescence intensities at ROI1 and ROI2 were normalized and data analysed as described (Nissim-Rafinia and Meshorer, 2011). Both photobleaching experiments have been done using a Leica TCS SP2-AOBS confocal microscope.

Polytene Chromosomes Immunostaining

Apart from the changes detailed below, the procedure was mostly as previously described (Rugjee et al., 2013). Briefly, actively wandering 3rd instar larvae were dissected in 1X PBS and salivary glands were fixed first with 3.7% formaldehyde in 1X PBS and then with 3.7% formaldehyde in 45% acetic acid for 1 min each (Singh and Lakhotia, 2012). For Pol II immunostaining, salivary glands dissected in 1XPBS were incubated directly with 3.7% formaldehyde in 45% acetic acid for 3 minutes. Salivary glands were squashed in the same solution under the coverslip. Slides were briefly dipped in liquid nitrogen, the coverslips were flipped off with a sharp blade and then immediately immersed in 90% ethanol and stored at 4^{0}C. For immunostaining, the chromosomes were air dried and then rehydrated by incubating the slide with 1XPBS in a plastic Coplin jar. Chromosomes were incubated in blocking solution (as for the tissue immunostaining) for 1 hr at RT and then incubated with primary antibodies diluted in blocking solution in a humid chamber overnight at 4^{0}C. Chromosomes were washed with 1X PBS three times and further incubated with fluorescent tagged appropriate secondary antibodies diluted in blocking solution for 2 hrs at RT in the humid chamber. After washing, chromosomes were counterstained with DAPI and mounted in

PromoFluor mounting media. Chromosomes were examined under Nikon Eclipse Ti epifluorescence microscope, equipped with ORCA-R2 camera (Hamamatsu Photonics).

Fluorescent Oligo (dT) *in situ* hybridization (FISH)

Oligo (dT) FISH was done as previously described for mammalian cells with some adaptations (Tripathi et al., 2015). Salivary glands of 3rd instar larvae were dissected in 1XPBS and fixed in 4% formaldehyde for 15 min at RT. Glands were then washed with 1XPBS and incubated in 0.1% Triton X-100 with 1U/µL Ribolock RNase Inhibitor (ThermoFisher Scientific, EO0381) in 1XPBS for 10 min on ice and then rinsed further with 1XPBS three times with 5 min intervals and then with 2XSSC for 10 min. Salivary glands were incubated with 5ng/µL rhodamine-labelled oligo(dT)45 probe (IDT) in hybridization solution (25% Formamide, 2X SSC pH 7.2, 10% w/v Dextran sulfate (Sigma Aldrich), 1 mg/mL *E. coli* tRNA (Sigma-Aldrich, R1753) for 12 hrs at 42^{0}C. Glands were then washed with freshly made wash buffer (50% Formamide in 2XSSC pH 7.2), followed by 2XSSC, 1XSSC and finally with 1XPBS 3 times each with 5 min interval. Nuclei were counterstained with DAPI and tissues were mounted in PromoFluor Antifade mounting medium and examined under Leica TCS SP2-AOBS confocal microscope.

For polytene chromosomes oligo(dT) FISH, salivary glands were dissected in 1XPBS and incubated with fixing solution (1.85% formaldehyde in 45% acetic acid) for 5 min at RT. Chromosomes were squashed in the same solution and examined immediately under phase-contrast microscope to check if properly spread. Slides with good chromosomes were briefly dipped in liquid nitrogen and the coverslips were flipped off with a sharp blade. Slides were immediately dipped in 90% alcohol and stored at 4^{0}C. Before hybridization, slides were air dried and rehydrated in 1XPBS and then washed and hybridized as described above for whole salivary glands. Chromosomes were counterstained with DAPI and mounted in PromoFluor Antifade mounting medium and examined under Nikon Eclipse Ti epifluorescence microscope.

Immunoprecipitation

Immunoprecipitation was performed as previously described (Hintermair et al., 2016), with some modifications as detailed below. S2 cells (4 X 10^7) were harvested and washed with ice-cold 1X PBS containing 1X PhosSTOP (Roche, 04906845001) and 1X cOmplete™, Mini, EDTA-free Protease Inhibitor Cocktail (Roche, 04693159001). Cells were incubated in the hypotonic AT buffer (15 mM HEPES pH 7.6, 10 mM KCl, 5mM MgOAc, 3mM CaCl2, 300 mM Sucrose, 0.1% Triton X-100, 1mM DTT, 1X PhosSTOP, 1X cOmplete™, Mini, EDTA-free Protease Inhibitor Cocktail and 1U/µL Ribolock RNase Inhibitor) for 20 min on ice and lysed with 2mL Dounce homogenizer by 30 strokes with the tight pestle. Lysate was centrifuged at 5000 RPM for 5 min at 4^0C in microcentrifuge and the nuclear pellet was resuspended in 500 µL IP buffer (50 mM Tris-HCl pH 8.0, 150 mM NaCl, 1% NP-40 (Roche), 1X PhosSTOP, 1X cOmplete™, Mini, EDTA-free Protease Inhibitor Cocktail, 1U/µL Ribolock RNase Inhibitor) for 20 min on ice. Nuclear lysates were sonicated using a Bioruptor sonicator (Diagenode) for 3 cycles of 30 sec ON and 30 sec OFF with maximum intensity. Following sonication, the lysates were centrifuged at 13000 RPM for 15 min at 4^0C in a microfuge and the antibody (5µg) was added to the clear supernatant, with or without addition of RNase A (100µg/mL), and incubated overnight at 4^0C on a rocker. Following incubation, 20 µL of prewashed paramagnetic Dynabeads (ThermoFisher Scientific, 10004D) were added and incubated further for 2 hrs at 4^0C on a rocker. Beads were washed 5 times with IP buffer using a magnetic rack and proteins were extracted by adding 40µL SDS-PAGE sample buffer.

ChIP-Seq

S2 cells (2 X 10^7) were harvested and fixed with 1% formaldehyde (EM grade, Polyscience) for 10 min at RT. Following fixation, cross-linking reaction was stopped by adding 125 mM Glycine for 5 min at RT. Cells were centrifuged at 2000 RPM for 5 min at 4°C, the pellet was washed twice with ice-cold 1X PBS containing 1X cOmplete™, Mini, EDTA-free Protease Inhibitor Cocktail. The cell pellet was resuspended in 1 mL of cell lysis buffer (5mM PIPES pH 8.0, 85mM KCl, 0.5%

NP-40) supplemented with 1X cOmplete™, Mini, EDTA-free Protease Inhibitor Cocktail and 1X PhosStop and incubated for 10 min at 4^0C. Cells were centrifuged and the pellet was resuspended in 1 mL nuclear lysis buffer (50mM Tris pH 8.0, 10 mM EDTA, 1.0% SDS) supplemented with 1X cOmplete™, Mini, EDTA-free Protease Inhibitor Cocktail and 1X PhosStop and incubated for 10 min at 4^0C. The cell suspension was further diluted with 500 µL IP dilution buffer (16.7 mM Tris pH 8.0, 1.2 mM EDTA, 167 mM NaCl, 1.1% Triton X-100, 0.01% SDS) and sonicated for 5 cycles at 30sec ON, 30 sec OFF with maximum intensity by using a Bioruptor sonicator (Diagenode); this produced an average fragment size of ~500 bp. Samples were centrifuged at 13000 RPM for 20 min in a microcentrifuge and the clear supernatant was transferred to a 15 mL tube. An aliquot of 100 µL supernatant was kept to extract input DNA. The supernatant was further diluted with 5 volume of IP dilution buffer. For each ChIP, typically we added 5 to 10 µg of antibody to this supernatant and incubated overnight at 4^0C on a rocker. Prewashed 20 µL Dynabeads were added to the lysate-antibody mix and incubated further for 1 hr at 4^0C on a rocker. Beads were washed 6 times with low salt buffer (0.1% SDS, 1% Triton X-100, 2mM EDTA, 20 mM Tris pH 8.0, 150 mM NaCl), once with high salt buffer (0.1% SDS, 1% Triton X 100, 2mM EDTA, 20 mM Tris pH 8.0, 500 mM NaCl) and once with 1X TE buffer (10mM Tris pH 8.0, 1mM EDTA). The beads were then incubated with 250 µL elution buffer (0.1M NaHC03, 1% SDS) at RT for 15 min and eluted chromatin was reverse cross-linked by adding 38 µL de-crosslinking buffer (2M NaCl, 0.1M EDTA, 0.4M Tris pH 7.5) and then incubated at 65°C for overnight on a rotator. Proteins were digested by adding 2 µL Proteinase K (50 mg/mL) and incubated at 50^0C for 2 hrs on a rocker. DNA was isolated by using Monarch® PCR and DNA Cleanup Kits. Real-time PCR quantification of DNA samples was carried out using the SensiFAST SYBR Hi-ROX Kit (Bioline, BIO-92005) in 96-well plates using an ABI PRISM 7000 system (Applied Biosystems). For NGS sequencing, ChIP and input DNA were further fragmented to 200 bp fragment size using a Bioruptor Pico (Diagenode). All ChIP-DNA libraries were produced using the NEBNext Ultra II DNA Library Prep Kit (New England Biolab E7645L) and NEBnext Multiplex Oligos

for Illumina Dual Index Primers (New England Biolabs E7600S), using provided protocols with 10ng of fragmented ChIP DNA. Constructed libraries were assessed for quality using the Tapestation 2200 (Agilent G2964AA) with High Sensitivity D1000 DNA ScreenTape (Agilent 5067-5584). Libraries were tagged with unique barcodes and sequenced simultaneously on a HiSeq4000 sequencer.

Nascent RNA isolation from S2 cells

Nascent RNA isolation was performed as previously described (Khodor et al., 2011). Briefly, S2 cells (4 X 10^7) were harvested and washed twice with ice-cold 1X PBS via centrifugation at 2000g for 5 min each. Cells were resuspended in 1 mL ice-cold buffer AT and incubated on ice for 10 minutes. Cells were lysed using a 2mL Dounce homogenizer by 30 strokes with the tight pestle. The lysate was divided into two aliquots and each aliquot of 500 µL was layered over a 1mL cushion of buffer B (15 mM HEPES-KOH at pH 7.6, 10 mM KCl, 5 mM MgOAc, 3 mM CaCl2, 1 M sucrose, 1 mM DTT, 1X cOmplete™, Mini, EDTA-free Protease Inhibitor Cocktail), and centrifuged at 8000 RPM for 15 min at 4°C in a microcentrifuge. The supernatant was removed and the pellet was resuspended in 5 volumes of nuclear lysis buffer (10 mM HEPES-KOH pH 7.6, 100 mM KCl, 0.1 mM EDTA, 10% Glycerol, 0.15 mM Spermine, 0.5 mM Spermidine, 0.1 M NaF, 0.1 M Na3VO4, 0.1 mM ZnCl2, 1 mM DTT, 1X cOmplete™, Mini, EDTA-free Protease Inhibitor Cocktail and 1U/µL Ribolock RNase Inhibitor) and resuspended using a 2mL Dounce homogenizer by 3 strokes with loose pestle and 2 strokes with tight pestle. Equal volume of 2X NUN buffer (50 mM HEPES-KOH pH 7.6, 600 mM NaCl, 2 M Urea, 2% NP-40, 1 mM DTT, 1X cOmplete™, Mini, EDTA-free Protease Inhibitor Cocktail and 1U/µL Ribolock RNase Inhibitor) was added to the nuclear suspension drop by drop while vortexing and the suspension was placed on ice for 20 min prior to spinning at 13,000 RPM for 30 min at 4°C. The supernatant was removed and TRI Reagent (Sigma, T9424) was added to the histone–DNA-Pol II-RNA pellet. The TRI Reagent–pellet suspension was incubated at 65°C with intermittent vortexing to dissolve the pellet, and RNA was extracted following the manufacturer's protocol. Poly(A) depletion was

performed with Dynabeads™ Oligo(dT)25 (ThermoFisher Scientific). The purification of nascent RNA was assessed by RT-PCR of CG12030, CG5059 and CG10802 genes which have slow rates of co-transcriptional splicing (Khodor et al., 2011); cDNA synthesis was performed using qScript cDNA synthesis kit (Quanta Biosciences, 95047-025).

RNA-seq

Extracted RNA samples were quantified using a Nanodrop-8000 Spectrophotometer (ThermoFisher ND-8000-GL) to assess quality and to determine concentrations. Aliquots of each sample were diluted to ~5ng/µl, and tested with an Agilent Tapestation 2200 (Agilent G2964AA) using High Sensitivity RNA ScreenTapes kit (Agilent 5067- 5579) to determine the RNA Integrity Number.

Total-RNA (1µg) was first poly(A) selected using the NEBNext® Poly(A) mRNA Magnetic Isolation Module (New England Biolabs E7490L) prior to library construction. Nascent RNA samples (100 ng) were processed without poly(A) selection. RNA libraries were prepared using a NEBNext Ultra Directional RNA Library Prep Kit (New England Biolab E7420L) and NEBnext Multiplex Oligos for Illumina Dual Index Primers (New England Biolabs E7600S), following standard protocols. RNA libraries were checked for quality using the Tapestation 2200 (Agilent G2964AA) with High Sensitivity D1000 DNA ScreenTape (Agilent 5067-5584). Multiplexed libraries were sequenced (50-bp single-end reads) on a HiSeq4000 sequencer.

CHIP-seq and RNA-seq data analysis

ChIP-seq and RNA-seq data were initially viewed and analysed using the Lasergene Genomics Suite version 14 (DNASTAR). Pre-processing, assembly and mapping of the sequencing reads in the FASTQ files were performed by the SeqMan NGen software of this package automatically after selecting the NCBI *D. melanogaster* Dm6 genome release and accompanying annotations. Assembly and alignment output files for each genome contig were then analysed with the ArrayStar and GenVision Pro

software (from the same package) to view and compare data track on the genome. Profiles at selected regions were saved as high-resolution images.

To perform the metagene analyses, an index for Dm6 was downloaded from the HISAT2 website. HISAT2 v2.1.0 was then used to align the FASTQ files on it. The resulting SAM files were converted to BAM format, sorted, and indexed with Samtools 1.6. For the cytoplasmic RNA-seq data, the NCBI RefSeq gene annotations for Dm6 were downloaded as a GTF file from UCSC Table Browser (genome.ucsc.edu). Custom scripts were then used to produce read counts per gene in an HTSeq-count compatible format based on the GTF file. Transcript lengths were also obtained from the GTF file and used together with total mapped sequencing reads to convert counts into RPKM values. For both ChIP-seq and nascent RNA-seq data, the BAM files were converted to Bedgraph files. This was carried out with the genomeCoverageBed command and options -bga and -ibam from the Bedtools v2.26.0 suite. Custom Perl scripts were then used to filter the Dm6 annotations either for genes separated by a minimum distance to avoid overlapping signals or RNA-seq expression levels. Subsequently, custom scripts were used to extract the signal from the Bedgraph files for each entry in the filtered gene list. A single base resolution was used for flanking regions, while the signal in gene bodies was binned into 16 bins to take account of different gene lengths. Each dataset was normalized by the total mapped sequencing reads in that dataset. Cross-referencing between different datasets was done based on the 'name' field, after filtering the annotations for multiple entries with the identical name.

A custom script was used to extract from the Bedgraph files the sequencing read coverage for each exon/intron/exon region in the dm6 annotation file xon_fly_gene (downloaded from UCSC Table Browser). To normalise for any bias in the sequencing, the UPF1 signal of each exon or intron was divided by the average coverage in the input sample. The fold change of UPF1 signal/input signal in introns was compared to that of their flanking exons using Wilcox.test (two sided and unpaired) in R (www.r-project.org). This analysis was done using either all introns

annotated in Dm6 (151623) or those longer than 100bp (76708), in either case flanking exons are significantly more enriched than introns. Here we have shown the result of analysis using just the longer introns as these were considered to be more informative because of the predicted lower resolution of ChIP at discriminating between closely adjacent sequences and because the lower sequencing coverage of shorter introns compared to longer introns. All ChIP-seq and RNA-seq raw sequencing data and Bedgraph files were deposited in the GEO repository (Accession No GSE116808)

Acknowledgments

We thank Bob Michell for critically reading the manuscript and valuable discussions. Thanks also to Michael Rosbash and Michael Marr (USA) for providing a detailed Nascent RNA-seq protocol, Harald Saumweber (Germany) for the P11 antibody and Laszlo Tora (France) for the 7G5 antibody. Bloomington is also acknowledged for providing fly stocks. Thanks also to Alessandro Di Maio and the Birmingham Advanced Light Microscopy (BALM) facility; our School Drosophila research community, fly food facility and Shrikant Jondhale for fly stocks maintenance; our NGS facility; and, Mike Tomlinson for providing Odyssey infrared imaging system for Western blot detection. We thank also Pawel Grzechnik for reagents, and his and our group for help and continuous discussions. This project was funded by a Leverhulme Trust (RPG-2014-291) and BBSRC (BB/M022757/1) project grants, and at its start, Wellcome Trust (9340/Z/09/Z) to SB. DH was supported by BBSRC grants BB/M017982/1 and BB/L006340/1.

Author Contributions

A.K.S. designed the study, performed experiments, interpreted data and wrote the manuscript. S.R.C., S.D., V.D. and P.R. designed the study and performed experiments. S.K. and L.O. conducted the sequencing experiments and wrote the manuscript. J.Z. and D.H. conducted bioinformatic analyses and wrote the manuscript. S.B. provided expertise, supervision, funding, data interpretation and manuscript writing.

References

Abruzzi, K.C., Belostotsky, D.A., Chekanova, J.A., Dower, K., and Rosbash, M. (2006). 3'-end formation signals modulate the association of genes with the nuclear periphery as well as mRNP dot formation. EMBO J *25*, 4253-4262.

Adelman, K., and Lis, J.T. (2012). Promoter-proximal pausing of RNA polymerase II: emerging roles in metazoans. Nat Rev Genet *13*, 720-731.

Ajamian, L., Abel, K., Rao, S., Vyboh, K., Garcia-de-Gracia, F., Soto-Rifo, R., Kulozik, A.E., Gehring, N.H., and Mouland, A.J. (2015). HIV-1 Recruits UPF1 but Excludes UPF2 to Promote Nucleocytoplasmic Export of the Genomic RNA. Biomolecules *5*, 2808-2839.

Altamura, N., Groudinsky, O., Dujardin, G., and Slonimski, P.P. (1992). Nam7 nuclear gene encodes a novel member of a family of helicases with a Zn-ligand motif and is involved in mitochondrial functions in *Saccharomyces cerevisiae*. Journal of Molecular Biology *224*, 575-587.

Azzalin, C.M., and Lingner, J. (2006). The human RNA surveillance factor UPF1 is required for S phase progression and genome stability. Curr Biol *16*, 433-439.

Azzalin, C.M., Reichenbach, P., Khoriauli, L., Giulotto, E., and Lingner, J. (2007). Telomeric repeat containing RNA and RNA surveillance factors at mammalian chromosome ends. Science *318*, 798-801.

Bensaude, O. (2011). Inhibiting eukaryotic transcription: Which compound to choose? How to evaluate its activity? Transcription *2*, 103-108.

Bhattacharya, A., Czaplinski, K., Trifillis, P., He, F., Jacobson, A., and Peltz, S.W. (2000). Characterization of the biochemical properties of the human Upf1 gene product that is involved in nonsense-mediated mRNA decay. RNA *6*, 1226-1235.

Boehm, A.K., Saunders, A., Werner, J., and Lis, J.T. (2003). Transcription factor and polymerase recruitment, modification, and movement on dhsp70 in vivo in the minutes following heat shock. Mol Cell Biol *23*, 7628-7637.

Brogna, S., McLeod, T., and Petric, M. (2016). The Meaning of NMD: Translate or Perish. Trends Genet *32*, 395-407.

Brogna, S., and Wen, J. (2009). Nonsense-mediated mRNA decay (NMD) mechanisms. Nat Struct Mol Biol *16*, 107-113.

Brooks, A.N., Duff, M.O., May, G., Yang, L., Bolisetty, M., Landolin, J., Wan, K., Sandler, J., Booth, B.W., Celniker, S.E., *et al.* (2015). Regulation of alternative splicing in Drosophila by 56 RNA binding proteins. Genome Res *25*, 1771-1780.

Carastro, L.M., Tan, C.K., Selg, M., Jack, H.M., So, A.G., and Downey, K.M. (2002). Identification of delta helicase as the bovine homolog of HUPF1: demonstration of an interaction with the third subunit

of DNA polymerase delta. Nucleic Acids Res *30*, 2232-2243.

Chakrabarti, S., Jayachandran, U., Bonneau, F., Fiorini, F., Basquin, C., Domcke, S., Le Hir, H., and Conti, E. (2011). Molecular mechanisms for the RNA-dependent ATPase activity of Upf1 and its regulation by Upf2. Mol Cell *41*, 693-703.

Chawla, R., Redon, S., Raftopoulou, C., Wischnewski, H., Gagos, S., and Azzalin, C.M. (2011). Human UPF1 interacts with TPP1 and telomerase and sustains telomere leading-strand replication. EMBO J *30*, 4047-4058.

Choudhury, S.R., Singh, A.K., McLeod, T., Blanchette, M., Jang, B.Y., Badenhorst, P., Kanhere, A., and Brogna, S. (2016). Exon junction complex proteins bind nascent transcripts independently of pre-mRNA splicing in Drosophila melanogaster. Elife *5*.

Conic, S., Desplancq, D., Ferrand, A., Fischer, V., Heyer, V., Reina San Martin, B., Pontabry, J., Oulad-Abdelghani, M., Babu, N.K., Wright, G.D., *et al.* (2018). Imaging of native transcription factors and histone phosphorylation at high resolution in live cells. J Cell Biol *217*, 1537-1552.

Culbertson, M.R., Underbrink, K.M., and Fink, G.R. (1980). Frameshift suppression in Saccharomyces Cerevisiae II. Genetic properties of group II suppressors. Genetics *95*, 833-853.

Czaplinski, K., RuizEchevarria, M.J., Paushkin, S.V., Han, X., Weng, Y.M., Perlick, H.A., Dietz, H.C., TerAvanesyan, M.D., and Peltz, S.W. (1998). The surveillance complex interacts with the translation release factors to enhance termination and degrade aberrant mRNAs. Genes & development *12*, 1665-1677.

Czaplinski, K., Weng, Y., Hagan, K.W., and Peltz, S.W. (1995). Purification and characterization of the Upf1 protein - a factor involved in translation and messenger RNA degradation. RNA *1*, 610-623.

de Turris, V., Nicholson, P., Orozco, R.Z., Singer, R.H., and Muhlemann, O. (2011). Cotranscriptional effect of a premature termination codon revealed by live-cell imaging. RNA *17*, 2094-2107.

Fatscher, T., Boehm, V., and Gehring, N.H. (2015). Mechanism, factors, and physiological role of nonsense-mediated mRNA decay. Cell Mol Life Sci *72*, 4523-4544.

Fiorini, F., Bagchi, D., Le Hir, H., and Croquette, V. (2015). Human Upf1 is a highly processive RNA helicase and translocase with RNP remodelling activities. Nature communications *6*, 7581.

Flury, V., Restuccia, U., Bachi, A., and Muhlemann, O. (2014). Characterization of Phosphorylation- and RNA-Dependent UPF1 Interactors by Quantitative Proteomics. J Proteome Res *13*, 3038-3053.

Fukaya, T., Lim, B., and Levine, M. (2017). Rapid Rates of Pol II Elongation in the Drosophila Embryo. Curr Biol *27*, 1387-1391.

Fukuda, M., Asano, S., Nakamura, T., Adachi, M., Yoshida, M., Yanagida, M., and Nishida, E. (1997). CRM1 is responsible for intracellular transport mediated by the nuclear export signal. Nature *390*, 308-311.

Gao, Z., and Wilkinson, M. (2017). An RNA decay factor wears a new coat: UPF3B modulates translation termination. F1000Res *6*, 2159.

Ghosh, A., and Lima, C.D. (2010). Enzymology of RNA cap synthesis. Wiley Interdiscip Rev RNA *1*, 152-172.

Goetz, A.E., and Wilkinson, M. (2017). Stress and the nonsense-mediated RNA decay pathway. Cell Mol Life Sci *74*, 3509-3531.

He, F., and Jacobson, A. (2015). Nonsense-Mediated mRNA Decay: Degradation of Defective Transcripts Is Only Part of the Story. Annu Rev Genet.

Henderson, K.D., and Andrew, D.J. (2000). Regulation and function of Scr, exd, and hth in the Drosophila salivary gland. Dev Biol *217*, 362-374.

Hintermair, C., Voss, K., Forne, I., Heidemann, M., Flatley, A., Kremmer, E., Imhof, A., and Eick, D. (2016). Specific threonine-4 phosphorylation and function of RNA polymerase II CTD during M phase progression. Sci Rep *6*, 27401.

Hodgkin, J., Papp, A., Pulak, R., Ambros, V., and Anderson, P. (1989). A new kind of informational suppression in the nematode Caenorhabditis elegans. Genetics *123*, 301-313.

Hogg, J.R., and Goff, S.P. (2010). Upf1 senses 3'UTR length to potentiate mRNA decay. Cell *143*, 379-389.

Hovemann, B.T., Dessen, E., Mechler, H., and Mack, E. (1991). Drosophila snRNP associated protein P11 which specifically binds to heat shock puff 93D reveals strong homology with hnRNP core protein A1. Nucleic Acids Res *19*, 4909-4914.

Hurt, J.A., Robertson, A.D., and Burge, C.B. (2013). Global analyses of UPF1 binding and function reveal expanded scope of nonsense-mediated mRNA decay. Genome Res *23*, 1636-1650.

Ivanov, P.V., Gehring, N.H., Kunz, J.B., Hentze, M.W., and Kulozik, A.E. (2008). Interactions between UPF1, eRFs, PABP and the exon junction complex suggest an integrated model for mammalian NMD pathways. Embo J *27*, 736-747.

Jensen, T.H., Patricio, K., McCarthy, T., and Rosbash, M. (2001). A block to mRNA nuclear export in S. cerevisiae leads to hyperadenylation of transcripts that accumulate at the site of transcription. Mol Cell *7*, 887-898.

Karousis, E.D., Nasif, S., and Muhlemann, O. (2016). Nonsense-mediated mRNA decay: novel mechanistic insights and biological impact. Wiley Interdiscip Rev RNA *7*, 661-682.

Kashima, I., Yamashita, A., Izumi, N., Kataoka, N., Morishita, R., Hoshino, S., Ohno, M., Dreyfuss, G., and Ohno, S. (2006). Binding of a novel SMG-1-Upf1-eRF1-eRF3 complex (SURF) to the exon junction complex triggers Upf1 phosphorylation and nonsense-mediated mRNA decay. Genes Dev *20*, 355-367.

Keeling, K.M., Lanier, J., Du, M., Salas-Marco, J., Gao, L., Kaenjak-Angeletti, A., and Bedwell, D.M. (2004). Leaky termination at premature stop codons antagonizes nonsense-mediated mRNA decay in S. cerevisiae. RNA *10*, 691-703.

Khodor, Y.L., Rodriguez, J., Abruzzi, K.C., Tang, C.H., Marr, M.T., 2nd, and Rosbash, M. (2011). Nascent-seq indicates widespread cotranscriptional pre-mRNA splicing in Drosophila. Genes Dev *25*, 2502-2512.

Klonis, N., Rug, M., Harper, I., Wickham, M., Cowman, A., and Tilley, L. (2002). Fluorescence photobleaching analysis for the study of cellular dynamics. Eur Biophys J *31*, 36-51.

Kurosaki, T., and Maquat, L.E. (2016). Nonsense-mediated mRNA decay in humans at a glance. J Cell Sci *129*, 461-467.

Lakhotia, S.C., Mallik, M., Singh, A.K., and Ray, M. (2012). The large noncoding hsromega-n transcripts are essential for thermotolerance and remobilization of hnRNPs, HP1 and RNA polymerase II during recovery from heat shock in Drosophila. Chromosoma *121*, 49-70.

Leeds, P., Peltz, S.W., Jacobson, A., and Culbertson, M.R. (1991). The product of the yeast Upf1 gene is required for rapid turnover of messenger RNAs containing a premature translational termination codon. Genes & development *5*, 2303-2314.

Leeds, P., Wood, J.M., Lee, B.S., and Culbertson, M.R. (1992). Gene products that promote mRNA turnover in Saccharomyces cerevisiae. Mol Cell Biol *12*, 2165-2177.

Lykke-Andersen, S., and Jensen, T.H. (2015). Nonsense-mediated mRNA decay: an intricate machinery that shapes transcriptomes. Nat Rev Mol Cell Biol *16*, 665-677.

McLeod, T., Abdullahi, A., Li, M., and Brogna, S. (2014). Recent studies implicate the nucleolus as the major site of nuclear translation. Biochem Soc Trans *42*, 1224-1228.

Mendell, J.T., ap Rhys, C.M., and Dietz, H.C. (2002). Separable roles for rent1/hUpf1 in altered splicing and decay of nonsense transcripts. Science *298*, 419-422.

Metzstein, M.M., and Krasnow, M.A. (2006). Functions of the nonsense-mediated mRNA decay pathway in Drosophila development. PLoS genetics *2*, e180.

Mizuguchi-Hata, C., Ogawa, Y., Oka, M., and Yoneda, Y. (2013). Quantitative regulation of nuclear pore complex proteins by O-GlcNAcylation. Biochim Biophys Acta *1833*, 2682-2689.

Mouaikel, J., Verheggen, C., Bertrand, E., Tazi, J., and Bordonne, R. (2002). Hypermethylation of the cap structure of both yeast snRNAs and snoRNAs requires a conserved methyltransferase that is localized to the nucleolus. Mol Cell *9*, 891-901.

Muhlemann, O., and Karousis, E.D. (2017). New functions in translation termination uncovered for NMD factor UPF3B. EMBO J *36*, 2928-2930.

Muse, G.W., Gilchrist, D.A., Nechaev, S., Shah, R., Parker, J.S., Grissom, S.F., Zeitlinger, J., and

Adelman, K. (2007). RNA polymerase is poised for activation across the genome. Nat Genet *39*, 1507-1511.

Nazarenus, T., Cedarberg, R., Bell, R., Cheatle, J., Forch, A., Haifley, A., Hou, A., Wanja Kebaara, B., Shields, C., Stoysich, K., *et al.* (2005). Upf1p, a highly conserved protein required for nonsense-mediated mRNA decay, interacts with the nuclear pore proteins Nup100p and Nup116p. Gene *345*, 199-212.

Neu-Yilik, G., Raimondeau, E., Eliseev, B., Yeramala, L., Amthor, B., Deniaud, A., Huard, K., Kerschgens, K., Hentze, M.W., Schaffitzel, C., *et al.* (2017). Dual function of UPF3B in early and late translation termination. EMBO J *36*, 2968-2986.

Nissim-Rafinia, M., and Meshorer, E. (2011). Photobleaching assays (FRAP & FLIP) to measure chromatin protein dynamics in living embryonic stem cells. J Vis Exp.

Paul, B., and Montpetit, B. (2016). Altered RNA processing and export lead to retention of mRNAs near transcription sites and nuclear pore complexes or within the nucleolus. Mol Biol Cell *27*, 2742-2756.

Phair, R.D., and Misteli, T. (2000). High mobility of proteins in the mammalian cell nucleus. Nature *404*, 604-609.

Pulak, R., and Anderson, P. (1993). Messenger RNA surveillance by the *Caenorhabditis elegans* smg genes. Genes & development *7*, 1885-1897.

Rugjee, K.N., Roy Chaudhury, S., Al-Jubran, K., Ramanathan, P., Matina, T., Wen, J., and Brogna, S. (2013). Fluorescent protein tagging confirms the presence of ribosomal proteins at Drosophila polytene chromosomes. PeerJ *1*, e15.

Singh, A.K., and Lakhotia, S.C. (2012). The hnRNP A1 homolog Hrp36 is essential for normal development, female fecundity, omega speckle formation and stress tolerance in Drosophila melanogaster. J Biosci *37*, 659-678.

Singh, A.K., and Lakhotia, S.C. (2015). Dynamics of hnRNPs and omega speckles in normal and heat shocked live cell nuclei of Drosophila melanogaster. Chromosoma *124*, 367-383.

Singh, G., Rebbapragada, I., and Lykke-Andersen, J. (2008). A competition between stimulators and antagonists of Upf complex recruitment governs human nonsense-mediated mRNA decay. PLoS Biol *6*, e111.

Tripathi, V., Fei, J., Ha, T., and Prasanth, K.V. (2015). RNA fluorescence in situ hybridization in cultured mammalian cells. Methods Mol Biol *1206*, 123-136.

Varsally, W., and Brogna, S. (2012). UPF1 involvement in nuclear functions. Biochem Soc Trans *40*, 778-783.

Wang, W.R., Czaplinski, K., Rao, Y., and Peltz, S.W. (2001). The role of Upf proteins in modulating the

translation read-through of nonsense-containing transcripts. Embo Journal *20*, 880-890.

Zund, D., Gruber, A.R., Zavolan, M., and Muhlemann, O. (2013). Translation-dependent displacement of UPF1 from coding sequences causes its enrichment in 3' UTRs. Nat Struct Mol Biol *20*, 936-943.

Figures and legends

Figure 1

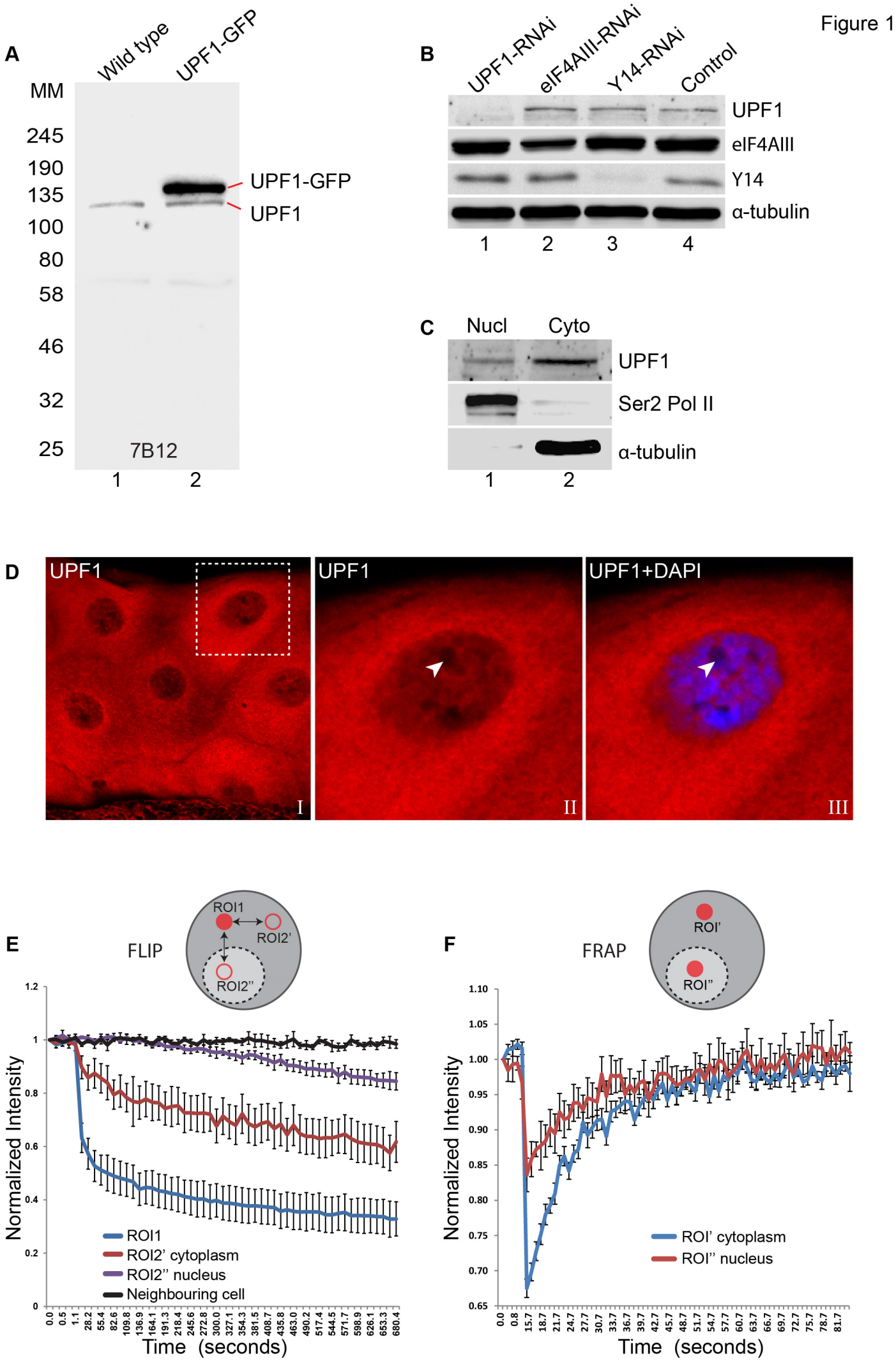
A
Wild type
UPF1-GFP
MM
245
190
135
100
80
58
46
32
25
UPF1-GFP
UPF1
7B12
1
2
B
UPF1-RNAi
eIF4AIII-RNAi
Y14-RNAi
Control
UPF1
eIF4AIII
Y14
α-tubulin
1
2
3
4
C
Nucl
Cyto
UPF1
Ser2 Pol II
α-tubulin
1
2
D
UPF1
UPF1
UPF1+DAPI
I
II
III
E
FLIP
ROI1
ROI2'
ROI2''
Normalized Intensity
Time (seconds)
ROI1
ROI2' cytoplasm
ROI2'' nucleus
Neighbouring cell
F
FRAP
ROI'
ROI''
Normalized Intensity
Time (seconds)
ROI' cytoplasm
ROI'' nucleus

Figure 1. UPF1 continuously shuttles between nucleus and cytoplasm. (**A**) Western blotting of whole-cell lysate from either normal (lane 1) or transfected S2 cells expressing UPF1-GFP (lane 2), probed with the UPF1 monoclonal antibody 7B12. The proteins run according to their expected molecular weights: UPF1 (~130 kDa), and UPF1-GFP (~157 kDa) (**B**) Western blotting of S2 cells treated with dsRNA targeting UPF1 or the other RNA binding proteins indicated, used as controls. Separate sections of the membrane were probed with anti-UPF1 (7B12, top row), anti-eIF4AIII (row 2), anti-Y14 (row 3) or anti-α-tubulin (row 4) as a loading control. (**C**) Western blotting of UPF1 following nuclear (Nucl) and cytoplasmic (Cyto) fractionation of S2 cell. RNA Pol II and α-tubulin were detected by the corresponding antibodies using the same blot (shown below). (**D**) Fluorescence immunolocalization of UPF1 (Cy3, red) in 3rd instar larval salivary gland. The arrowheads in panel II and III (magnified view of boxed area in panel I) point to the nucleolus, identified by no DAPI staining, which as other nucleoli shows no UPF1 signal in its centre. (**E**) Plot shows fluorescence loss in photobleaching (FLIP) of UPF1-GFP in salivary gland cells photobleached in ROI1 (red circle, cytoplasm) and then GFP signal measured at the identical time points in two separate ROI2s (red rings), in either cytoplasm or nucleus; both equidistant from ROI1. The different lines show rate of GFP fluorescence loss in either the photobleached ROI1 (blue line), or ROI2' in the cytoplasm (red line) or ROI2'' in nucleus (purple line). Change during in fluorescence intensity at equivalent regions in neighbouring cells was measured as a control during the same time-course (black line). Y-axis shows normalized relative fluorescence intensity and X-axis time (seconds) from start of imaging. Quantification based on imaging experiments in 8 different cells. (**F**) Plot shows fluorescence recovery after photobleaching (FRAP) of UPF1-GFP in either cytoplasm (ROI', blue line) or nucleus (ROI'', red line) of salivary gland cells. Line values are the average of 8 separate measurements in different cells.

Figure 2

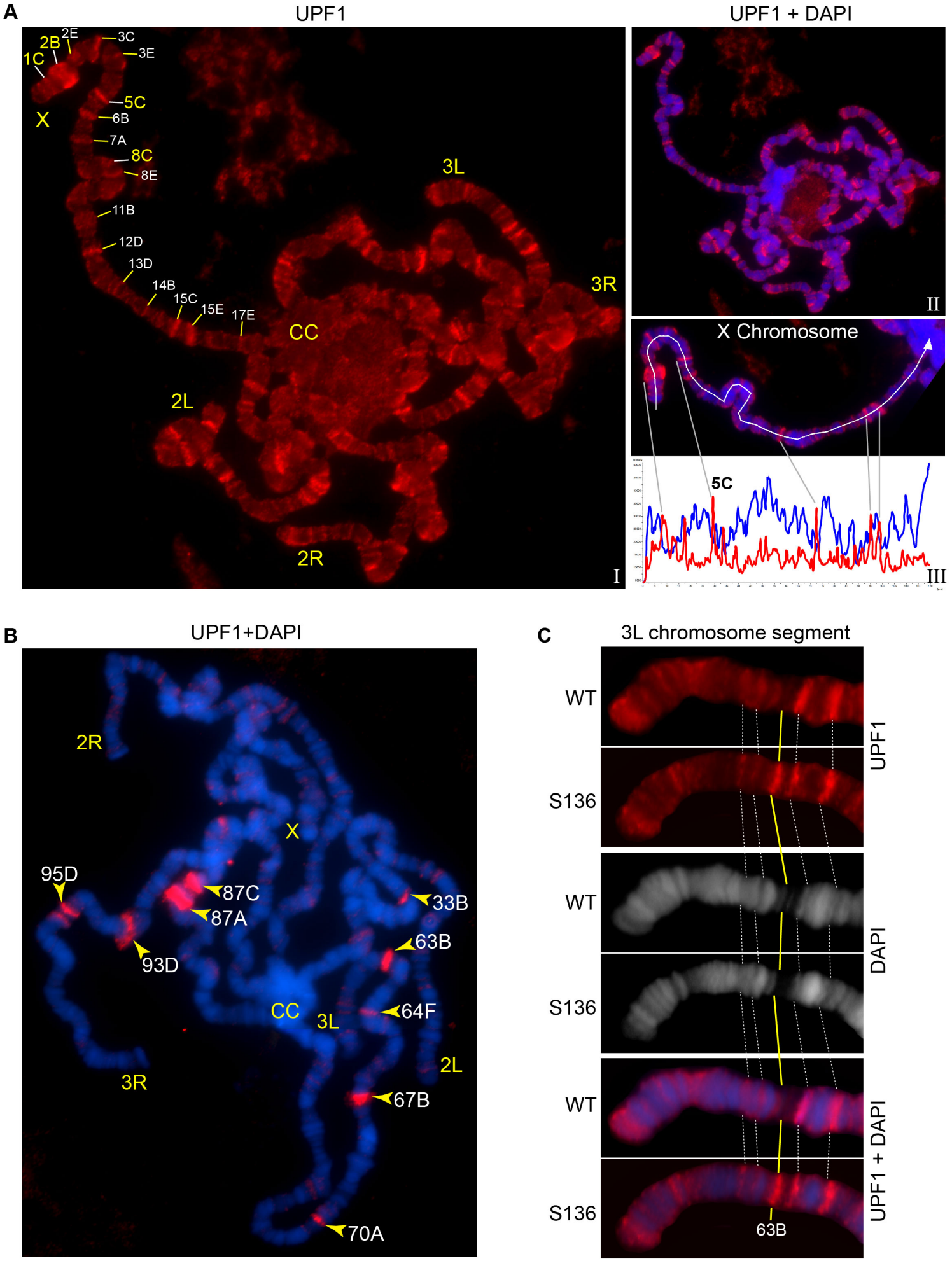
A
UPF1
UPF1 + DAPI
1C
2B
2E
3C
3E
X
5C
6B
7A
8C
8E
11B
12D
13D
14B
15C
15E
17E
3L
3R
CC
2L
2R
I
II
X Chromosome
5C
III
B
UPF1+DAPI
2R
X
95D
87C
87A
33B
63B
93D
CC
3L
64F
2L
3R
67B
70A
C
3L chromosome segment
WT
S136
UPF1
WT
S136
DAPI
WT
S136
UPF1 + DAPI
63B

Figure 2. UPF1 binds at transcriptionally active sites on the polytene chromosomes. (**A**) Fluorescence immunolocalization of UPF1 (Cy3, red, I) on polytene chromosomes (DAPI, blue, II). Chromosome arms (X, 2L, 2R, 3L and 3R) and chromocentre (CC) are labelled. The labels indicate cytological locations of interband regions at the X chromosome, presenting apparent UPF1 signal. The line profile (III, white panel) shows signal intensities along the white line drawn on the X chromosome, UPF1 (red) and DAPI (blue). (**B**) Immunolocalization of UPF1 (red) on polytene chromosomes derived from larvae subjected to a 40 min heat shock at 37^0C. UPF1 signals are primarily detected at heat shock gene loci, indicated by their cytological locations, using their standard nomenclature. (**C**) Immunolocalization of UPF1 (red) at an ecdysone induced transgene (named S136) located at cytological position 63B (Yellow line) and the same region on the wild type chromosome after ecdysone treatment. The white dotted lines indicate flanking bands as mapping reference. Chromosomes were stained with DAPI (grey in middle panel or blue in bottom panel).

Figure 3

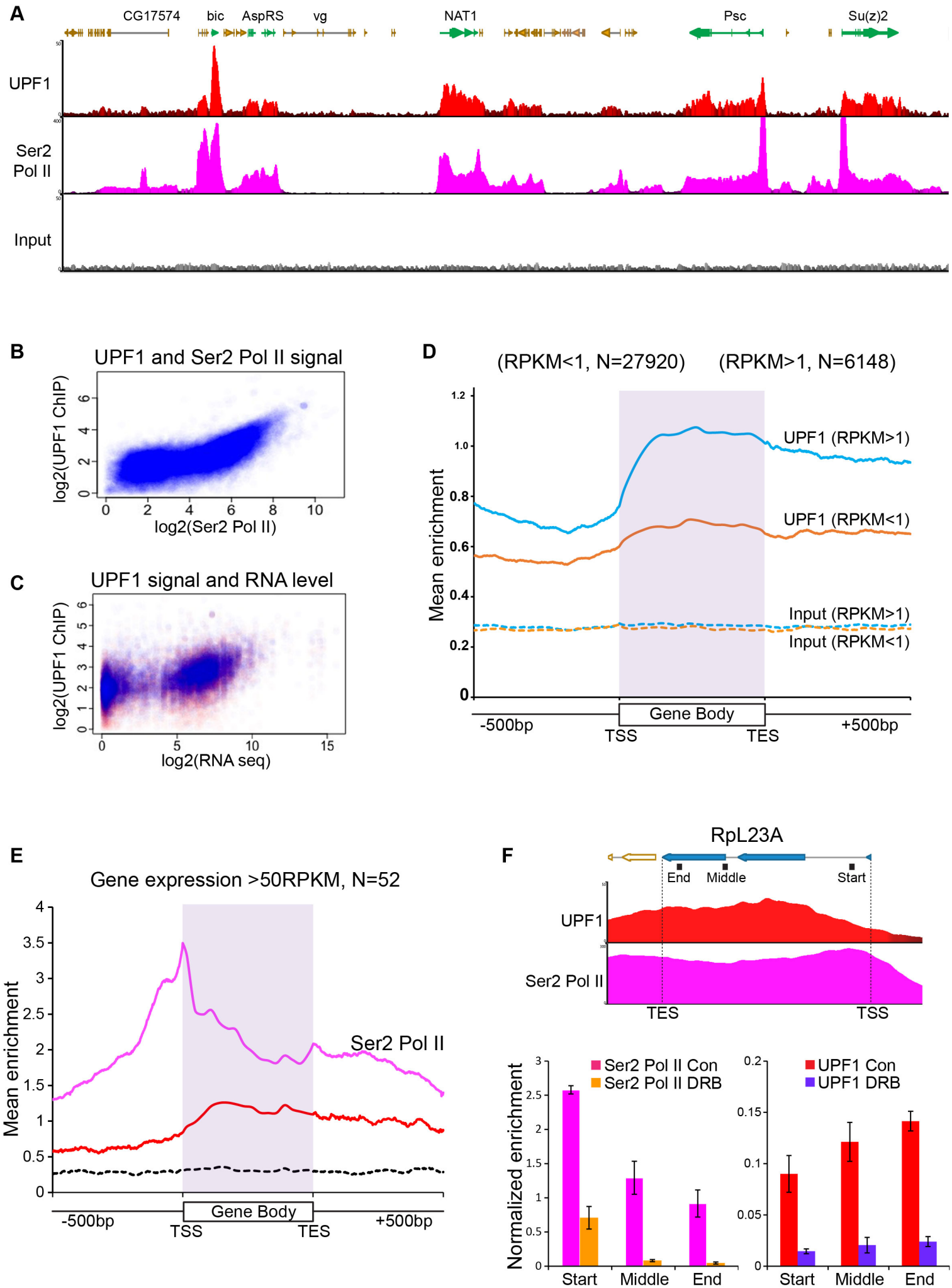
A
CG17574
bic
AspRS
vg
NAT1
Psc
Su(z)2
UPF1
Ser2 Pol II
Input
B
UPF1 and Ser2 Pol II signal
log2(UPF1 ChIP)
log2(Ser2 Pol II)
C
UPF1 signal and RNA level
log2(UPF1 ChIP)
log2(RNA seq)
D
(RPKM<1, N=27920)
(RPKM>1, N=6148)
Mean enrichment
UPF1 (RPKM>1)
UPF1 (RPKM<1)
Input (RPKM>1)
Input (RPKM<1)
-500bp
TSS
Gene Body
TES
+500bp
E
Gene expression >50RPKM, N=52
Mean enrichment
Ser2 Pol II
-500bp
TSS
Gene Body
TES
+500bp
F
RpL23A
End
Middle
Start
UPF1
Ser2 Pol II
TES
TSS
Normalized enrichment
Ser2 Pol II Con
Ser2 Pol II DRB
UPF1 Con
UPF1 DRB
Start
Middle
End

Figure 3. UPF1 associates at Pol II transcription sites. (**A**) Genome browser visualization of UPF1 (red) and Ser2 Pol II (pink) ChIP-seq enrichment profiles at a representative chromosomal region in S2 cells, including highly active genes (green) and low or inactive genes (orange). The input profile (grey) is shown in the bottom panel on the same scale as that of UPF1 (**B**) Scatter plot showing correlation between normalised exon reads in UPF1 and Ser2 Pol II ChIP-seq samples. (**C**) Scatter plot showing relationship between normalised UPF1 ChIP-reads vs. mRNA-seq expression levels; data points corresponding to either exons (blue) or introns (red). (**D**) Metagene profiles showing average UPF1 occupancy at either active (blue, RPKM >1) or inactive/low expressed transcription units (RPKM <1, orange), gene body (scaled to 16 bins of gene full length) plus 500 bp from either end. The number of individual transcription units (N) used for this analysis is given on the top. Corresponding normalised input profiles are shown by dotted lines. (**E**) Superimposed metagene plots of UPF1 (red), Ser2 Pol II (pink) at highly expressed gene loci (RPKM >50). The input enrichment profile for same gene set is shown by the dotted line (black). (**F**) Graph shows ChIP-seq enrichment profiles of UPF1 (red) and Ser2 Pol II (pink) at the RpL23A gene. Bottom, shows real-time PCR quantification of Ser2 Pol II (left) and UPF1 (right) average enrichment at RpL23A gene based on two separate ChIP replicates from either normal or DRB treated S2 cells. The relative position of the three amplicons tested (Start, Middle and End of the gene) are indicated by black boxes underneath the gene schematic on top.

Figure 4

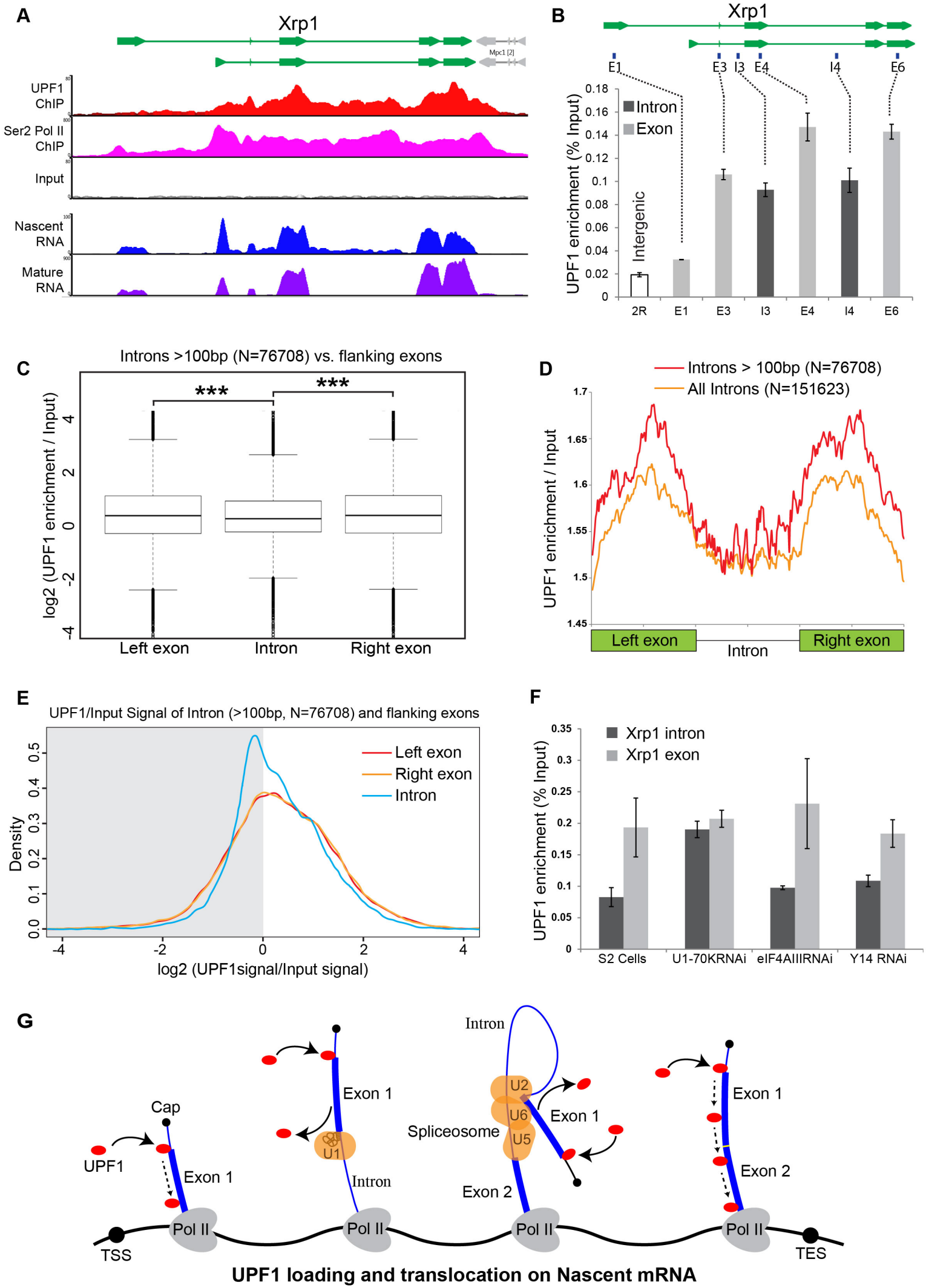
A
Xrp1
Mpc1 [2]
UPF1 ChIP
Ser2 Pol II ChIP
Input
Nascent RNA
Mature RNA
B
Xrp1
E1
E3
I3
E4
I4
E6
Intron
Exon
Intergenic
UPF1 enrichment (% Input)
2R
E1
E3
I3
E4
I4
E6
C
Introns >100bp (N=76708) vs. flanking exons
***
***
log2 (UPF1 enrichment / Input)
Left exon
Intron
Right exon
D
Introns > 100bp (N=76708)
All Introns (N=151623)
UPF1 enrichment / Input
Left exon
Intron
Right exon
E
UPF1/Input Signal of Intron (>100bp, N=76708) and flanking exons
Left exon
Right exon
Intron
Density
log2 (UPF1signal/Input signal)
F
Xrp1 intron
Xrp1 exon
UPF1 enrichment (% Input)
S2 Cells
U1-70KRNAi
eIF4AIIIRNAi
Y14 RNAi
G
Cap
UPF1
Exon 1
Pol II
TSS
Exon 1
U1
Intron
Pol II
Intron
U2
U6
U5
Spliceosome
Exon 1
Exon 2
Pol II
Exon 1
Exon 2
Pol II
TES
UPF1 loading and translocation on Nascent mRNA

Figure 4. Intron recognition interferes with UPF1 association on nascent transcripts. (**A**) Schematic of the Xrp1 locus (top) showing its two main transcription units. Below, UPF1 (red) and Ser2 Pol II (pink) ChIP-seq profiles at this gene; that of the input is shown below (grey). The bottom two panels show nascent RNA-seq (blue) and poly(A) RNA-seq (purple) profiles. (**B**) Real-time PCR quantification of average enrichment in different regions in either exons (E1, E3, E4 and E6) or introns (I3 or I4) in multiple UPF1 ChIP replicates. (**C**) Box plots of normalised UPF1 ChIP-seq reads mapping at either left exon (shown on left), intron (middle) or right exon (on right). Whiskers correspond to +/- 1.5 interquartile range with respect to quartiles. Wilcoxon rank sum test values are: left exon vs. intron, p-value = 6.737e-08; right exon vs intron, p-value = 2.391e-09; and, left exon vs. right exon p-value = 0.606. *** $p < 0.001$ for difference in UPF1 signal between intron and its flanking exon. (**D**) Line profile of average UPF1 ChIP-seq/input enrichment expressed as percentage of full length in either exons or intron. Analysis is based on 151623 introns of any length (orange line) or 76708 introns longer than 100 bp (red line) as annotated in the dm6 genome release (**E**) Density plots of UPF1 enrichment at either the exon before (red line), exon after (orange line) or the intron (blue line). The x-axis shows the log2 of the normalized (by input) UPF1 ChIP signal; the right half of the graph shows the density of the values that are enriched, the left half (shadowed) those that are not. (**F**) Real-time PCR quantification of UPF1 ChIP enrichment (two replicates) at intron (I4) or exon (E6) of the Xrp1 gene, in either normal S2 cells or cells RNAi depleted of the proteins indicated. (**G**) Proposed model of how UPF1 scanning of the nascent transcript is connected to intron recognition during spliceosome assembly; spliceosomal snRNPs (U1, U2/U6 and U5) are represented by orange oval shapes, the squiggle drawing within U1 snRNP signifies the base pairing between U1snRNA and the 5’ ss; TSS indicate the transcription start site; and TES, the transcription end site.

Figure 5

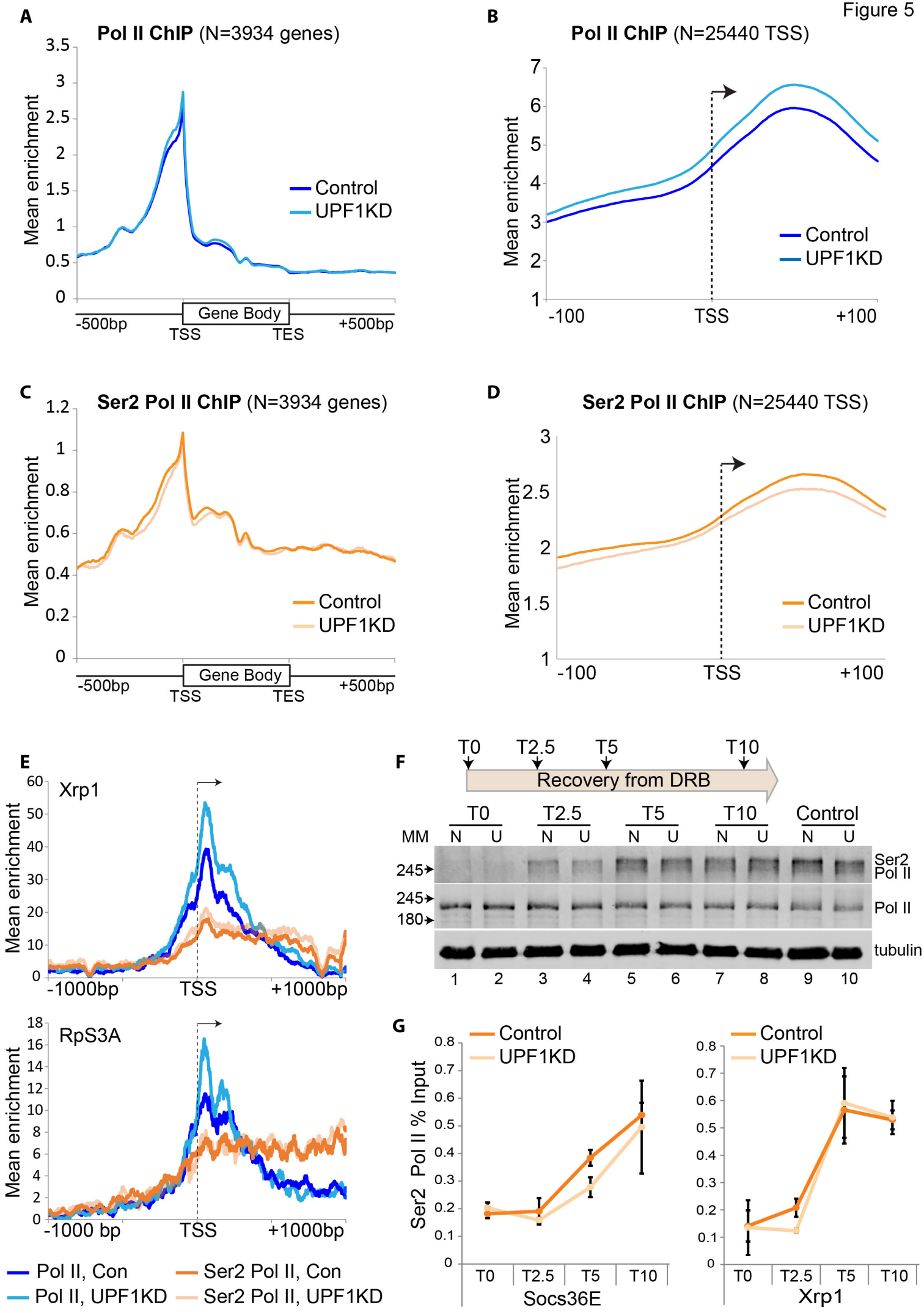
A
Pol II ChIP (N=3934 genes)
Mean enrichment
Control
UPF1KD
Gene Body
-500bp
TSS
TES
+500bp
B
Pol II ChIP (N=25440 TSS)
Mean enrichment
Control
UPF1KD
-100
TSS
+100
C
Ser2 Pol II ChIP (N=3934 genes)
Mean enrichment
Control
UPF1KD
Gene Body
-500bp
TSS
TES
+500bp
D
Ser2 Pol II ChIP (N=25440 TSS)
Mean enrichment
Control
UPF1KD
-100
TSS
+100
E
Xrp1
Mean enrichment
-1000bp
TSS
+1000bp
RpS3A
Mean enrichment
-1000 bp
TSS
+1000bp
Pol II, Con
Pol II, UPF1KD
Ser2 Pol II, Con
Ser2 Pol II, UPF1KD
F
T0
T2.5
T5
T10
Recovery from DRB
T0
T2.5
T5
T10
Control
MM
N
U
245
245
180
Ser2 Pol II
Pol II
tubulin
1
2
3
4
5
6
7
8
9
10
G
Control
UPF1KD
Ser2 Pol II % Input
T0
T2.5
T5
T10
Socs36E
Control
UPF1KD
T0
T2.5
T5
T10
Xrp1

Figure 5. Depletion of UPF1 increases Pol II stalling at TSSs. (**A**) Metagene line plots showing average occupancy of unphosphorylated Pol II at gene bodies (scaled as 16 bins of full length) and ± 500 bp from either end, in normal S2 cells (control, dark blue) or UPF1-RNAi S2 cells (UPF1KD, light blue); analysis based on 3934 (N) transcription units that do not overlap within 500 bp of either ends. (**B**) Metagene plots showing unphosphorylated Pol II at TSS ± 100bp, based on 25440 TSSs that are not closer than 200 bp. (**C**) Metagene plots as in **A** showing Ser2 Pol II occupancy; in normal S2 cells (control, dark orange line) and UPF1-RNAi S2 cells (UPF1KD, light orange line). (**D**) As for B but showing the Ser2 Pol II profiles. (**E**) Normalised ChIP-seq profile of either Pol II (blue lines) or Ser2 Pol II (orange lines) at the Xrp1 gene, ± 1000bp from the TSS (transcript, NM_001275790, the shorter of the two transcripts shown in Figure 3A). The equivalent plots for RpS3A (NM_166714) are shown below. Dark lines refer to normal S2 cells, light lines to UPF1-RNAi, as indicated in the legend below the plots. (**F**) Schematics of the timeframe (top) of the recovery from DRB treatment in S2 cells. Panel below shows Western blot of Ser2 Pol II (top row) and un-phosphorylated Pol II (middle row) at different time points from DRB removal in normal (N) and UPF1-RNAi (U) cells. The α-tubulin was detected as a loading control (bottom row). (**G**) Line graphs show real-time PCR quantifications of average Ser2 Pol II enrichment at either Socs36E gene (on left) or Xrp1 gene (on right) following DRB treatment (T0), at three time points from recovery: 2.5 min (T2.5), 5 minutes (T5) and 10 minutes (T10). Both primer pairs are ~ 4kb downstream of the TSS (see Table S4).

Figure 6

A

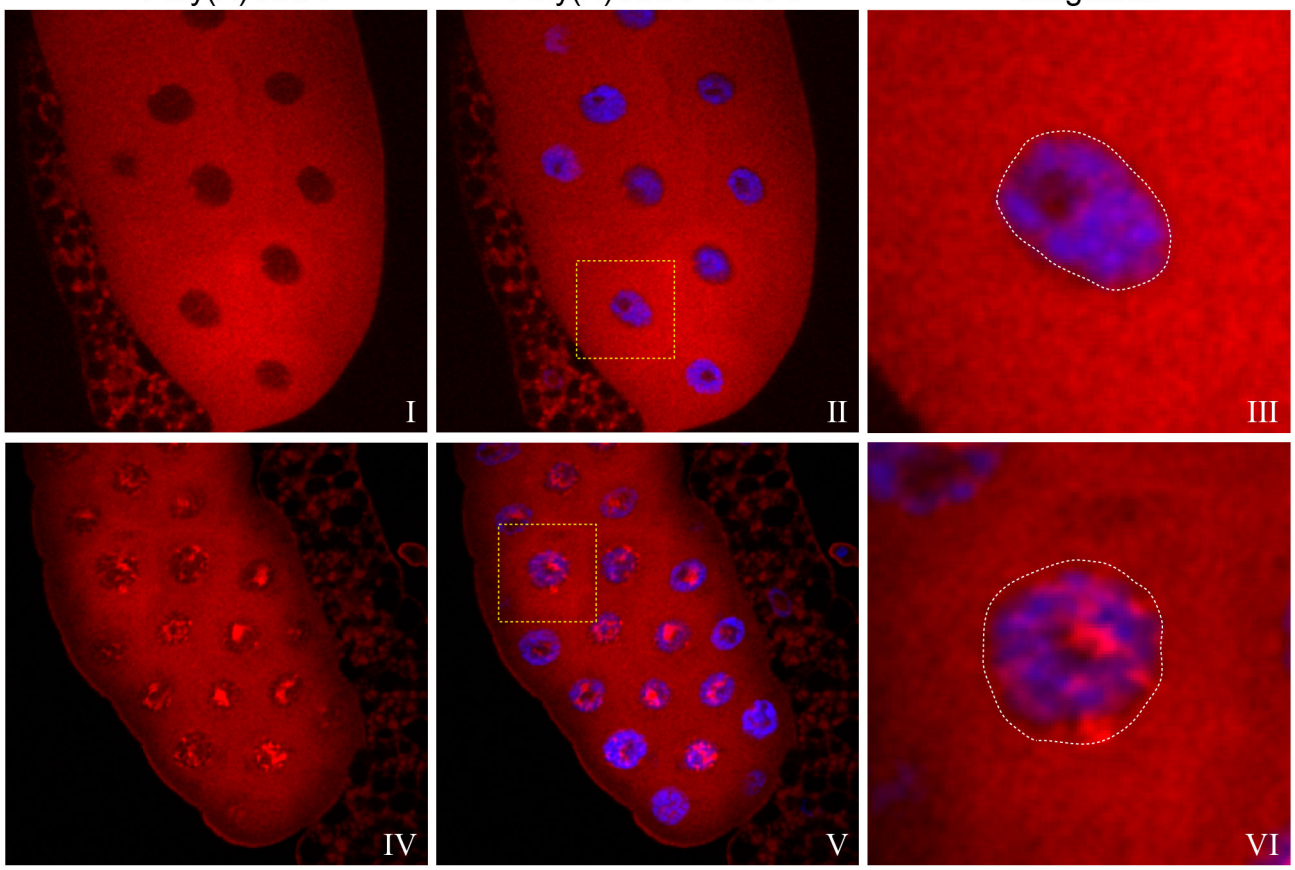
Poly(A) RNA
Poly(A) RNA + DAPI
Magnified
Wild type
FkhGAL4>UPF1RNAi
I
II
III
IV
V
VI

B

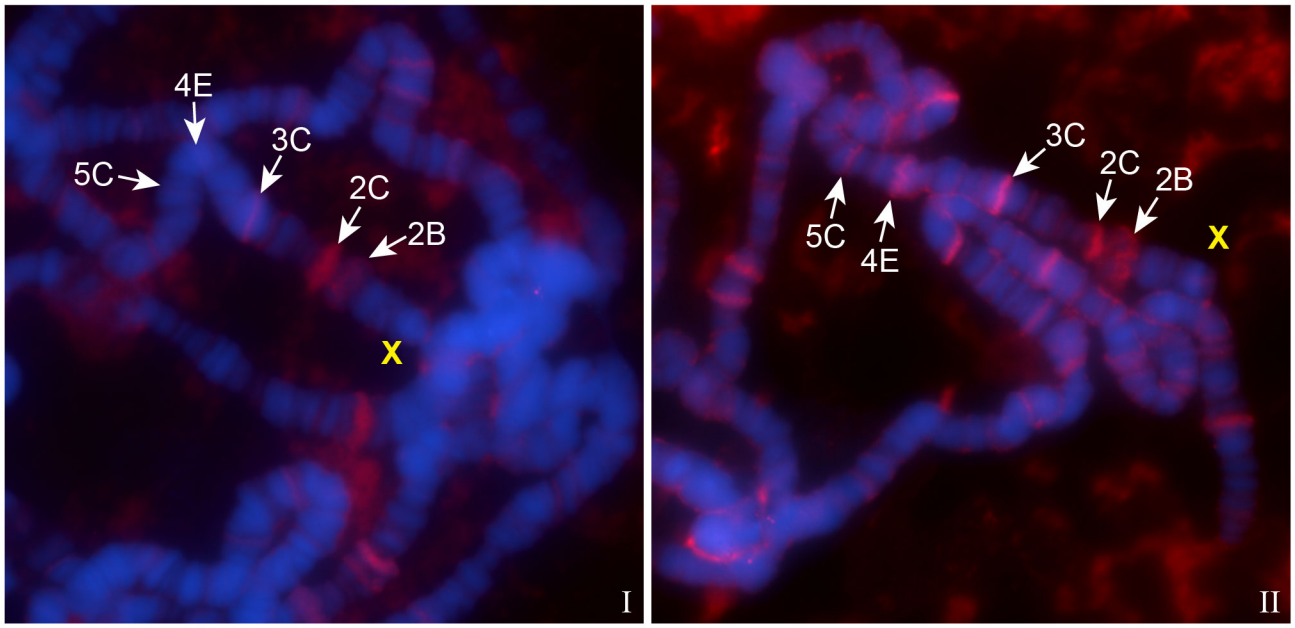
Wild type
FkhGAL4>UPF1RNAi
Poly(A) RNA + DAPI
4E
3C
5C
2C
2B
X
I
II

C

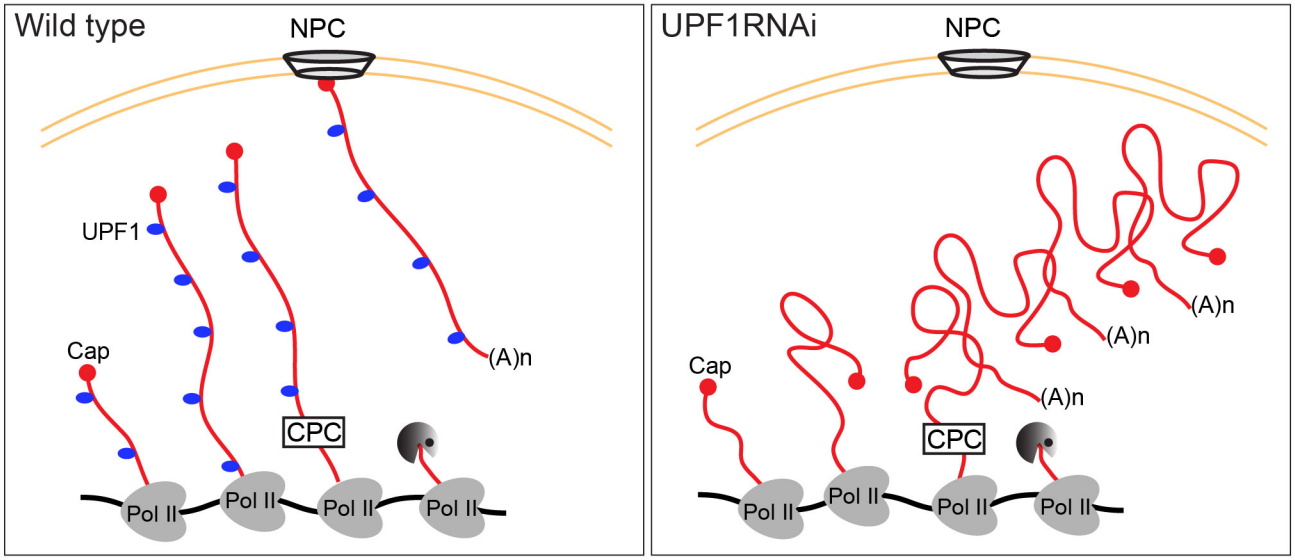
Wild type
NPC
UPF1
Cap
(A)n
CPC
Pol II
UPF1RNAi

Figure 6. UPF1 knockdown results in nuclear accumulation and transcription sites retention of poly(A) mRNA. (**A)** Fluorescence *in situ* hybridization (FISH) of rhodamine-labelled oligo (dT)45 mer in salivary gland cells of either wild type (top panel) or UPF1-RNAi (bottom panel) 3rd instar larva. Chromosomes were counterstained with DAPI (blue). (**B**) Oligo (dT) 45 mer FISH (as above) of 3rd instar larval salivary gland polytene chromosomes from either wild type or UPF1-RNAi. Chromosomes were counterstained with DAPI (blue). (**C**) Proposed model of accumulation of newly transcribed poly(A) mRNA at the site of transcription in UPF1KD (right) compared with wild type (left). Abbreviations: NPC for nuclear pore complex and CPC for cleavage and polyadenylation complex.

Supplementary Figures and legends

Figure S1

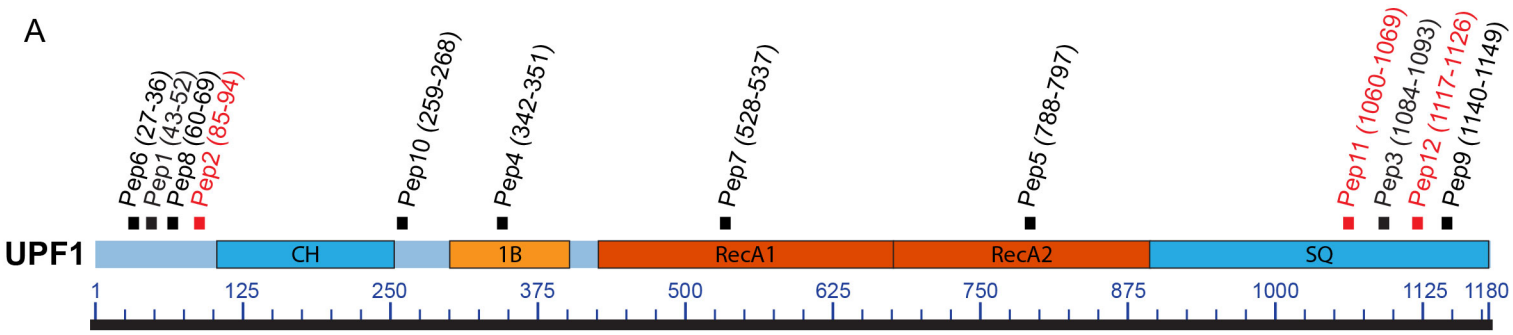
A
Pep6 (27-36)
Pep1 (43-52)
Pep8 (60-69)
Pep2 (85-94)
Pep10 (259-268)
Pep4 (342-351)
Pep7 (528-537)
Pep5 (788-797)
Pep11 (1060-1069)
Pep3 (1084-1093)
Pep12 (1117-1126)
Pep9 (1140-1149)
UPF1
CH
1B
RecA1
RecA2
SQ
1
125
250
375
500
625
750
875
1000
1125
1180

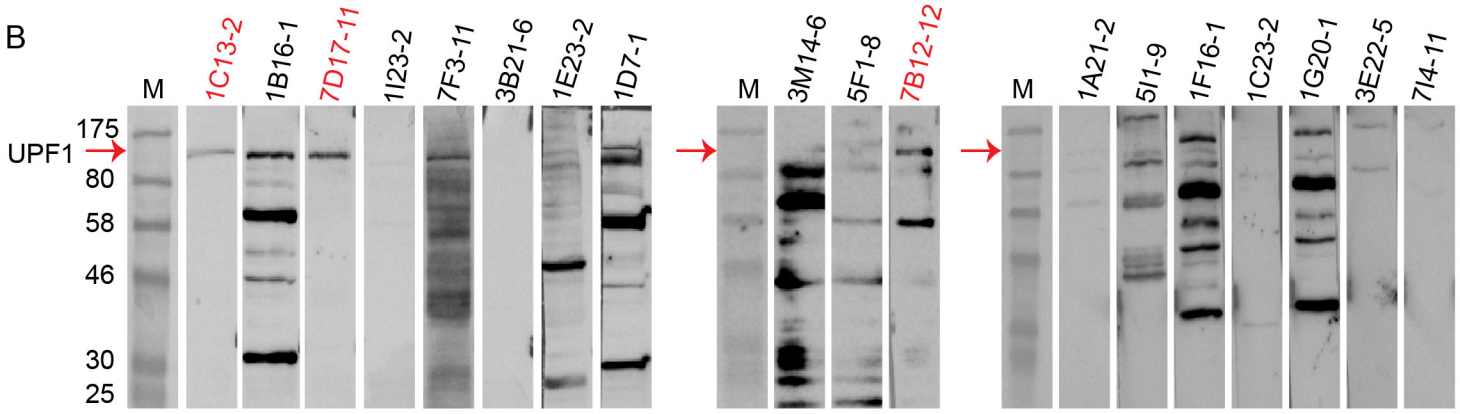
B
M
1C13-2
1B16-1
7D17-11
1I23-2
7F3-11
3B21-6
1E23-2
1D7-1
M
3M14-6
5F1-8
7B12-12
M
1A21-2
5I1-9
1F16-1
1C23-2
1G20-1
3E22-5
7I4-11
UPF1
175
80
58
46
30
25

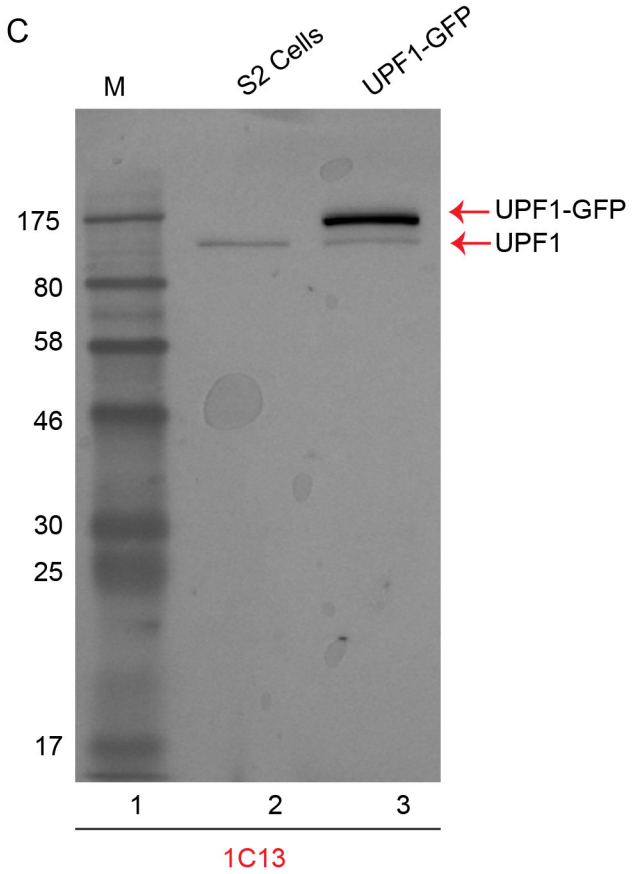
C
M
S2 Cells
UPF1-GFP
175
80
58
46
30
25
17
UPF1-GFP
UPF1
1
2
3
1C13

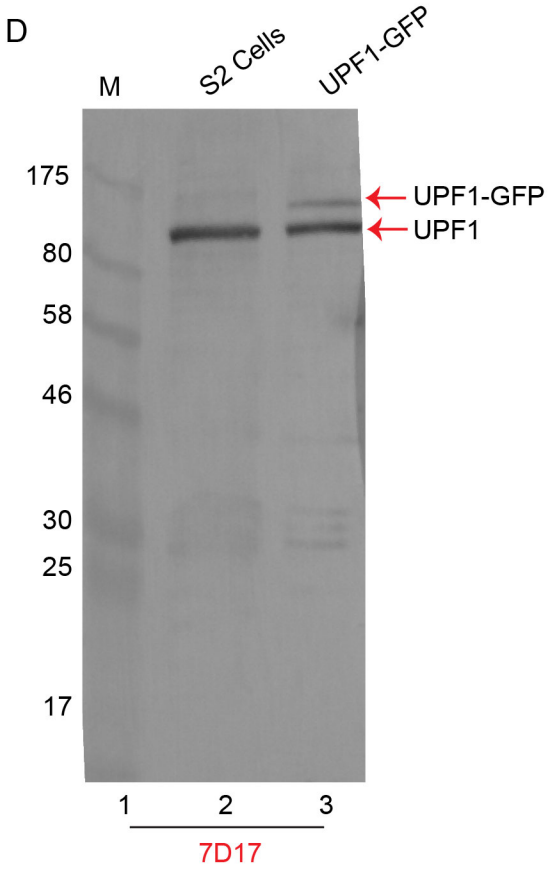
D
M
S2 Cells
UPF1-GFP
175
80
58
46
30
25
17
UPF1-GFP
UPF1
1
2
3
7D17

Figure S1. Generation of monoclonal antibodies against Drosophila UPF1. (**A**) Schematics of UPF1 showing its different structural domains. The peptides used as immunogens and their respective amino acid locations are given in brackets (sequences are in Table S1). The peptides indicated by red color produced the monoclonal antibodies with highest specificity, as shown below (**B**) Western blotting of S2 cell protein extracts, probed with 18 ascites induced with hybridomas previously screened for their reactivity to the corresponding peptides (terminal numbers correspond to different peptides indicated in A). Lanes labelled M show a molecular weight marker. (**C**) Western blotting of whole-cell S2 lysate with the UPF1 monoclonal antibody (mab) 1C13. From either normal (lane 2) or transfected S2 cells expressing UPF1-GFP (lane 3) in which the two bands correspond to either endogenous UPF1 or UPF1-GFP. (**D**) As in C, using mab 7D17. Western blotting with 7B12 is shown in Figure 1A.

Figure S2

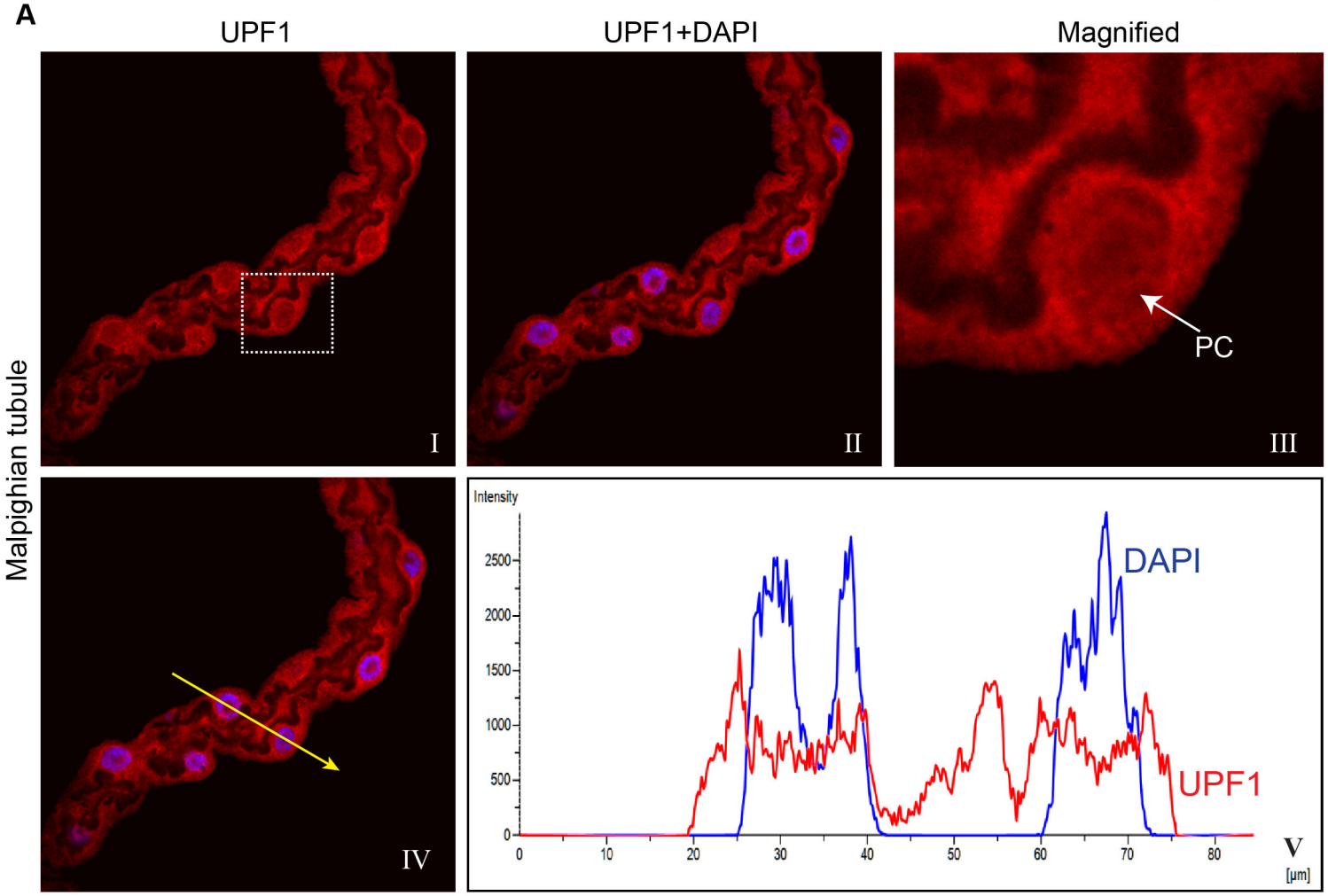
A
UPF1
UPF1+DAPI
Magnified
Malpighian tubule
I
II
III
PC
IV
Intensity
DAPI
UPF1
V
[µm]

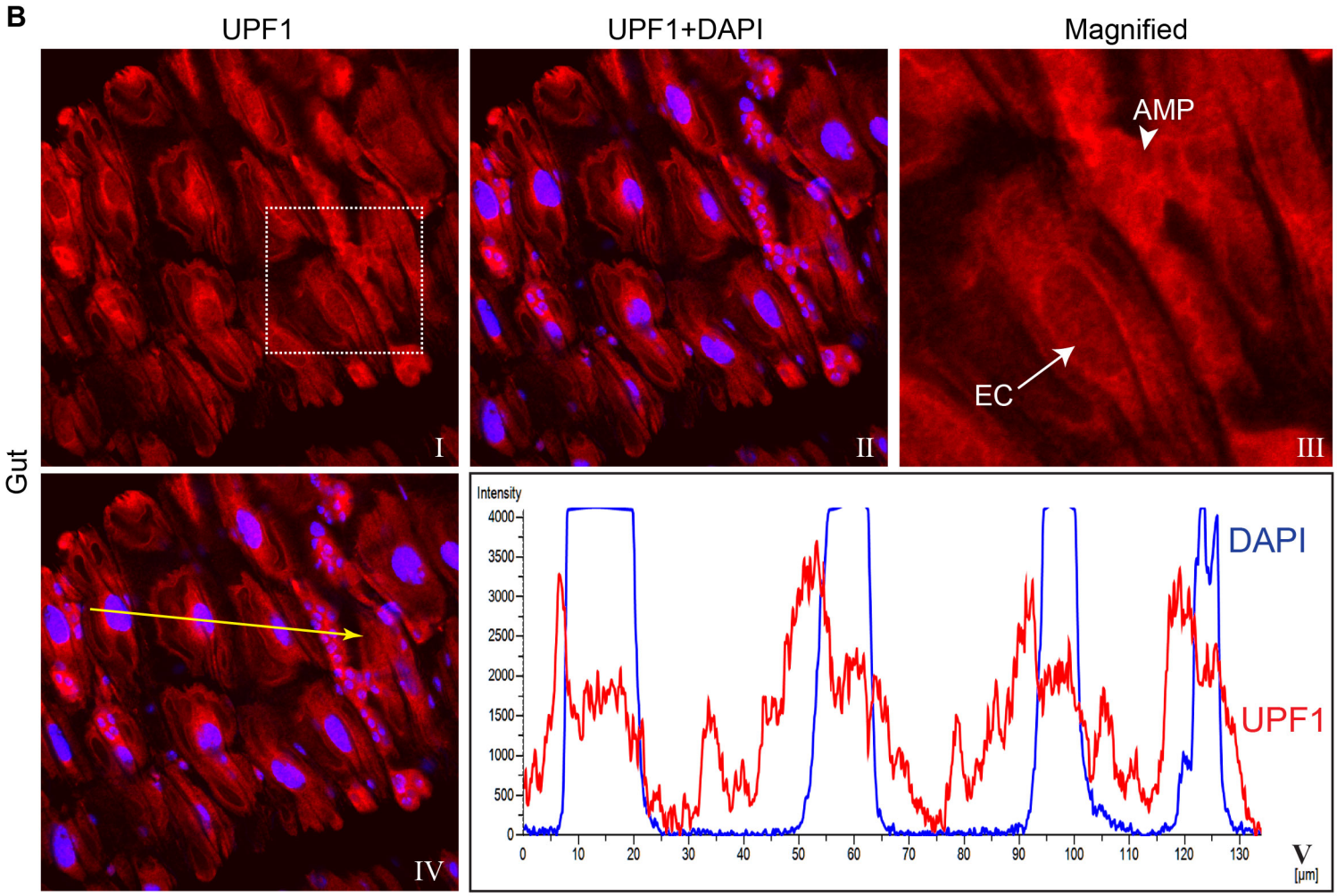
B
UPF1
UPF1+DAPI
Magnified
Gut
I
II
III
AMP
EC
IV
Intensity
DAPI
UPF1
V
[µm]

Figure S2. UPF1 subcellular localization in different larval tissues. (**A**) Fluorescence immunolocalization of UPF1 (Cy3, red) in 3rd instar larval Malpighian tubule (I to IV). Panel III shows magnified view of boxed area in panel I, white arrow indicates UPF1 signal within nucleus of a Principal Cell (PC). Tissues were counter-stained with DAPI (blue). Line profiles (V) show both Cy3 and DAPI fluorescence intensities along the yellow line drawn (IV). (**B**) Immunolocalization of UPF1 (Cy3, red) in gut cells (I to IV). Panel III shows magnified view of boxed area panel I. Arrow and arrowhead in (III) indicate presence of UPF1 within nuclei of Enterocytes Cell (EC) and Adult Midgut Progenitor Cells (AMPs), respectively. The line profiles show both Cy3 and DAPI fluorescence intensities along the yellow line (IV) across both EC and AMPs cells (V).

Figure S3

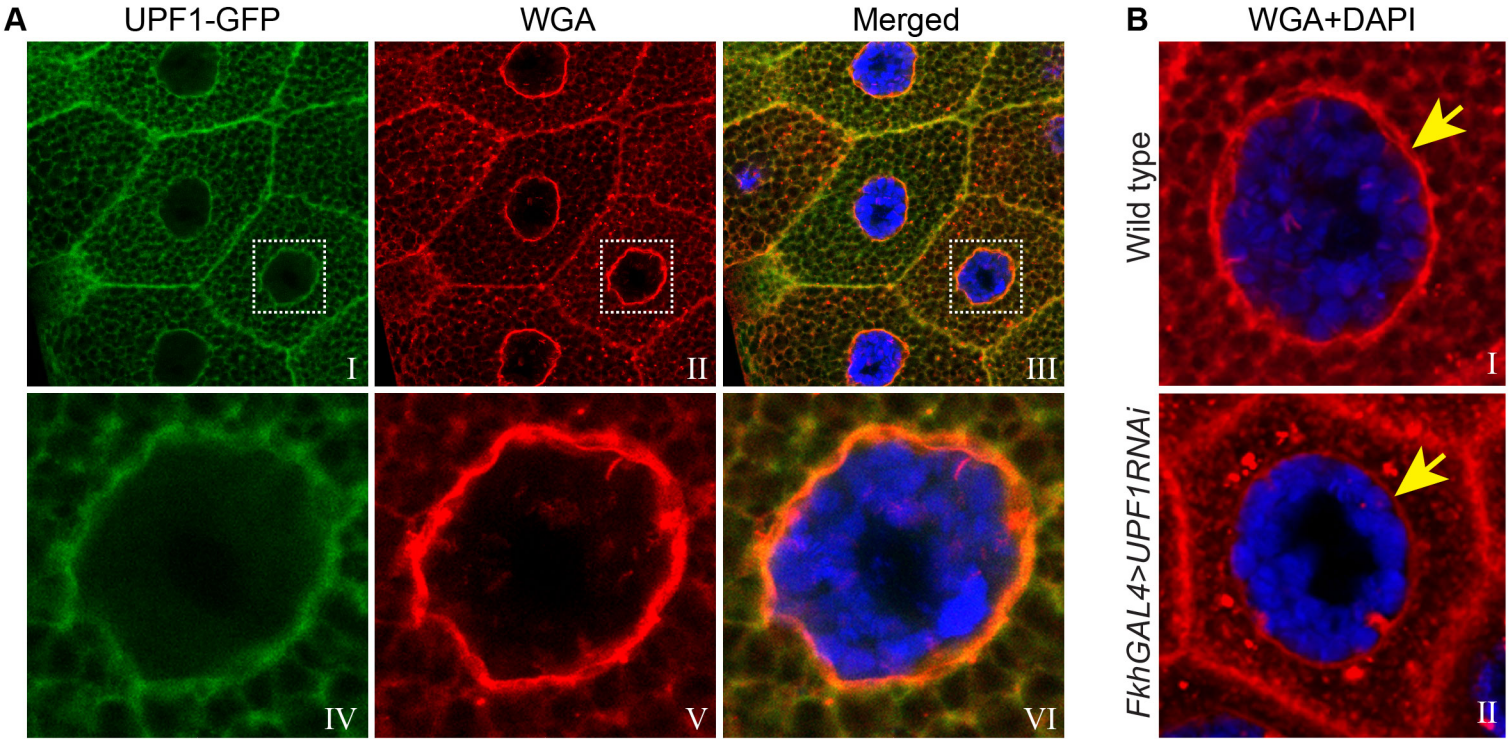
A
UPF1-GFP
WGA
Merged
I
II
III
IV
V
VI
B
WGA+DAPI
Wild type
FkhGAL4>UPF1RNAi
I
II

Figure S3. UPF1 may associate with nuclear membrane. (**A**) Fluorescence imaging of tetramethylrhodamine conjugated Wheat Germ Agglutinin (WGA, red) and UPF1-GFP (green) in salivary gland cells. Lower panels are magnified view of boxed area in upper panels. (**B**) Imaging of WGA (red) in wild type (upper panel) and FkhGAL4>UPF1-RNAi (lower panel) salivary gland cells. Yellow arrow indicates nuclear envelope. Cells were counter-stained with DAPI (blue).

Figure S4

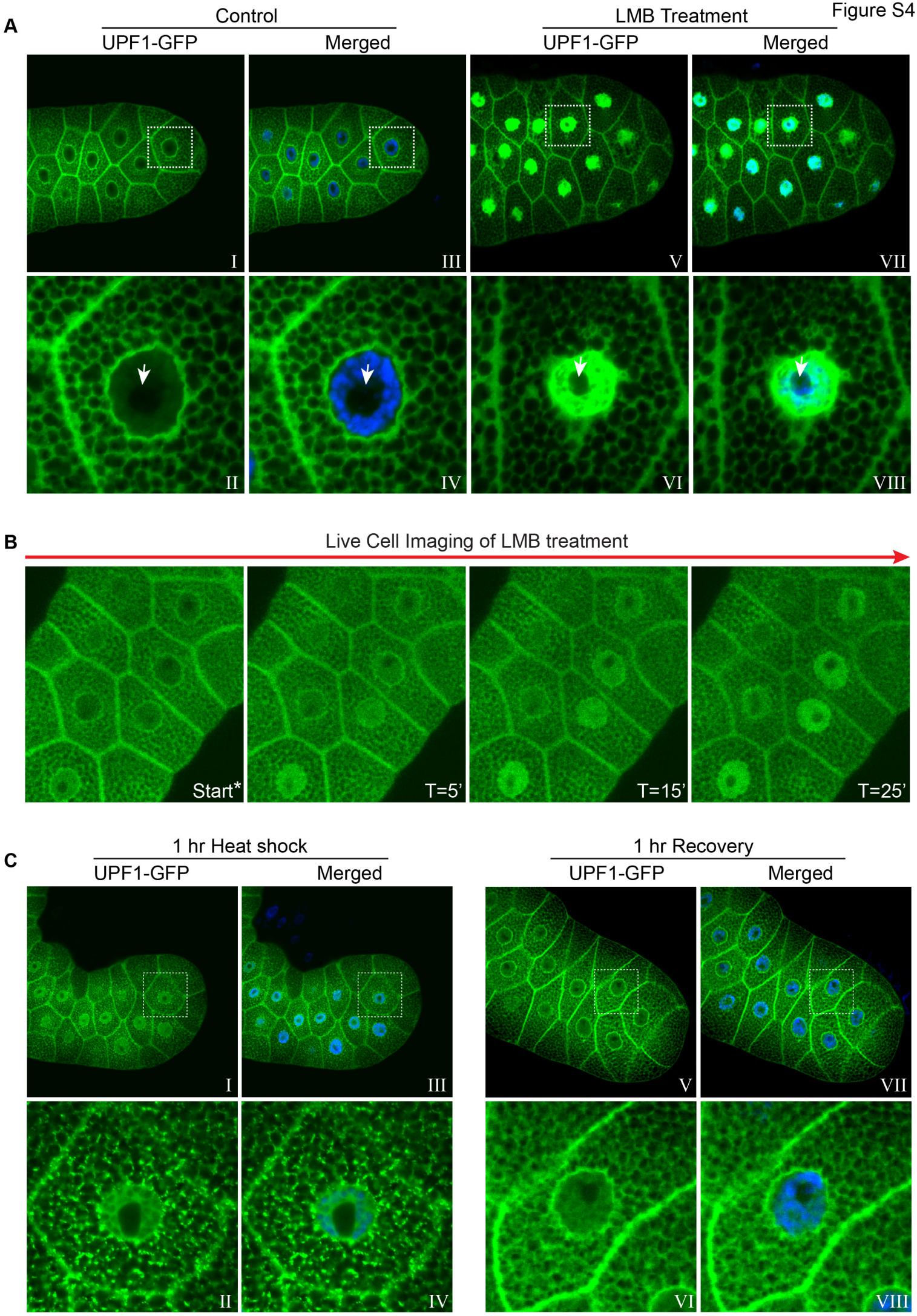
A
Control
LMB Treatment
UPF1-GFP
Merged
UPF1-GFP
Merged
I
III
V
VII
II
IV
VI
VIII
B
Live Cell Imaging of LMB treatment
Start*
T=5'
T=15'
T=25'
C
1 hr Heat shock
1 hr Recovery
UPF1-GFP
Merged
UPF1-GFP
Merged
I
III
V
VII
II
IV
VI
VIII

Figure S4. UPF1 is highly dynamic within both nucleus and cytoplasm. (**A**) Imaging of 3rd instar larval salivary glands transgenically expressing UPF1-GFP (green), incubated for 1 hr in either normal M3 media (Control, I to IV) or supplemented with 100µM LMB (LMB, V to VIII). Panels II, IV, VI and VIII are magnified views of the boxed areas in panel I, III, V and VII, respectively. The arrows in II, IV, VI and VIII indicate the nucleoli. Nuclei were counter-stained with DAPI (blue). (**B**) Time-lapse live cell imaging showing changes in the cellular distribution of UPF1-GFP in 3rd instar larval salivary gland at different time intervals of LMB treatment. Start* refers to the first image acquired straight after dissection and mounting of the tissues in a cavity slide, the procedure takes ~5-6 minutes in which cells have been exposed to LMB. (**C**) Localization of UPF1-GFP (green) in salivary glands after 1 hr heat shock (I to IV) or after 1 hr recovery following heat shock (V to VIII). Lower panels are magnified views of boxed area in upper panel, with or without DAPI counter-staining (blue).

Figure S5

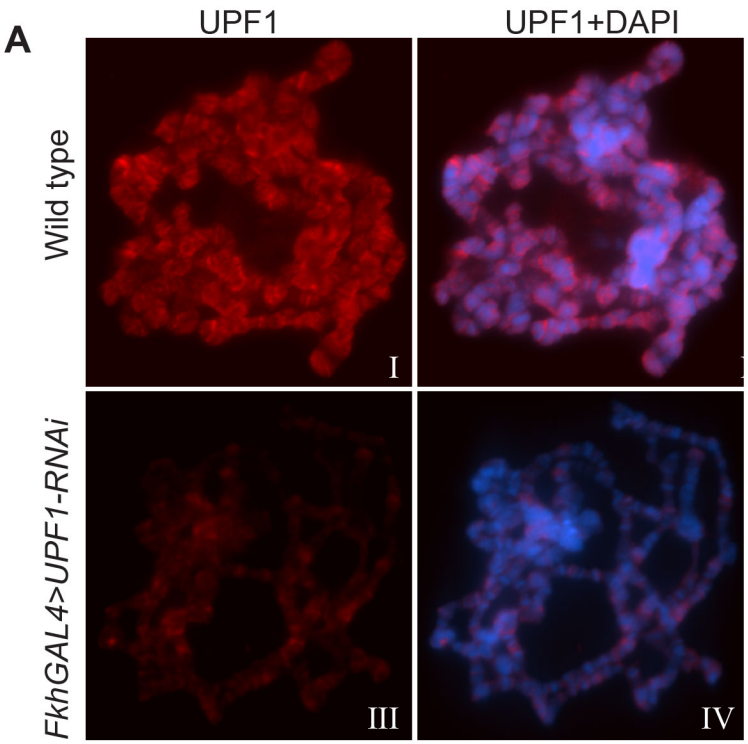
A
UPF1
UPF1+DAPI
Wild type
FkhGAL4>UPF1-RNAi
I
III
IV

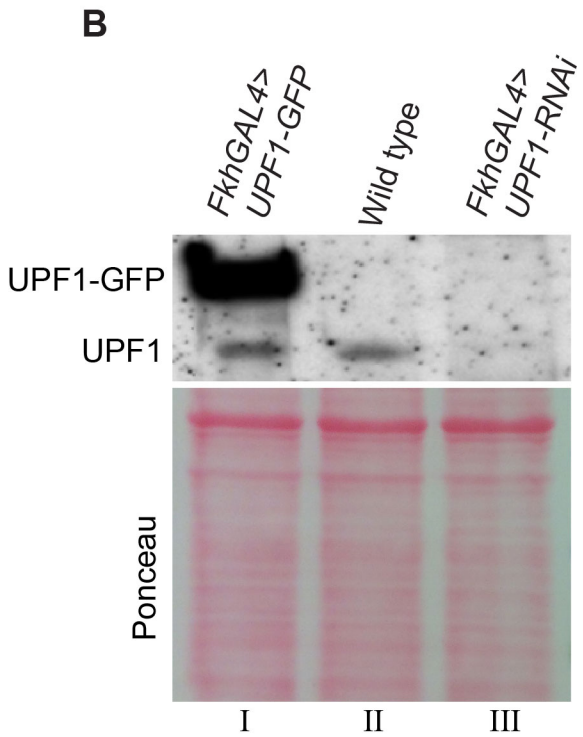
B
FkhGAL4> UPF1-GFP
Wild type
FkhGAL4> UPF1-RNAi
UPF1-GFP
UPF1
Ponceau
I
II
III

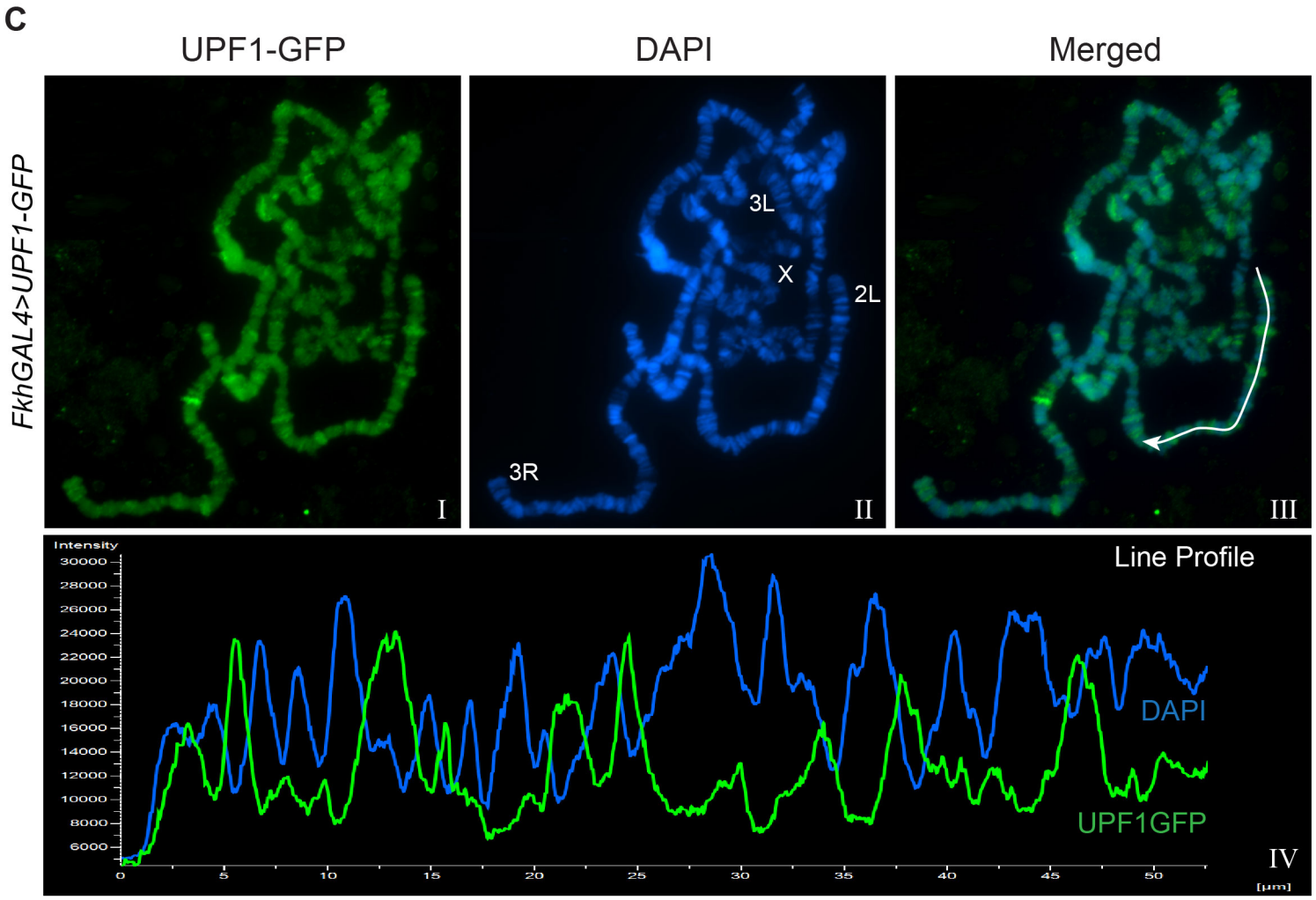
C
UPF1-GFP
DAPI
Merged
FkhGAL4>UPF1-GFP
3L
X
2L
3R
I
II
III
Intensity
Line Profile
DAPI
UPF1GFP
IV
[µm]

Figure S5. UPF1 RNAi depletes 7B12 mab signal. (**A**) Fluorescence immunolocalization of UPF1 using the 7B12 monoclonal antibody (Cy3, red) on polytene chromosomes (blue) of wild type (I, II) and UPF1-RNAi (III, IV) salivary glands. (**B**) Western blotting probed with 7B12 mab for protein extracts of 3rd instar larval salivary gland from *FkhGAL4>UPF1-GFP* (lane I), wild type (lane II) and *FkhGAL4>UPF1-RNAi* (lane III). Ponceau staining of the same blot showing equal protein loading. (**C**) Immunolocalization of UPF1-GFP (FITC, green, I, III) on polytene chromosomes of *FkhGAL4>UPF1-GFP* salivary glands, detected using anti-GFP antibody. Chromosomes were counter stained with DAPI (blue, II, III). Line profiles in IV show both signal intensities along the white line traced on the chromosome arm in III. Note that UPF1 signal peaks at chromatin-decondensed regions characterised by low DAPI signal.

Figure S6

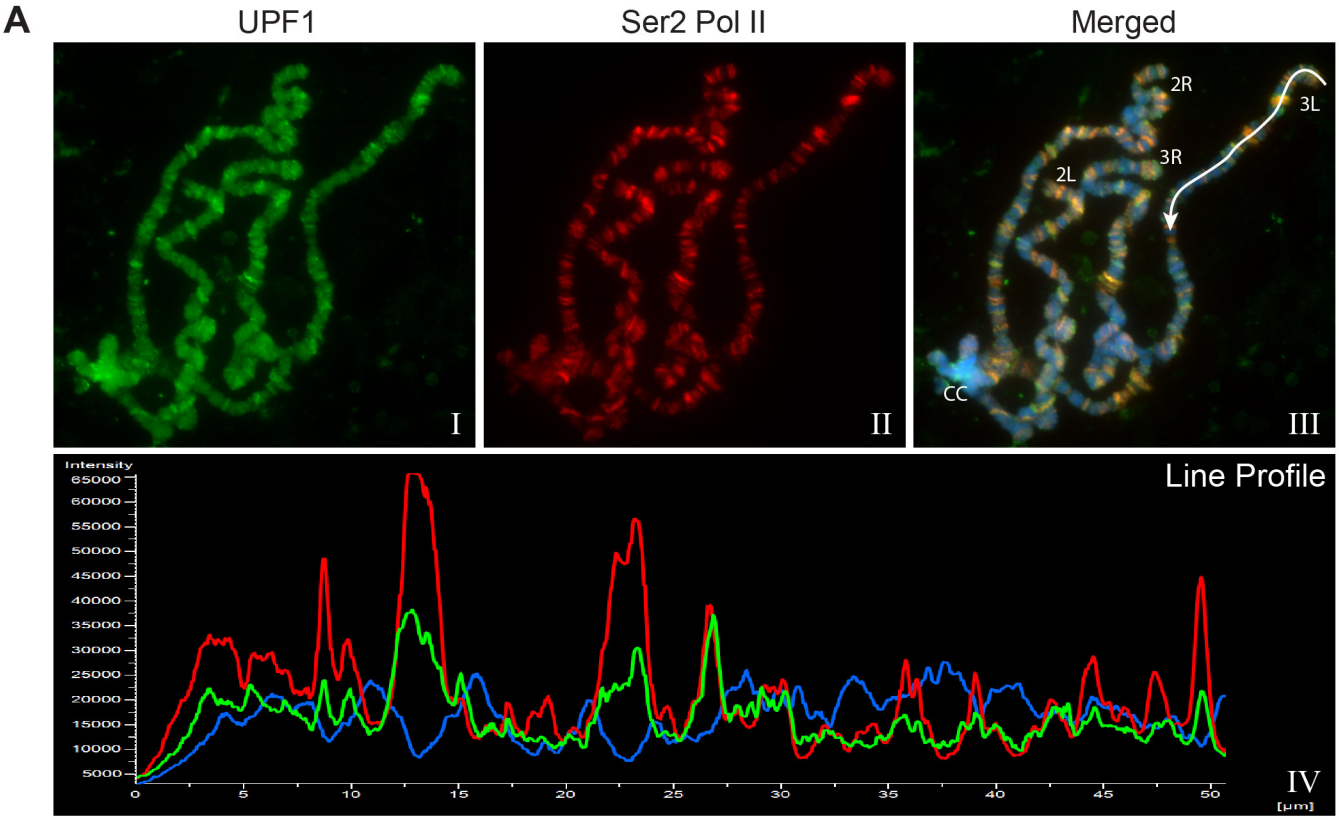
A
UPF1
Ser2 Pol II
Merged
2R
3L
3R
2L
CC
I
II
III
Line Profile
Intensity
65000
60000
55000
50000
45000
40000
35000
30000
25000
20000
15000
10000
5000
0
5
10
15
20
25
30
35
40
45
50
[µm]
IV

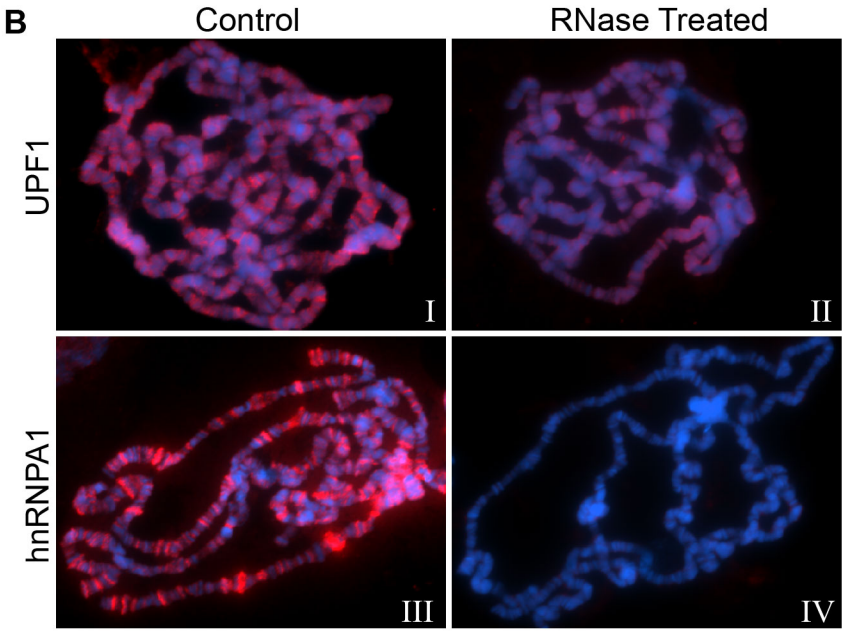
B
Control
RNase Treated
UPF1
hnRNPA1
I
II
III
IV

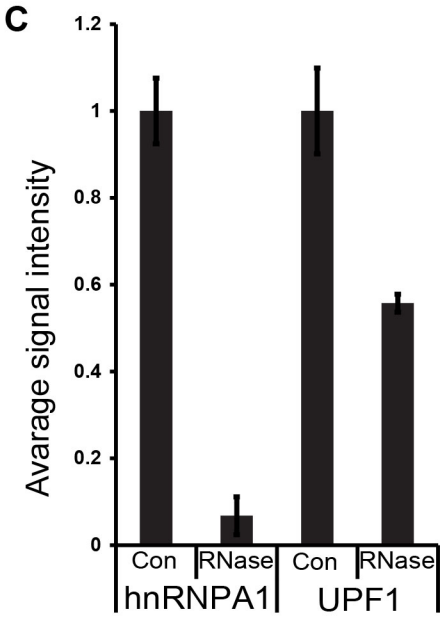
C
Avarage signal intensity
1.2
1
0.8
0.6
0.4
0.2
0
Con
RNase
Con
RNase
hnRNPA1
UPF1

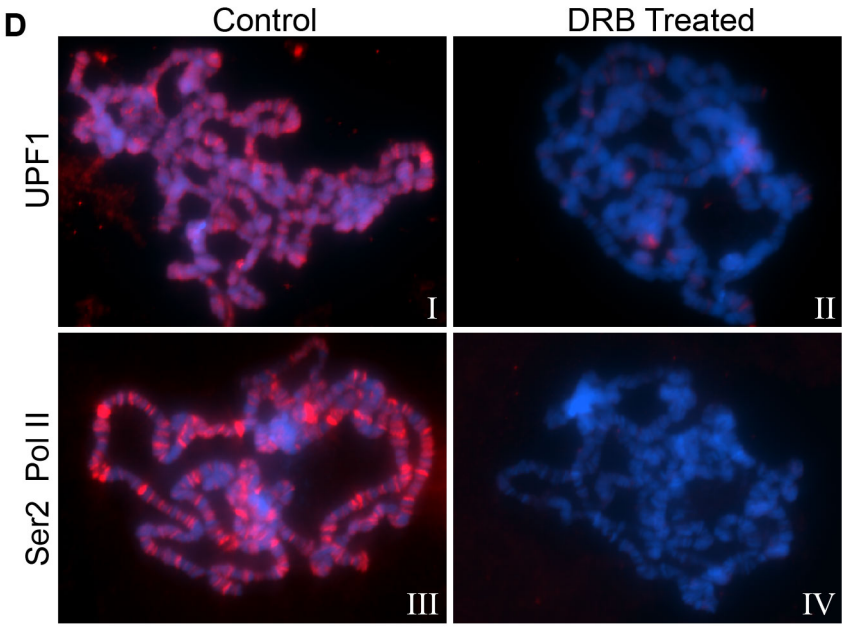
D
Control
DRB Treated
UPF1
Ser2 Pol II
I
II
III
IV

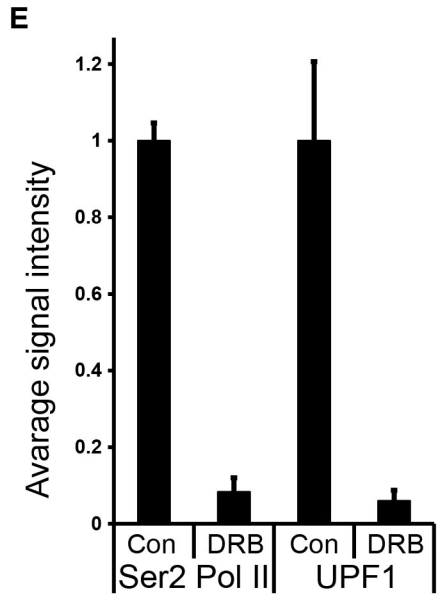
E
Avarage signal intensity
1.2
1
0.8
0.6
0.4
0.2
0
Con
DRB
Con
DRB
Ser2 Pol II
UPF1

Figure S6. UPF1 chromosomal association is transcription and nascent RNA dependent. (**A**) Co-immunolocalization of UPF1 (FITC, green, I, III) and Ser2 Pol II (Cy3, red, II, III) at polytene chromosomes, counterstained with DAPI (blue). Line profiles in IV show all signal intensities along the white line drawn in III. (**B**) Immunolocalization of UPF1 (red, I and II) and hnRNPA1 (red, III and IV) at polytene chromosomes of either untreated (I and III) or RNase treated salivary glands (II and IV). (**C**) Graph shows normalized fluorescence intensity of the hnRNPA1 and UPF1 signals in control and after RNase treatment, based on mean intensities of 8-10 different nuclear spreads. (**D**) Immunolocalization of UPF1 (red, I and II) and Ser2 Pol II (red, III and IV) at polytene chromosomes from untreated (I and III) or DRB treated glands (II and IV). (**E**) Graph shows normalized fluorescence intensity of Ser2 Pol II and UPF1 in control and after DRB treatment, based on mean intensities of 8 different nuclear spreads.

Figure S7

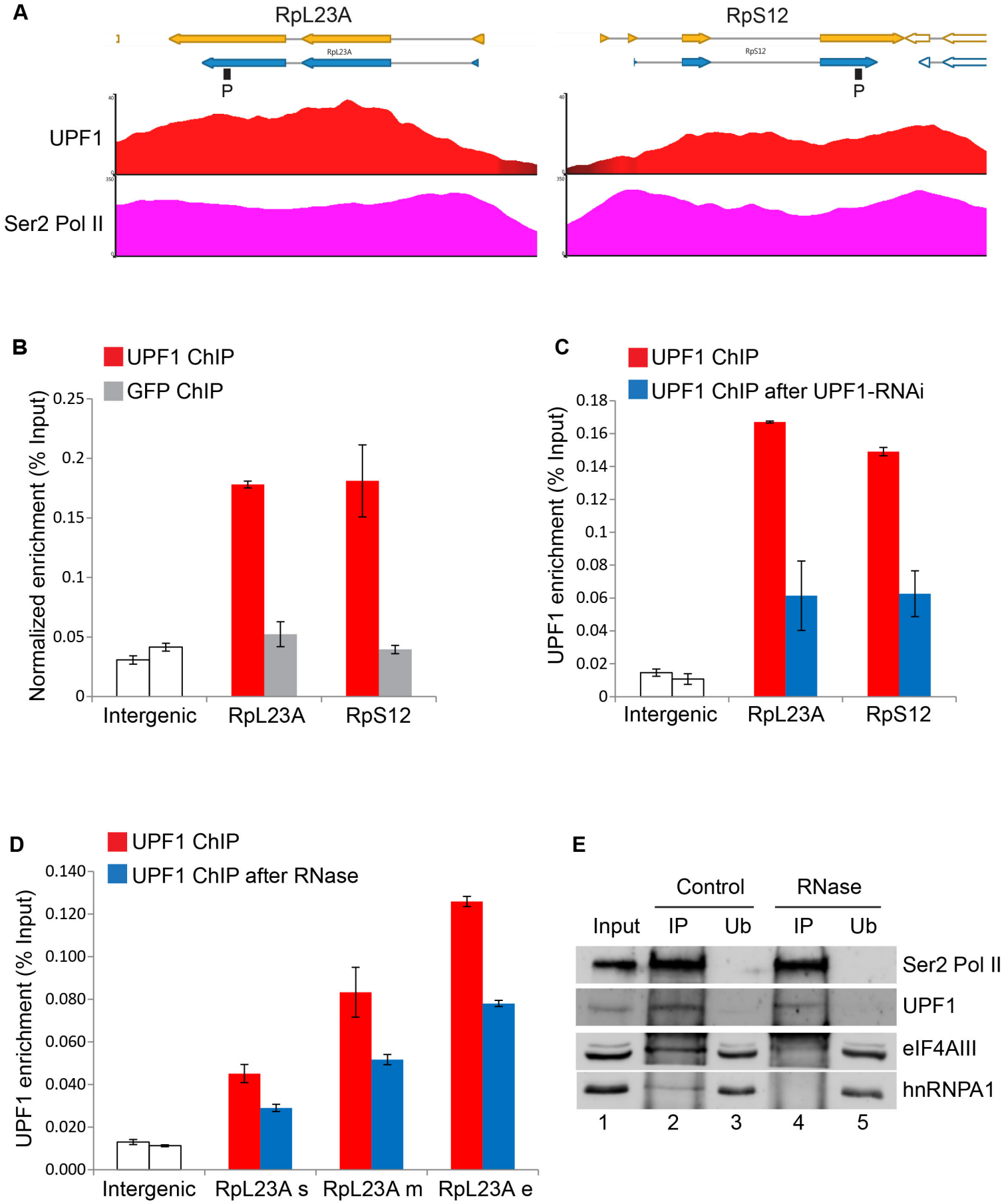
A
RpL23A
RpS12
P
P
UPF1
Ser2 Pol II
B
UPF1 ChIP
GFP ChIP
Normalized enrichment (% Input)
0.25
0.2
0.15
0.1
0.05
0
Intergenic
RpL23A
RpS12
C
UPF1 ChIP
UPF1 ChIP after UPF1-RNAi
UPF1 enrichment (% Input)
0.18
0.16
0.14
0.12
0.1
0.08
0.06
0.04
0.02
0
Intergenic
RpL23A
RpS12
D
UPF1 ChIP
UPF1 ChIP after RNase
UPF1 enrichment (% Input)
0.140
0.120
0.100
0.080
0.060
0.040
0.020
0.000
Intergenic
RpL23A s
RpL23A m
RpL23A e
E
Control
RNase
Input
IP
Ub
IP
Ub
Ser2 Pol II
UPF1
eIF4AIII
hnRNPA1
1
2
3
4
5

Figure S7. Real-time PCR validation of UPF1 ChIP association at selected genes. (**A**) UPF1 (red) and Ser2 Pol II (pink) ChIP-seq enrichment profiles at RpL23A (on left) and RpS12 (on right) gene loci. (**B**) Real-time PCR quantification of average ChIP signal of either endogenous UPF1 (red) or GFP (as negative control, grey) at the RpL23 and RpS12 genes in salivary glands expressing GFP. The locations of the primer pairs used are indicated by the black boxes (P) shown below the genes schematics in A. (**C**) Real-time PCR quantification of average UPF1 association in control (red) or UPF1-RNAi (blue) S2 cells. (**D**) Real-time PCR quantification of average UPF1 association at three distinct regions of RpL23 in S2 cells (same primers pairs as in Figure 3F) with (blue) or without (red) RNase A treatment. (**E**) Ser2 Pol II immunoprecipitation of S2 cell nuclear extracts using anti-Ser2 Pol II antibody (ab5095) and detection (same blot) of Ser2 Pol II, UPF1, eIF4AIII and hnRNPA1, in control (lanes 2-3) or RNase treated samples (lanes 4-5). IP refers to immunoprecipitated fractions, Ub to unbound fractions.

Figure S8

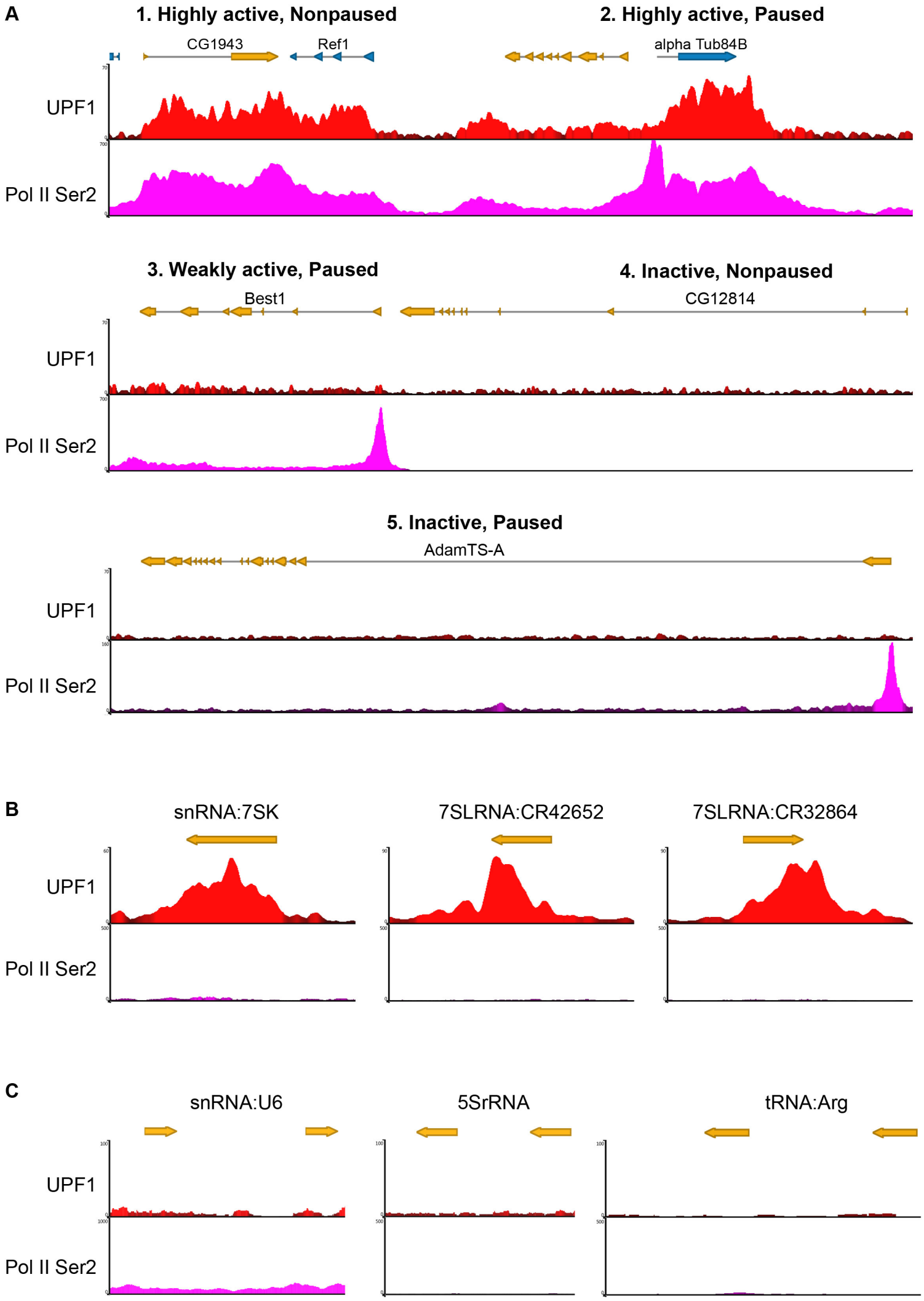
A
1. Highly active, Nonpaused
2. Highly active, Paused
CG1943
Ref1
alpha Tub84B
UPF1
Pol II Ser2
3. Weakly active, Paused
4. Inactive, Nonpaused
Best1
CG12814
UPF1
Pol II Ser2
5. Inactive, Paused
AdamTS-A
UPF1
Pol II Ser2
B
snRNA:7SK
7SLRNA:CR42652
7SLRNA:CR32864
UPF1
Pol II Ser2
C
snRNA:U6
5SrRNA
tRNA:Arg
UPF1
Pol II Ser2

Figure S8. ChIP-seq profiles of UPF1 at representative Pol II genes and some Pol III loci. (**A**) ChIP-seq profiles of UPF1 (red) and Ser2 Pol II (pink) at different active genes characterised by either paused or not paused Pol II at the TSS (panels 1-3). Panels 4 and 5 show absence of Upf1 at two inactive genes, with or without paused Pol II. (**B**) ChIP-seq profile of UPF1 (red) and Ser2 Pol II (pink) at the three Pol III transcribing gene loci indicated. (**C**) ChIP-seq profiles showing no UPF1 signal at three highly transcribing Pol III genes (snRNPU6, 5SrRNA and tRNA:Arg).

Figure S9

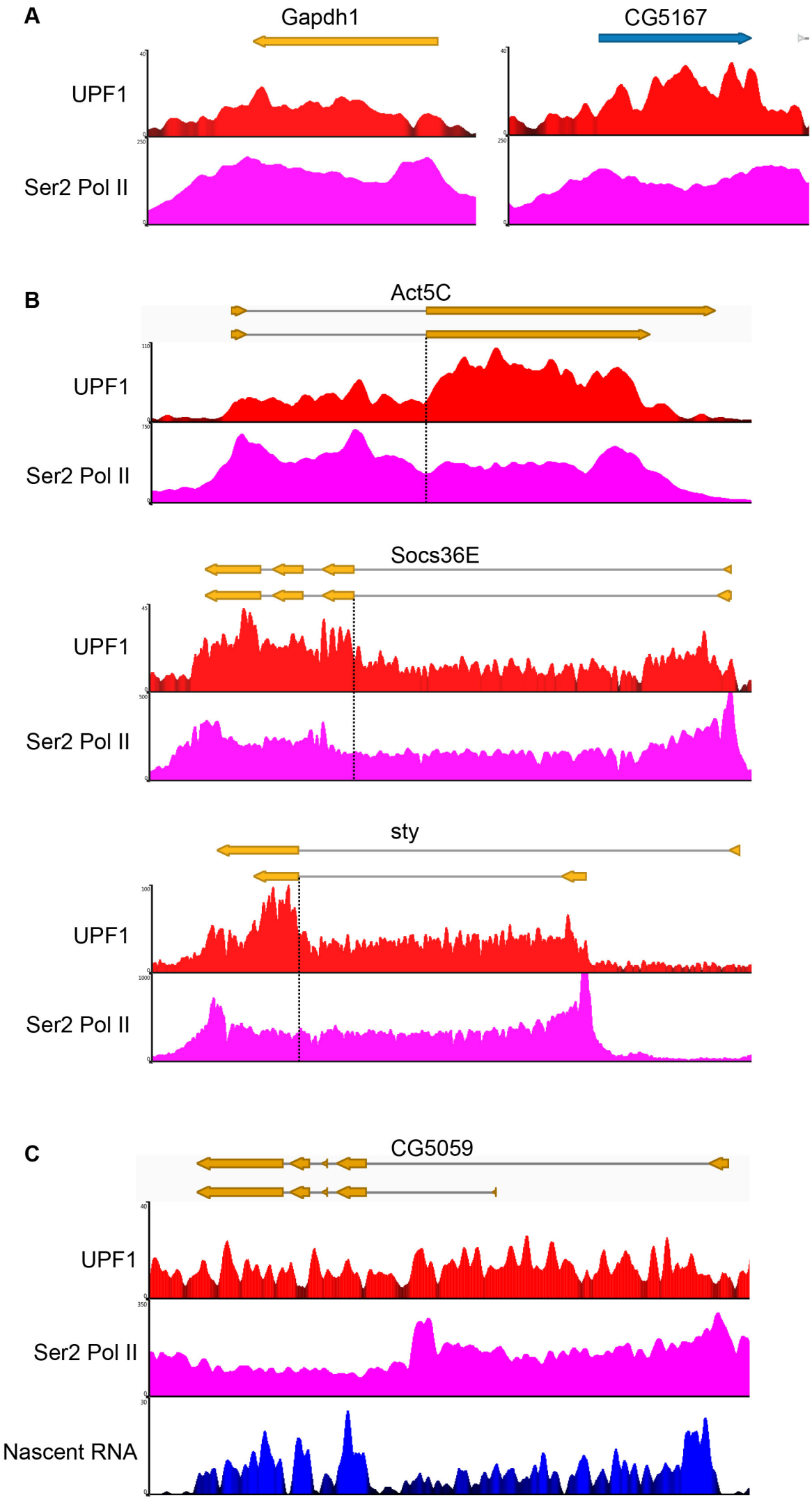
A
Gapdh1
CG5167
UPF1
Ser2 Pol II
B
Act5C
UPF1
Ser2 Pol II
Socs36E
UPF1
Ser2 Pol II
sty
UPF1
Ser2 Pol II
C
CG5059
UPF1
Ser2 Pol II
Nascent RNA

Figure S9. Additional examples of UPF1 ChIP-seq profiles at genes with or without introns. (**A**) ChIP-seq profiles showing enrichment of UPF1 (red) and Ser2 Pol II (pink) at genes without intron. (**B**) ChIP-seq profile showing enrichment of UPF1 (red) and Ser2 Pol II (pink) at other highly expressing intron-containing genes. Dotted lines demarcate regions around intron/exon borders at which UPF1 shows higher association with exons despite uniform Ser2 distribution. (**C**) UPF1 ChIP-seq profile (red) and Ser2 Pol II (pink) at CG5059 gene, which as indicated by the nascent RNA-seq profile underneath (blue) show high intronic sequencing reads, indicative of inefficient co-transcriptional splicing.

Figure S10

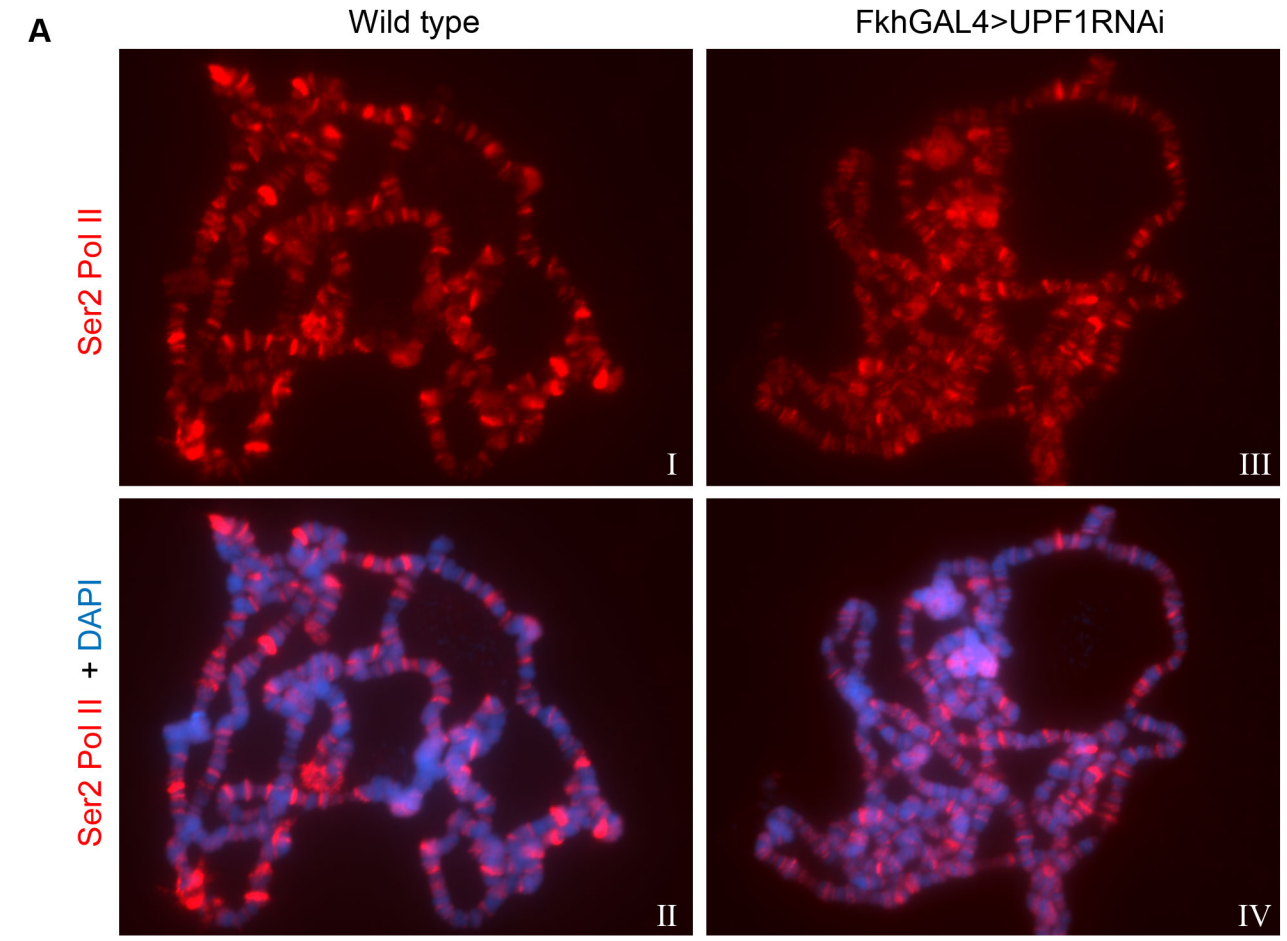
A
Wild type
FkhGAL4>UPF1RNAi
Ser2 Pol II
Ser2 Pol II + DAPI
I
II
III
IV

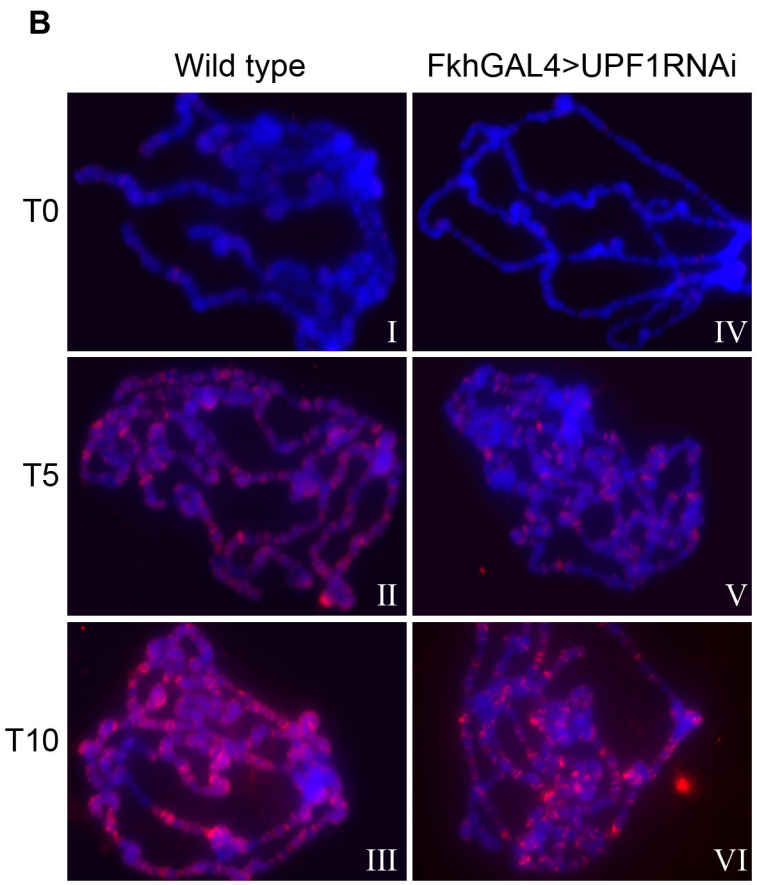
B
Wild type
FkhGAL4>UPF1RNAi
T0
T5
T10
I
II
III
IV
V
VI

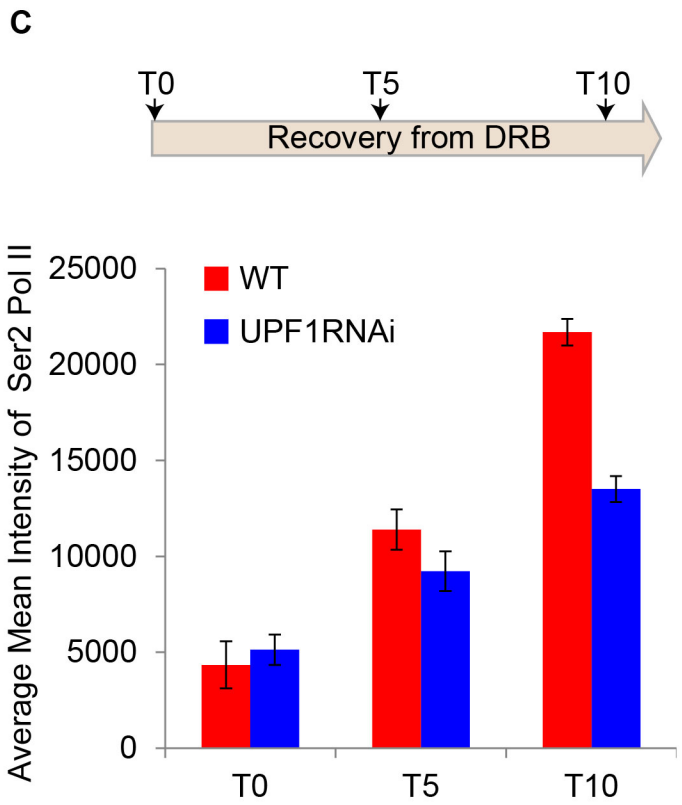
C
T0
T5
T10
Recovery from DRB
Average Mean Intensity of Ser2 Pol II
25000
20000
15000
10000
5000
0
WT
UPF1RNAi
T0
T5
T10

Figure S10. Depletion of UPF1 slows Pol II transcription recovery from DRB treatment. (**A**) Immunolocalization of Ser2 Pol II (Cy3, red) on polytene chromosomes (DAPI, blue) of wild type (I, II) or *FkhGAL4>UPF1-RNAi* (III, IV) 3rd instar larval salivary glands. (**B**) Immunolocalization of Ser2 Pol II (Cy3, red) on polytene chromosomes (DAPI, blue) of wild type (I-III) or *FkhGAL4>UPF1-RNAi* (IV-VI) salivary glands, at different time points after recovery from DRB treatment for 0 min (T0), 5 min (T5) and 10 min (T10). (**C**) Top, schematics of the timeframe of the recovery from DRB treatment in S2 cells. Panel below shows average mean intensity of Ser2 Pol II signal on polytene chromosomes of wild type (red) or UPF1-RNAi (blue) salivary glands treated with DRB and at two time points after its removal. The mean of intensity was calculated by measuring signals in 10 different chromosome spreads.

Table S1. Peptides used for UPF1 antibody generation (positions refer to full length sequence FBpp0073433)			
No.	Start	End	Peptide
1	43	52	TSQSQTQNDQ
2	85	94	DEPGSSYVKE
3	1084	1093	PGGNKKTNKL
4	342	351	HYVGELYNPW
5	788	797	QYQGSLHSRL
6	27	36	DTQPTQYDYR
7	528	537	KSREAIDSPV
8	60	69	SAGDSHPRLA
9	1140	1149	SQQPELSQDF
10	259	268	KPGIDSEPAH
11	1060	1069	QTGNFSPGNS
12	1117	1126	AAPYSQHPMP

Table S2. Most enriched transcription units by UPF1 ChIP-seq (black=Protein coding genes, red=Noncoding RNAs).						
No.	**Transcript**	**Chromosome**	**Cytological Location**	**Strand**	**Gene**	**UPF1 Enrichment**
1	NR_002554	chr2R	60A3	-	snoRNA:Psi18S-176	20.92784248
2	NR_073860	chr2R	45F1	+	CR43651	19.84962099
3	NR_073861	chr2R	45F1	+	CR43651	19.58870612
4	NM_078901	chr2R	42A7	-	Act42A	16.53573972
5	NM_166890	chrX	2B1	-	sta	15.7976555
6	NM_001297856	chrX	2B1	-	sta	14.65188523
7	NM_057402	chrX	2B1	-	sta	14.65188523
8	NM_001316458	chr3L	70A6	+	Nplp2	14.2141182
9	NM_144173	chr3L	70A6	+	Nplp2	14.2141182
10	NM_166889	chrX	2B1	-	sta	14.0181416
11	NM_206272	chr3L	63F5	-	Ubi-p63E	13.10522634
12	NR_001992	chr3R	84A5	-	7SLRNA:CR32864	13.04190544
13	NR_037753	chr3R	84A5	-	7SLRNA:CR42652	13.04190544
14	NM_001274454	chr3L	63F5	-	Ubi-p63E	12.94301365
15	NM_168043	chr3L	63F5	-	Ubi-p63E	12.86980148
16	NM_079185	chr3L	63F5	-	Ubi-p63E	12.8624403
17	NM_001299392	chr2R	48C5	+	Ef1alpha48D	12.7336405
18	NR_002067	chr3R	93D	+	Hsromega	12.6383098
19	NR_002069	chr3R	93D	+	Hsromega	12.6383098
20	NM_001300130	chr3L	70A6	+	Nplp2	12.582198
21	NM_001316502	chr3R	86D8	+	Tctp	11.88147055
22	NM_058027	chr2R	48C5	+	Ef1alpha48D	11.51812571
23	NM_001014455	chr2L	21 E2	+	PNUTS	11.50911291
24	NR_048444	chr3R	93D	+	Hsromega	11.47018513
25	NM_001297855	chrX	2B1	+	rush	11.45428524
26	NM_130567	chrX	2B1	+	rush	11.36293998
27	NM_170070	chr3R	94 E10-94 13	-	pnt	11.36070171
28	NM_141791	chr3R	86D8	+	Tctp	11.3160895
29	NM_001298659	chr2L	23F3-23F6	+	Thor	11.29086613
30	NM_057284	chr3R	93 E13	+	RpS3	10.9579823
31	NM_001014454	chr2L	21 E2	+	PNUTS	10.86549487
32	NM_001298210	chrX	10-E3 to 10 E4	-	Hsc70-3	10.85467784
33	NR_133429	chr3R	93D	+	Hsromega	10.74841913
34	NM_167307	chrX	10-E3 to 10 E4	-	Hsc70-3	10.70276539
35	NM_165850	chr2R	48C5	+	Ef1alpha48D	10.69805745
36	NM_001202085	chr3L	61B2	-	CG42846	10.5511492
37	NM_001275943	chr3R	94 E10-94 13	-	pnt	10.42349043
38	NM_079983	chr2R	57C3	+	Xbp1	10.40232605
39	NM_166427	chr2R	57C3	+	Xbp1	10.39685831
40	NM_001202063	chr2R	59B6	-	CG3800	10.39235699
41	NM_079175	chr3L	63B11	+	Hsp83	10.35797394
42	NM_001299393	chr2R	48C5	+	Ef1alpha48D	10.3424767

43	NM_143714	chrX	5D2	-	mab-21	10.22106132
44	NM_167180	chrX	8C14	-	His3.3B	10.19996373
45	NM_057947	chr2L	23F3-23F6	+	Thor	10.10779488
46	NM_001103474	chrX	9D2	-	spri	10.09939045
47	NM_001272490	chrX	9D2	-	spri	10.0968423
48	NM_001272491	chrX	9D2	-	spri	10.0968423
49	NM_001298516	chrX	18D3	+	RpS10b	10.05584386
50	NM_001274433	chr3L	63B11	+	Hsp83	9.962334214
51	NM_167065	chrX	5 E4	-	Ubi-p5E	9.845904641
52	NM_167306	chrX	10 E3-10 E4	-	Hsc70-3	9.739493741
53	NM_167308	chrX	10 E3-10 E4	-	Hsc70-3	9.739493741
54	NM_206223	chr3L	61B2	+	CG33229	9.726778964
55	NM_169625	chr3R	88 E4	+	Hsc70-4	9.714744345
56	NM_001300552	chr3R	94 E13	+	RpS3	9.705903021
57	NM_176503	chr3R	88 E4	+	Hsc70-4	9.687864086
58	NM_001347750	chrX	2B1	+	mei-38	9.661728876
59	NM_078497	chrX	5C7	+	Act5C	9.593373151
60	NM_168070	chr3L	64A10	-	ImpL2	9.571757664
61	NM_134543	chrX	19C5	+	l(1)G0004	9.506154816
62	NM_169841	chr3R	91D3	+	Xrp1	9.489137734
63	NM_079879	chr4	101 F1	-	RpS3A	9.472988193
64	NM_166714	chr4	101 F1	-	RpS3A	9.472988193
65	NM_001275657	chr3R	88 E4	+	Hsc70-4	9.464906214
66	NM_001298008	chrX	5 E4	-	Ubi-p5E	9.44989544
67	NM_169626	chr3R	88 E4	+	Hsc70-4	9.391845758
68	NM_176502	chr3R	88 E4	+	Hsc70-4	9.391845758
69	NM_176719	chrX	8C14	-	His3.3B	9.373510295
70	NM_169627	chr3R	88 E4	+	Hsc70-4	9.333994534
71	NM_137895	chr2R	59B6	-	CG3800	9.317056284
72	NM_001272174	chrX	1C5	+	Sec22	9.263596844
73	NM_130507	chrX	1C5	+	Sec22	9.263596844
74	NM_164617	chr2L	25C1	+	Col4a1	9.208538686
75	NM_057786	chrX	1C4	-	RpL22	9.203239849
76	NM_164615	chr2L	25C1	+	Col4a1	9.190852727
77	NM_165869	chr2R	48 E8-48 E9	-	RpS11	9.137225506
78	NM_001014453	chr2L	21 E2	+	PNUTS	9.022927536
79	NM_001272921	chr2L	21 E2	+	PNUTS	9.022927536
80	NM_164616	chr2L	25C1	+	Col4a1	9.013677552
81	NM_001275501	chr3R	85 E1	-	Calr	9.013384298
82	NM_001014725	chrX	5C7	+	Act5C	8.989781735
83	NM_132656	chrX	11F1	+	CG1673	8.981761268
84	NM_079569	chr3R	85 E1	-	Calr	8.981419499
85	NM_079632	chr3R	88 E4	+	Hsc70-4	8.957987156
86	NM_001273288	chr2L	85 E1	-	Rack1	8.945814985
87	NM_057921	chr2L	85 E1	-	Rack1	8.945814985

88	NM_132800	chrX	13C4	-	CG15642	8.919897052
89	NM_001014726	chrX	5C7	+	Act5C	8.909849299
90	NM_001299958	chr3L	61B2	+	CG33229	8.850750946
91	NM_079355	chr3L	71B5	-	Pdi	8.830574597
92	NM_080366	chr2L	39 E7	-	EF2	8.804229445
93	NM_001298794	chr2L	85 E1	-	Rack1	8.793822499
94	NM_165395	chr2L	39 E7	-	EF2	8.793744101
95	NM_165394	chr2L	39 E7	-	EF2	8.732148442
96	NR_123764	chrX	1C4	+	CR44965	8.355359116
97	NR_002545	chr2R	54A2	+	snoRNA:U3:54Ab	8.034844038
98	NR_002544	chr2R	54A2	+	snoRNA:U3:54Aa	7.685229313
99	NR_002493	chr3R	84D4	-	snRNA:7SK	7.602249655
100	NR_073616	chr4	102B7	+	CR44027	7.389972024
101	NR_133116	chr2R	50A1-A3	-	CR44206	7.36480527
102	NR_047918	chr2L	27F4	+	mir-305	7.207345421

Table S3. Transcription units with increased unphosphorylated Pol II at TSS in UPF1 depleted S2 cells							
No.	**Transcript**	**Chromosomes**	**Strand**	**Genes**	**Control**	**UPF1KD**	**Ratio**
8	NM_001201633	chrX	-	CG15347	1.029076	3.690992	3.586707
19	NM_078758	chr2L	+	TotM	1.150733	3.240686	2.816192
28	NM_001259329	chr2R	+	stan	1.123977	2.963514	2.636632
30	NM_080176	chr3R	+	GstD6	1.134011	2.97221	2.620972
47	NM_078909	chr2R	+	Tsp42Eg	1.69464	4.053704	2.392073
52	NM_001273063	chr2L	-	Mad	1.257132	2.864851	2.278879
65	NM_079000	chr2R	-	Mdr49	2.383408	5.241766	2.199273
70	NM_168173	chr3L	+	CG8398	2.433995	5.29505	2.175457
73	NR_124533	chr2R	+	CR45140	4.407069	9.507183	2.157258
75	NM_001274215	chr2R	+	Reep1	1.042245	2.242202	2.15132
77	NM_136328	chr2R	-	CG30440	1.228076	2.627998	2.139931
81	NM_001300045	chr3L	+	CG32365	1.249607	2.64792	2.119003
83	NM_079535	chr3R	-	alpha-Est8	1.381507	2.913392	2.10885
91	NM_137110	chr2R	-	CG8617	2.225169	4.610262	2.07187
92	NR_125056	chr3L	-	CR45174	1.604756	3.319743	2.06869
95	NM_134978	chr2L	+	bdl	1.778463	3.670754	2.064003
112	NM_137127	chr2R	-	CG12868	1.712826	3.422832	1.998353
113	NM_141775	chr3R	-	CG14695	2.77702	5.548821	1.998121
118	NM_001169157	chrX	-	CG13375	1.032629	2.050411	1.985622
121	NM_001169497	chr2L	+	CG44085	5.326819	10.50741	1.972548
124	NM_001272492	chrX	-	spri	1.997113	3.910928	1.958291
143	NM_001299801	chr2R	+	CG4269	1.701957	3.244165	1.906138
152	NM_136294	chr2L	+	CG3635	1.419133	2.677962	1.88704
163	NM_001273395	chr2L	-	CG5381	5.247804	9.80238	1.867901
164	NM_001297962	chrX	+	CG15784	1.096594	2.047407	1.867061
166	NM_169568	chr3R	+	Npc2b	2.965778	5.530954	1.864926
171	NM_001103965	chr2R	+	CG43795	5.672353	10.55958	1.861588
187	NM_137526	chr2R	+	Cyp12b2	1.685234	3.062018	1.816969
196	NR_073936	chr3L	-	CR43971	1.159304	2.078397	1.792797
199	NM_001144421	chr3L	+	PGRP-LD	5.392874	9.615648	1.783029
201	NM_132388	chrX	+	CG2909	1.354751	2.412648	1.780879
202	NM_206407	chr3L	+	siz	3.179829	5.650172	1.776879
203	NR_125016	chr3L	-	CR45677	1.552706	2.757176	1.775723
204	NM_140770	chr3L	-	CG13698	2.428978	4.312535	1.775453
207	NM_00120207	chr2R	-	Mmp1	1.21198	2.149231	1.773322

	2						
214	NM_001298798	chr2L	+	lectin-28C	1.355169	2.393674	1.766329
216	NM_168961	chr3L	+	SPoCk	1.125231	1.986059	1.765023
226	NM_001299324	chr2R	-	CG1648	1.748362	3.055536	1.747656
227	NM_001259456	chr2R	-	CG43103	7.397721	12.884	1.741618
228	NM_001260323	chr3R	-	p53	2.809002	4.889648	1.740706
233	NM_001272217	chrX	-	CG14818	1.355587	2.345134	1.729976
240	NM_001272687	chrX	-	AnxB11	1.066284	1.839646	1.725288
243	NM_079177	chr3L	+	Drs	1.873574	3.22614	1.721918
245	NM_001144410	chr3L	+	CG10359	13.40286	23.07186	1.721414
246	NM_166424	chr2R	+	Treh	4.17086	7.155566	1.715609
251	NM_001038842	chr2L	-	CG2201	2.905576	4.972183	1.711256
252	NM_001038843	chr2L	-	CG2201	2.905576	4.972183	1.711256
257	NM_141658	chr3R	+	CG8301	1.528876	2.609341	1.706705
260	NM_165416	chr2R	+	CG3107	1.37879	2.349719	1.704189
269	NM_167534	chrX	-	Sep-04	4.446994	7.541204	1.695798
271	NM_001104305	chr3R	+	CG34383	6.187204	10.48622	1.694823
272	NM_142053	chr3R	+	CG34383	6.187204	10.48622	1.694823
274	NR_124532	chr2R	+	CR45140	7.73782	13.1022	1.693268
277	NM_137111	chr2R	-	Arc1	54.63151	92.43434	1.69196
282	NM_135181	chr2L	+	CG13982	1.249607	2.107964	1.686902
288	NM_141217	chr3R	-	CG31523	2.061705	3.460305	1.678371
291	NM_206122	chr2R	+	CG33462	2.486671	4.170865	1.677289
297	NM_169167	chr3R	+	CG1943	1.512154	2.530916	1.673716
299	NM_001274141	chr2R	+	CG10916	5.2292	8.738595	1.671115
306	NM_206554	chr3R	-	p38c	1.494595	2.48285	1.66122
310	NM_132212	chrX	+	CG1575	1.7446	2.885564	1.653998
311	NM_001299242	chr2R	+	CG30377	1.387151	2.294221	1.653909
313	NM_001272980	chr2L	-	aop	4.699299	7.768413	1.653101
314	NM_001299270	chr2R	-	Cyp6a14	1.591587	2.624203	1.648797
315	NM_001276150	chr3R	+	CG1969	1.218461	2.008036	1.648011
317	NM_138186	chr3L	-	mthl10	1.773028	2.915131	1.644154
323	NM_001144328	chr2L	-	CG9527	1.277826	2.093734	1.638512
324	NM_166895	chrX	+	br	1.563158	2.558744	1.636907
326	NM_167100	chrX	-	CG32732	1.640292	2.681598	1.63483

331	NM_142133	chr3R	+	CG14855	2.545828	4.149678	1.629992
333	NM_001275812	chr3R	+	CG4662	1.190868	1.938309	1.627643
334	NM_169877	chr3R	+	CG4662	1.190868	1.938309	1.627643
340	NM_176503	chr3R	+	Hsc70-4	1.436692	2.335331	1.625491
344	NR_124415	chr2L	+	CR44993	1.187732	1.926608	1.622089
349	NR_124437	chr2L	+	CR44809	8.738885	14.14417	1.618532
350	NM_137480	chr2R	+	GstE2	7.147925	11.56155	1.617469
352	NM_001103791	chr2R	+	CG7220	1.795604	2.900743	1.615469
353	NR_124538	chr2R	-	CR45142	1.004409	1.622399	1.615276
355	NM_001299705	chr2R	-	CG30148	1.965967	3.174595	1.614775
361	NM_001298884	chr2L	-	CG17124	6.169018	9.932981	1.61014
364	NM_001316511	chr3R	-	Bin1	5.658139	9.099883	1.608282
366	NM_001298321	chrX	-	CG9518	1.40262	2.251214	1.605007
372	NM_142316	chr3R	-	CG14906	2.565477	4.110783	1.602346
377	NM_137897	chr2R	-	CG3831	5.798191	9.269064	1.598613
379	NM_057805	chr2L	-	toc	1.719516	2.747531	1.597852
390	NR_047772	chrX	+	CR43461	2.038084	3.239896	1.589677
394	NR_124767	chr3L	+	CR45424	1.180834	1.87285	1.586039
395	NM_001276235	chr3L	-	CG40178	1.529712	2.423241	1.584116
399	NM_001038756	chrX	+	drd	1.128785	1.780986	1.57779
403	NR_124544	chr2R	+	CR44366	1.210726	1.906528	1.574698
406	NM_168492	chr3L	+	CG32099	1.056459	1.661452	1.572662
407	NM_001273130	chr2L	-	hoe1	4.204305	6.608337	1.571802
408	NM_168468	chr3L	+	CG32091	12.99712	20.42394	1.571421
410	NM_001298857	chr2L	-	CG5853	2.551054	4.007377	1.570871
413	NM_001260068	chr3R	+	CG8369	2.024287	3.174437	1.568175
414	NM_141514	chr3R	+	CG18249	1.478081	2.316041	1.566924
418	NM_001273626	chr2L	+	mib2	5.335808	8.344103	1.563794
420	NM_170484	chr3R	+	Fer2LCH	1.287024	2.008511	1.560586
421	NM_001169919	chr3L	+	CG5021	1.821942	2.84319	1.560527
423	NM_130655	chrX	-	eIF3ga	4.732326	7.375976	1.558637
425	NM_001272499	chrX	-	Rph	1.544972	2.404426	1.556291
438	NM_001103885	chr2R	-	CG30460	1.86354	2.889359	1.550468
443	NM_135175	chr2L	+	CG9505	2.710338	4.19901	1.549257
444	NM_170219	chr3R	-	CG10550	3.654127	5.654915	1.547542

445	NM_001038945	chr3L	-	CG33969	2.677519	4.138927	1.545806
446	NM_135327	chr2L	-	Wwox	1.589496	2.455496	1.544827
451	NM_080174	chr3R	+	GstD4	3.653082	5.631514	1.541579
452	NM_144186	chr3L	+	CG13315	1.909737	2.941852	1.540449
453	NR_073874	chr2R	-	CR43918	1.057713	1.628249	1.539405
459	NM_001274148	chr2R	-	Jabba	3.721854	5.720374	1.536969
460	NM_137527	chr2R	-	Jabba	3.721854	5.720374	1.536969
464	NM_205901	chr2L	-	CG34394	3.812366	5.855086	1.535814
468	NM_141260	chr3R	-	CG2604	1.680635	2.57756	1.533682
474	NM_001169707	chr2R	-	Sema1b	3.332842	5.104998	1.531725
475	NM_001104123	chr3L	-	CG10663	1.596185	2.444903	1.531716
479	NM_176214	chr2R	-	mthl4	2.097449	3.210645	1.530738
481	NM_001300537	chr3R	-	pinta	1.841383	2.816152	1.529369
485	NM_001297917	chrX	+	CG2930	4.304642	6.574975	1.527415
492	NM_167198	chrX	-	Ptpmeg2	2.940275	4.482032	1.524358
493	NM_078499	chrX	-	Tsp5D	1.289323	1.964872	1.523956
496	NM_078914	chr2R	+	Tsp42El	4.519111	6.876655	1.521683
502	NM_136945	chr2R	+	Dh44-R2	2.946546	4.472703	1.517948
503	NM_165907	chr2R	+	Dh44-R2	2.946546	4.472703	1.517948
509	NM_001299591	chr2R	+	CG11400	3.981057	6.027746	1.514107
514	NM_168070	chr3L	-	ImpL2	3.674613	5.556569	1.512151
516	NM_001273397	chr2L	+	GATAd	2.089715	3.15657	1.510526
518	NM_135525	chr2L	-	CG5604	2.471412	3.730837	1.509597
520	NM_170440	chr3R	-	Zip99C	1.651998	2.492969	1.509064
522	NM_001259659	chr3L	-	CG11537	12.7352	19.20189	1.50778
523	NM_001274425	chr3L	-	CG11537	12.7352	19.20189	1.50778
524	NM_080175	chr3R	+	GstD5	10.76025	16.21956	1.507359
527	NM_078513	chrX	-	fz4	1.019878	1.537017	1.50706
528	NM_001144160	chr2R	-	KCNQ	2.826352	4.254349	1.505244
532	NM_001275243	chr3L	-	Wnk	2.503812	3.763724	1.503198
533	NM_001297887	chrX	-	CG3091	1.205082	1.811344	1.503087
535	NM_134877	chr2L	-	CG18557	7.171128	10.77478	1.502522
536	NM_001298631	chr2L	-	NLaz	2.276592	3.420303	1.502379
542	NM_136206	chr2L	+	CG2617	1.91559	2.869753	1.498104
547	NM_136290	chr2L	+	CG42748	2.311082	3.458408	1.496445
556	NM_133101	chrX	+	CG7101	1.804174	2.690769	1.491413

558	NM_167760	chrX	-	GCS2alpha	2.017598	3.007627	1.490697
559	NM_001300180	chr3L	-	Cyp12c1	2.170611	3.235152	1.490434
561	NM_001042794	chrX	+	sgg	1.555842	2.316041	1.488609
562	NM_001169494	chr2L	-	bun	4.503852	6.700991	1.487836
564	NM_079242	chr3L	+	RNaseX25	1.804593	2.684286	1.487475
566	NM_166625	chr2R	-	CG4797	2.350381	3.489082	1.484475
568	NM_142734	chr3R	+	CG6656	4.045858	6.000392	1.483095
569	NM_142983	chr3R	+	CG6356	3.393462	5.03274	1.48307
575	NM_170216	chr3R	+	CG31370	2.251508	3.33334	1.480493
580	NM_001273764	chr2L	+	CG17493	2.679401	3.957571	1.477036
581	NM_169083	chr3R	+	CG31549	1.974119	2.915447	1.476835
582	NM_001298049	chrX	-	unc-119	1.927087	2.845087	1.476367
583	NM_132161	chrX	-	unc-119	1.927087	2.845087	1.476367
589	NM_135323	chr2L	+	CG7231	4.658537	6.864638	1.473561
603	NM_001299594	chr2R	-	CG6568	2.024287	2.970471	1.467416
606	NM_165570	chr2R	+	Cul1	2.633622	3.859699	1.465548
607	NM_165512	chr2R	+	pk	3.973114	5.821882	1.46532
608	NR_048324	chr3R	-	snRNA:U4atac:82E	2.2467	3.289543	1.464167
611	NM_001273805	chr2R	+	Eb1	1.93064	2.825639	1.463576
614	NM_001300384	chr3R	+	Dic1	2.87213	4.202804	1.463306
620	NR_001982	chr3R	-	snRNA:U1:82Eb	25.57262	37.30252	1.45869
621	NM_001275275	chr3L	+	olf413	5.500318	8.022975	1.458638
624	NM_001276084	chr3R	-	dsd	2.533286	3.694471	1.458371
626	NM_001014498	chr2L	-	Clamp	5.707053	8.316749	1.457276
628	NM_136660	chr2R	+	CG1827	1.509645	2.199037	1.456658
629	NM_139552	chr3L	-	CG14969	1.265702	1.843599	1.456582
630	NM_140355	chr3L	+	CG14118	2.48918	3.624427	1.456073
631	NM_001274545	chr3L	-	ImpL3	5.37866	7.831026	1.455944
632	NR_073836	chr2R	-	CR44127	2.485417	3.61826	1.455796
634	NM_143322	chr3R	+	CG12883	2.20991	3.211435	1.453197
637	NM_135462	chr2L	+	CG13116	1.732894	2.515105	1.45139
639	NM_165690	chr2R	+	GstT2	3.316537	4.813279	1.451297
640	NM_057417	chr2R	-	tra2	2.492106	3.616363	1.451127
641	NM_001273924	chr2R	-	mlt	3.737741	5.422331	1.450697
644	NM_001299838	chr2R	-	CG9815	3.684228	5.340586	1.449581
646	NM_165689	chr2R	+	CG1902	1.363112	1.975623	1.449347

647	NM_057386	chr2L	-	aub	1.557305	2.256906	1.449239
652	NM_133088	chrX	-	Ing3	1.345553	1.94827	1.447932
653	NM_078585	chrX	+	CkIalpha	1.711572	2.477949	1.447762
654	NR_124023	chr2L	+	CR44976	2.440266	3.53114	1.447031
656	NM_141930	chr3R	-	lig3	5.873653	8.496207	1.446495
660	NM_001103544	chrX	+	upd3	5.715414	8.261093	1.445406
661	NM_142718	chr3R	-	Archease	4.072405	5.88576	1.445279
662	NR_123961	chrX	-	CR45501	1.019669	1.473614	1.445189
664	NM_080360	chr2L	+	Hrs	1.496685	2.162197	1.444657
666	NM_133049	chrX	-	upd2	4.396199	6.348715	1.444137
667	NM_001276121	chr3R	-	Inx3	12.86898	18.57892	1.443698
669	NM_169336	chr3R	-	Timp	6.984252	10.07671	1.442775
671	NM_001273200	chr2L	+	Cpr	1.111226	1.602318	1.441937
672	NM_168262	chr3L	-	BI-1	1.761531	2.539929	1.441887
676	NM_001103704	chr2L	+	Fas3	6.86991	9.899303	1.440965
679	NM_001275272	chr3L	+	CG14561	1.376908	1.983055	1.440222
680	NM_166783	chr4	-	gw	2.618572	3.768784	1.439252
682	NM_140058	chr3L	+	CG3529	2.270739	3.266775	1.43864
685	NM_167192	chrX	-	CG32700	1.332802	1.916647	1.438058
693	NM_164549	chr2L	-	CG31778	1.512363	2.171051	1.435536
696	NM_168513	chr3L	-	Hip1	1.486233	2.13089	1.433752
699	NM_170444	chr3R	-	Zip99C	10.03908	14.38054	1.432457
701	NM_132531	chrX	-	CG11802	1.589078	2.275406	1.431903
703	NM_137040	chr2R	-	CG6145	1.821733	2.608234	1.431732
705	NM_139627	chr3L	+	CG1311	1.549989	2.214216	1.428537
709	NM_130718	chrX	+	HIP	2.10602	3.005414	1.427059
713	NR_125316	chr2L	+	CR44268	1.546853	2.201092	1.422948
715	NM_137717	chr2R	+	Lapsyn	1.686279	2.397311	1.421657
716	NM_142019	chr3R	+	CG32473	1.672065	2.377072	1.421639
717	NM_136697	chr2R	+	Adam	1.61458	2.293905	1.420744
719	NM_134992	chr2L	-	CG15439	2.786426	3.956938	1.420076
720	NR_133475	chr3R	+	CR46104	1.000438	1.420172	1.41955
735	NM_166989	chrX	+	HIP-R	3.341412	4.726317	1.414467
739	NM_001272215	chrX	-	CG14812	3.494843	4.941509	1.413943
740	NM_001300075	chr3L	+	CG33926	5.22711	7.3891	1.413611
745	NM_001169555	chr2L	-	sky	3.339531	4.716039	1.412186
748	NM_001273438	chr2L	+	CG16743	2.446328	3.451135	1.410741
751	NM_001259522	chr2R	+	mahj	2.277428	3.210803	1.409837

754	NM_001104094	chr3L	-	I-2	1.433975	2.021318	1.409591
755	NM_137805	chr2R	+	CG11275	3.361479	4.737701	1.409409
756	NM_166740	chr4	-	CG2316	1.940256	2.734408	1.409303
759	NM_134998	chr2L	-	HP6	1.868139	2.632109	1.408947
760	NM_166968	chrX	+	dnc	2.302512	3.243848	1.40883
764	NM_135986	chr2L	-	beat-IIIc	3.601451	5.06626	1.406728
765	NM_135923	chr2L	-	Ku80	2.441938	3.434849	1.406608
766	NR_002129	chrX	-	snRNA:U5:14B	23.42103	32.94397	1.406598
768	NM_132317	chrX	-	CG12121	1.222014	1.718215	1.406052
771	NM_168306	chr3L	-	pix	2.589098	3.639447	1.405682
772	NM_167956	chr3L	+	dos	8.708784	12.24143	1.405642
773	NM_080198	chr3R	-	Pp1-87B	2.80733	3.946029	1.405616
776	NM_132196	chrX	-	mahe	3.790209	5.324617	1.404835
779	NM_001274955	chr3L	+	dop	3.205749	4.49816	1.403154
780	NM_206362	chr3L	+	CG9425	2.241474	3.144395	1.402825
783	NM_166780	chr4	-	gw	2.600177	3.645614	1.402064
784	NM_170046	chr3R	+	Gr94a	5.577242	7.819167	1.401977
786	NM_001042877	chr2L	+	Mnn1	1.754006	2.458501	1.401649
787	NM_167758	chrX	-	GCS2alpha	3.111475	4.360759	1.401509
789	NM_138221	chr3L	+	CG13890	1.381716	1.935937	1.40111
790	NM_001298939	chr2L	+	ThrRS	3.986492	5.585345	1.401068
792	NM_079858	chr3R	-	Sap-r	6.908163	9.674624	1.400463
793	NM_137537	chr2R	-	CG15099	3.05608	4.279015	1.400164
796	NM_140762	chr3L	-	CG5535	4.27266	5.980786	1.399781
797	NM_001298693	chr2L	+	Bub1	2.172284	3.040515	1.399686
798	NM_141832	chr3R	+	wkd	1.907646	2.669107	1.399162
799	NM_170445	chr3R	-	Zip99C	1.328831	1.859094	1.399045
801	NM_001298467	chrX	+	Vps4	1.697776	2.372803	1.397595
803	NM_169811	chr3R	+	koko	1.412235	1.973093	1.397142
807	NM_141659	chr3R	+	P58IPK	5.512024	7.6941	1.395876
810	NM_143666	chr4	-	bip2	3.717465	5.1869	1.395279
813	NM_132868	chrX	+	CG8931	1.098684	1.531642	1.394069
818	NM_166482	chr2R	-	Tango11	3.441331	4.78893	1.391592
822	NM_136176	chr2L	+	bwa	5.604208	7.79466	1.390858
823	NM_001273997	chr2R	-	CG17574	4.079303	5.671359	1.390276
824	NM_206309	chr3L	+	Pdxk	2.304811	3.202265	1.389382
825	NM_141932	chr3R	-	Cyp9f2	2.438593	3.387257	1.389021
827	NM_135061	chr2L	-	Rpn11	4.680485	6.50082	1.38892
828	NM_001272850	chrX	+	S6kII	2.243146	3.114354	1.388386
829	NM_00117038	chr3L	+	CG40160	1.068374	1.482943	1.388037

	4						
830	NR_124606	chr2R	+	CR44417	3.531424	4.900399	1.387655
832	NR_133522	chrX	+	CR32636	1.932521	2.679543	1.386553
833	NM_142644	chr3R	+	CG5466	1.204037	1.669358	1.386467
834	NM_169467	chr3R	+	Desat1	7.069538	9.801115	1.386387
835	NM_001300614	chr3R	+	tx	1.556051	2.156505	1.385883
838	NM_143401	chr3R	+	Cpsf100	1.519679	2.104802	1.385031
839	NM_001260059	chr3R	-	CG45263	9.144411	12.66344	1.384828
840	NM_169223	chr3R	-	CG45263	9.144411	12.66344	1.384828
841	NM_139527	chr3L	-	CG14966	2.022197	2.800025	1.384645
843	NM_206363	chr3L	+	CG17839	3.076775	4.259251	1.384323
845	NR_133323	chr3R	+	CR45999	1.709273	2.365846	1.384124
846	NR_133324	chr3R	+	CR45999	1.709273	2.365846	1.384124
847	NR_124416	chr2L	+	CR43144	3.013646	4.169601	1.383573
848	NR_048035	chr2L	+	CR43148	1.42645	1.972619	1.382887
851	NM_057251	chr2L	+	stc	2.380064	3.287329	1.381194
852	NM_078611	chrX	+	mRpL3	1.461149	2.017049	1.380454
853	NM_001275934	chr3R	+	Irk1	1.076526	1.485631	1.380023
856	NM_001276029	chr3R	-	CG33494	5.493211	7.575357	1.37904
857	NM_142123	chr3R	+	CG3505	1.320051	1.820356	1.379004
859	NM_142925	chr3R	-	CG10217	1.897195	2.615033	1.378368
860	NM_057614	chr2L	+	Ror	1.177281	1.620976	1.376881
862	NR_073662	chrX	-	CR43981	1.467629	2.019895	1.376298
865	NM_132683	chrX	-	CG12177	1.924578	2.646497	1.375105
867	NM_141526	chr3R	-	Sgt1	2.071947	2.848408	1.374749
868	NM_169558	chr3R	+	Dip-B	2.960343	4.069673	1.37473
871	NM_079850	chr3R	+	CecA2	1.092413	1.50081	1.373848
872	NM_170651	chr3R	-	pnt	5.19241	7.13185	1.373514
873	NM_142929	chr3R	-	CG10208	1.501702	2.062427	1.373393
874	NM_001273369	chr2L	+	CG13117	18.8829	25.93039	1.373221
875	NM_132539	chrX	-	Upf1	2.024915	2.780261	1.373026
876	NM_001202118	chr3L	-	Eip63F-1	1.591587	2.185123	1.372921
879	NM_139641	chr3L	+	slow	6.694948	9.186687	1.372182
883	NM_001274300	chr3L	+	Usp10	1.894059	2.59432	1.369714
884	NM_137371	chr2R	-	Tes	1.812118	2.481585	1.369439
885	NM_168692	chr3L	+	CG32170	4.154973	5.6897	1.369371
886	NM_001259338	chr2R	-	CG9005	2.481236	3.397376	1.369227
887	NM_001202089	chr3L	+	CG7991	14.96455	20.48513	1.368911
888	NM_142640	chr3R	-	CG16953	2.607493	3.569245	1.368842

893	NM_132790	chrX	-	CG9123	2.103302	2.877817	1.368237
894	NM_001298240	chrX	-	CG32647	8.492434	11.61878	1.368134
897	NM_001273199	chr2L	+	Cpr	1.793723	2.452809	1.36744
898	NM_001274994	chr3L	-	Zn72D	4.739851	6.479949	1.367121
903	NM_001042972	chr2R	-	IntS3	29.63353	40.47917	1.365992
905	NM_142218	chr3R	-	AOX1	12.31212	16.81185	1.365472
909	NM_136893	chr2R	-	EndoG	2.044146	2.789906	1.364827
911	NM_057214	chr2L	+	ab	5.344796	7.292334	1.36438
914	NM_001169571	chr2L	-	CG31612	1.187314	1.619394	1.363914
915	NM_001299536	chr2R	+	CG42524	4.579731	6.246258	1.363892
920	NR_001612	chr2L	+	snRNA:U5:23D	28.51812	38.87906	1.363311
921	NM_001274823	chr3L	-	Pbgs	1.063984	1.450371	1.363151
922	NM_170253	chr3R	+	Nf1	1.334056	1.818143	1.362868
930	NM_001347753	chr2R	-	cathD	9.573141	13.03437	1.361556
931	NM_001272270	chrX	+	CG3603	2.48479	3.382197	1.36116
932	NM_137887	chr2R	-	EMC8-9	2.876729	3.912351	1.36
934	NM_141619	chr3R	+	VhaM8.9	4.922547	6.6885	1.358748
935	NM_001316493	chr3R	-	agt	1.282843	1.743039	1.358731
936	NM_001299223	chr2R	-	Tsp42Ed	5.565745	7.561127	1.358511
937	NM_166469	chr2R	+	CG42365	2.813392	3.82191	1.358471
939	NM_137907	chr2R	+	l(2)k09913	3.613157	4.905459	1.357666
940	NM_001297869	chrX	+	east	1.494386	2.027801	1.356946
942	NR_001972	chr3L	+	snRNA:U12:73B	40.69855	55.21199	1.356608
943	NM_166435	chr2R	+	MFS16	2.673339	3.625692	1.356241
945	NM_001347812	chr2L	-	Sur	1.880681	2.549258	1.355497
948	NM_134670	chr2L	-	CG3625	9.920974	13.4393	1.354635
949	NM_137739	chr2R	-	CG10795	1.68398	2.28094	1.354493
952	NM_205893	chr2L	+	CG31690	5.317622	7.200945	1.354166
955	NM_001275073	chr3L	-	CG44006	13.21034	17.87247	1.352916
956	NM_166635	chr2R	-	SERCA	2.186289	2.957822	1.352896
958	NM_169562	chr3R	+	Ipp	1.043917	1.411476	1.352096
960	NM_166529	chr2R	+	Gp150	7.854879	10.6184	1.351822
961	NR_002465	chrX	+	snoRNA:U3:9B	61.05785	82.53678	1.35178
962	NM_141798	chr3R	-	GCC88	1.033883	1.397087	1.351301
964	NR_002076	chr3R	+	snRNA:U1:95Cc	71.28402	96.2806	1.350662
965	NM_00116994	chr3L	-	CG6091	1.593886	2.151761	1.350009

	6						
966	NM_206580	chr3R	-	Trc8	1.956142	2.640805	1.350007
968	NM_058130	chr2L	+	Sps2	1.863958	2.516212	1.349929
970	NM_001298169	chrX	-	CG1582	1.570474	2.119348	1.349496
971	NM_136044	chr2L	+	CG10333	1.481635	1.998866	1.349095
974	NR_073677	chr2L	+	CR44218	1.220342	1.645641	1.348508
977	NM_166279	chr2R	+	GstE9	5.758057	7.760665	1.347792
983	NM_135509	chr2L	-	CG5734	6.210198	8.36276	1.346617
984	NM_001299484	chr2R	-	Opa1	2.34411	3.155147	1.345989
985	NM_057858	chr2R	-	sktl	6.058648	8.154525	1.345931
986	NR_037757	chr3R	-	CR31514	1.268629	1.707305	1.345788
987	NM_138256	chr3L	+	msd1	2.158278	2.90438	1.345693
989	NM_143130	chr3R	-	CHKov2	14.6117	19.66026	1.345515
990	NM_080029	chrX	-	Smyd3	1.04329	1.403728	1.345482
991	NM_138249	chr3L	+	Rabex-5	3.222263	4.335303	1.345422
992	NM_143555	chr3R	-	CG9717	2.234576	3.006046	1.345242
994	NM_001104107	chr3L	+	Adi1	2.118144	2.84904	1.345064
995	NM_057473	chr2L	-	tam	1.099938	1.479464	1.345043
997	NM_133165	chr3L	+	Fie	2.693197	3.619525	1.343951
998	NM_140647	chr3L	+	Rpn12	2.540602	3.413029	1.343394
999	NM_167827	chr3L	-	fwd	6.288377	8.44403	1.3428
1002	NM_165390	chr2L	+	Cul2	1.68816	2.263547	1.340837
1003	NM_169139	chr3R	+	godzilla	2.495869	3.344883	1.340168
1006	NM_001260373	chr3R	+	Nup358	2.700931	3.614624	1.338288
1007	NM_001170207	chr3R	-	CG34034	1.364784	1.826364	1.338207
1009	NM_143738	chr2R	-	Ady43A	2.22496	2.97553	1.337341
1010	NM_136546	chr2R	+	Cyp6a13	1.457596	1.948902	1.337066
1011	NM_137728	chr2R	-	CG30392	1.126067	1.505395	1.33686
1012	NM_001258786	chrX	-	Pp2B-14D	2.469321	3.300137	1.336455
1013	NM_133105	chrX	-	CG7322	1.217206	1.626035	1.335875
1014	NM_141107	chr3L	+	CG7407	1.878173	2.507832	1.335251
1017	NM_001274328	chr3L	-	CG12084	3.44802	4.601566	1.334553
1018	NM_138268	chr3L	-	CG12084	3.44802	4.601566	1.334553
1019	NM_080199	chr2L	-	CIAPIN1	4.595409	6.132575	1.3345
1021	NR_073614	chr4	-	CR43956	1.38088	1.842176	1.334059
1023	NM_001275790	chr3R	+	Xrp1	27.5388	36.72762	1.333668
1025	NM_141970	chr3R	+	CG12279	1.840755	2.453915	1.333102
1026	NM_001275568	chr3R	-	CG4848	1.546017	2.060688	1.332901
1028	NM_137345	chr2R	+	CG15611	12.65347	16.85217	1.331822

1029	NM_166704	chr2R	-	zip	8.147736	10.85067	1.33174
1031	NM_001272166	chrX	+	CG32817	2.562969	3.411923	1.331239
1032	NM_141604	chr3R	-	CG11984	2.0454	2.722708	1.331137
1033	NM_167462	chrX	-	CG8974	2.791025	3.713761	1.330608
1034	NM_139887	chr3L	-	CG7506	1.301029	1.730864	1.330381
1035	NM_164909	chr2L	-	CYLD	1.206337	1.604532	1.330086
1037	NM_001104170	chr3L	+	Blos3	1.015906	1.350602	1.329455
1039	NM_001272501	chrX	-	Tango5	3.171049	4.212924	1.328558
1044	NM_164979	chr2L	+	escl	1.507346	2.001238	1.327657
1046	NM_164550	chr2L	-	CG31777	2.161832	2.867697	1.326513
1050	NM_058100	chr2L	+	Stam	5.500318	7.293915	1.32609
1051	NM_079245	chr3L	-	Nmt	1.645308	2.181645	1.325979
1052	NM_139833	chr3L	+	BHD	1.370219	1.81672	1.32586
1053	NM_079428	chr3L	-	CSN1b	2.135912	2.831648	1.325732
1055	NM_001316562	chr3R	+	Not10	1.201738	1.592831	1.32544
1056	NM_001275353	chr3R	-	PEK	1.046216	1.386178	1.324944
1058	NM_079054	chr2R	-	Dcr-2	3.532469	4.677934	1.324267
1059	NR_003121	chr3L	-	snRNA:U11	26.65395	35.29416	1.324162
1063	NM_137360	chr2R	-	CG6568	1.971402	2.608866	1.323356
1064	NM_169116	chr3R	-	CG2017	5.827038	7.709753	1.3231
1065	NM_001298196	chrX	+	Spase25	2.548963	3.37192	1.322859
1069	NM_001015476	chr3L	+	ND-AGGG	1.69485	2.239356	1.321271
1070	NM_134492	chrX	-	CG12237	4.504479	5.951535	1.321248
1071	NM_001299241	chr2R	+	CG1882	10.19606	13.47092	1.321188
1072	NM_143711	chr3R	-	Ref1	2.791443	3.687672	1.321063
1076	NM_136622	chr2R	+	Rad51D	1.178953	1.555991	1.319807
1077	NM_001014628	chr3R	+	gish	7.514153	9.910055	1.318852
1078	NM_001275696	chr3R	+	gish	7.514153	9.910055	1.318852
1079	NM_137543	chr2R	-	Jheh3	2.479146	3.269463	1.318786
1081	NM_001042981	chr2R	+	CG17486	2.960343	3.902548	1.318276
1082	NM_001201994	chr2R	-	CG6701	5.333508	7.029867	1.318057
1083	NM_166264	chr2R	+	pAbp	7.849026	10.34439	1.31792
1085	NM_001042932	chr2L	+	Slmap	1.910364	2.517002	1.317551
1086	NR_124833	chr3L	+	CR44526	3.321554	4.375938	1.317437
1087	NM_137694	chr2R	+	ND-B14.7	1.089486	1.435035	1.317166
1090	NM_142290	chr3R	+	CG14883	2.123997	2.796388	1.316569
1093	NM_140071	chr3L	-	CG3408	4.363799	5.740612	1.315508

1095	NM_080005	chrX	-	Rab18	2.565059	3.373185	1.315052
1096	NM_145191	chr3L	-	CG4098	3.055453	4.017654	1.314913
1097	NM_001299682	chr2R	+	CG7461	4.813431	6.326263	1.314294
1098	NM_140239	chr3L	-	CG11652	1.703629	2.23904	1.314277
1099	NM_001170362	chr2L	-	CG12567	3.245465	4.261781	1.313149
1100	NM_001275512	chr3R	-	FBXO11	5.062182	6.646126	1.312898
1101	NM_166924	chrX	-	CG4199	3.487736	4.578955	1.312873
1103	NM_001298000	chrX	-	sqh	4.664808	6.121349	1.31224
1104	NM_134791	chr2L	+	CG7289	1.516125	1.988747	1.31173
1105	NM_138028	chr2R	+	CG3163	1.719934	2.255641	1.31147
1106	NM_139888	chr3L	+	PGRP-SD	1.129621	1.480887	1.310959
1107	NM_001272244	chrX	+	Unc-76	1.652207	2.165517	1.310682
1108	NM_001259604	chr3L	-	mthl10	15.66795	20.53257	1.310482
1110	NM_140986	chr3L	+	CG4858	2.085116	2.73172	1.310104
1111	NM_135971	chr2L	-	CG13283	1.442336	1.889452	1.309994
1112	NM_057318	chrX	-	arm	5.330373	6.982591	1.309963
1115	NM_001042952	chr2L	+	lt	2.417481	3.165741	1.30952
1117	NM_001316533	chr3R	-	Tango9	1.868348	2.445852	1.309099
1118	NM_142745	chr3R	-	CG6028	1.934194	2.532023	1.309085
1121	NM_142122	chr3R	-	l(3)L1231	3.5193	4.606625	1.308961
1124	NM_135023	chr2L	+	CG11927	1.489996	1.949851	1.308628
1126	NM_001103805	chr2R	+	pyr	20.44313	26.74594	1.308309
1128	NM_143025	chr3R	+	CG42331	2.425215	3.172065	1.307952
1129	NM_142191	chr3R	-	CG6218	4.756783	6.221276	1.307875
1130	NM_001299957	chr3L	-	CG7028	5.076187	6.637114	1.3075
1133	NM_164784	chr2L	+	Bsg	5.400608	7.056904	1.306687
1134	NM_078520	chrX	-	sws	2.093478	2.73504	1.306458
1135	NM_167140	chrX	-	sws	2.093478	2.73504	1.306458
1136	NM_132796	chrX	+	CG11655	2.067767	2.701362	1.306415
1137	NM_142963	chr3R	+	Kal1	6.397911	8.35438	1.305798
1143	NM_001258811	chrX	+	CrebB	1.459059	1.904947	1.3056
1145	NM_001273767	chr2L	+	cta	2.142601	2.796072	1.30499
1146	NM_001169309	chrX	-	CG43658	2.160996	2.819631	1.304783
1147	NM_169029	chr3R	-	CG2604	2.562342	3.342985	1.30466
1148	NM_143687	chr4	-	CG11077	1.686697	2.200144	1.304409
1150	NM_142134	chr3R	+	CG14856	1.663285	2.168837	1.303948
1152	NM_169465	chr3R	+	Desat1	2.520953	3.286065	1.303501

1154	NM_001014478	chr2L	-	RapGAP1	11.32777	14.75828	1.30284
1156	NM_136412	chr2R	-	pgant3	2.212209	2.880504	1.302094
1157	NM_169115	chr3R	-	CG2017	1.034092	1.346333	1.301947
1158	NM_142986	chr3R	-	Nab2	1.799576	2.342762	1.301841
1159	NM_166139	chr2R	+	Rho1	3.463488	4.508437	1.301704
1160	NM_001272521	chrX	-	Evi5	4.279349	5.567479	1.301011
1161	NM_167285	chrX	-	Evi5	4.279349	5.567479	1.301011
1162	NM_001272885	chr2L	-	U2af38	3.402032	4.42606	1.301005
1163	NM_170365	chr3R	-	larp	3.475194	4.520612	1.300823
1164	NM_057990	chrX	+	dwg	2.035993	2.646497	1.299855
1167	NM_001042989	chr2R	+	conu	3.368587	4.378468	1.299794
1169	NM_135950	chr2L	-	CG5888	5.326192	6.922033	1.299621
1170	NM_166481	chr2R	-	Tango11	3.697606	4.804741	1.299419
1171	NM_170109	chr3R	-	KrT95D	5.83958	7.58769	1.299355
1172	NM_137273	chr2R	-	CG8060	1.230794	1.59884	1.299032
1173	NM_176097	chr2R	-	SCAP	6.073071	7.888895	1.298996
1176	NM_001274865	chr3L	+	Syx13	3.310266	4.297988	1.298382
1177	NM_001273030	chr2L	-	Pgk	2.520953	3.272941	1.298295
1178	NM_001103722	chr2R	-	Nipped-A	4.825137	6.264283	1.29826
1179	NM_001316406	chr2R	-	Nipped-A	4.825137	6.264283	1.29826
1180	NM_165959	chr2R	-	Nmda1	1.737702	2.255958	1.298242
1181	NM_141306	chr3R	+	CG12171	8.979901	11.65768	1.298197
1185	NM_165659	chr2R	-	Rab32	13.55733	17.59103	1.297529
1186	NR_003825	chr2R	-	snoRNA:Or-CD1	51.68518	67.06098	1.29749
1187	NM_168926	chr3L	+	CG32441	1.584898	2.056261	1.297409
1189	NM_176301	chr3L	+	ergic53	5.839371	7.574092	1.297073
1192	NM_001299592	chr2R	+	Gbp2	3.108757	4.030619	1.296537
1193	NM_001103392	chrX	-	CG3655	4.155182	5.385807	1.296166
1194	NM_079998	chr2R	-	arr	15.63304	20.26267	1.296144
1195	NM_143370	chr3R	+	Sid	1.198184	1.552987	1.296117
1196	NM_001299867	chr2R	-	SERCA	3.78561	4.906408	1.296068
1197	NM_166639	chr2R	-	SERCA	3.78561	4.906408	1.296068
1200	NR_133383	chr3R	+	CR46015	3.007794	3.897488	1.295796
1203	NM_001170089	chr3R	-	CG11984	1.914126	2.479372	1.295302
1204	NM_168145	chr3L	-	QC	8.687463	11.25259	1.295268
1206	NM_170217	chr3R	+	CG31436	4.587465	5.940467	1.294935
1207	NM_001298427	chrX	-	Ubr1	3.295843	4.267631	1.294853

1208	NM_167017	chrX	+	l(1)G0334	3.139485	4.065088	1.294826
1209	NM_167019	chrX	+	l(1)G0334	3.139485	4.065088	1.294826
1210	NM_001272473	chrX	-	alpha-Man-Ia	1.185224	1.534171	1.294415
1211	NM_001273770	chr2R	-	RNASEK	31.81752	41.17992	1.294253
1213	NM_137846	chr2R	-	CG17807	1.205709	1.560418	1.294191
1214	NM_001300127	chr3L	+	CG11279	1.845145	2.387033	1.293683
1215	NM_143679	chr4	-	MED26	3.35918	4.345422	1.293596
1218	NM_169595	chr3R	+	Hexim	7.416953	9.590034	1.292988
1220	NM_135005	chr2L	+	CG11929	1.634439	2.112707	1.292619
1221	NM_135329	chr2L	-	CG12560	13.82281	17.86599	1.292501
1222	NM_134687	chr2L	+	Tspo	9.505623	12.28555	1.29245
1224	NM_001300159	chr3L	-	CG9674	13.20323	17.06341	1.292366
1227	NM_168900	chr3L	+	CG32440	1.063357	1.373687	1.291839
1229	NM_001298254	chrX	+	CG2200	1.438992	1.85862	1.291612
1230	NM_169744	chr3R	-	Keap1	5.503453	7.107658	1.291491
1231	NM_001104459	chr3R	-	LpR2	5.379496	6.947015	1.291388
1232	NM_001201921	chr2L	-	CG10165	1.232884	1.592041	1.291314
1234	NM_001103902	chr2R	+	Phb2	3.103113	4.006112	1.290998
1235	NM_001297907	chrX	-	CG18508	3.057962	3.946503	1.290567
1236	NM_001316420	chr2R	+	PRAS40	18.93913	24.44207	1.290559
1238	NM_001275918	chr3R	-	wge	2.926688	3.776215	1.290269
1242	NM_142404	chr3R	-	CG7357	2.287671	2.950232	1.289623
1246	NM_206616	chrX	-	CG2658	1.081961	1.394558	1.288916
1249	NM_142100	chr3R	-	NK7.1	7.40441	9.53754	1.288089
1250	NM_079914	chr3L	-	skd	15.98464	20.58886	1.28804
1251	NM_168879	chr3L	-	skd	15.98464	20.58886	1.28804
1252	NR_037751	chr3L	-	CR32218	1.810654	2.332168	1.288025
1253	NM_138089	chr2R	+	uri	2.210328	2.846826	1.287966
1254	NM_167336	chrX	+	CG4004	3.334932	4.294826	1.28783
1256	NM_140664	chr3L	+	CG9706	1.378581	1.775136	1.287655
1257	NM_001202094	chr3L	-	Rap1	3.342248	4.30289	1.287424
1261	NM_142791	chr3R	-	Rpn7	2.916028	3.752498	1.286853
1262	NM_167476	chrX	-	ND-20	1.803547	2.320626	1.286701
1263	NM_001272720	chrX	+	CG12991	1.881517	2.420712	1.286574
1264	NM_168123	chr3L	-	Msr-110	13.47079	17.32761	1.28631
1265	NM_165957	chr2R	-	Nmda1	3.152863	4.055443	1.286273
1266	NM_165958	chr2R	-	Nmda1	3.152863	4.055443	1.286273

1267	NM_137558	chr2R	-	CG11906	1.617507	2.080452	1.286209
1268	NM_001170094	chr3R	-	Vps15	1.366039	1.756953	1.286166
1269	NM_141611	chr3R	-	Vps15	1.366039	1.756953	1.286166
1270	NM_135373	chr2L	+	Wdr82	1.643009	2.112707	1.285877
1271	NM_170033	chr3R	-	loco	14.11127	18.14459	1.285822
1273	NM_140995	chr3L	-	Pex16	2.150962	2.765556	1.28573
1276	NM_165960	chr2R	-	Nmda1	2.357279	3.029447	1.285146
1277	NM_141173	chr3L	+	BoYb	1.930013	2.480162	1.285049
1278	NM_169490	chr3R	+	CtBP	7.8461	10.08003	1.284718
1280	NM_001272668	chrX	-	CG42354	2.386544	3.064706	1.284161
1281	NM_169392	chr3R	-	PGRP-LB	1.205918	1.54856	1.284133
1285	NM_206737	chrX	+	Gbeta13F	5.721894	7.34467	1.283608
1286	NM_206739	chrX	+	Gbeta13F	5.721894	7.34467	1.283608
1287	NM_001274070	chr2R	-	Khc-73	4.875932	6.258591	1.283568
1288	NM_140901	chr3L	+	Rpn1	4.619866	5.929874	1.28356
1290	NM_001260229	chr3R	+	pasi1	1.473482	1.891191	1.283484
1293	NM_080188	chr3R	+	Hsp70Bb	182.2273	233.8322	1.28319
1295	NM_001274163	chr2R	-	hpo	2.389261	3.065339	1.282965
1296	NM_169033	chr3R	-	CG12163	8.017926	10.28557	1.282822
1297	NM_169034	chr3R	-	CG12163	8.017926	10.28557	1.282822
1299	NM_166709	chr2R	+	CG30428	1.212608	1.554884	1.282265
1300	NM_140288	chr3L	+	l(3)j2D3	1.176863	1.508873	1.282115
1302	NM_166192	chr2R	-	unc-104	1.98917	2.549732	1.281807
1303	NM_001201764	chr2L	+	Msp300	10.87647	13.94052	1.281713
1304	NM_001201766	chr2L	+	Msp300	10.87647	13.94052	1.281713
1306	NM_137318	chr2R	+	IntS8	1.308972	1.677264	1.281359
1308	NM_164839	chr2L	-	C1GalTA	2.645328	3.388364	1.280886
1309	NM_134929	chr2L	-	pgant2	2.663514	3.411132	1.280689
1311	NM_176148	chr2R	-	GalT1	1.089277	1.394558	1.280259
1312	NM_001273389	chr2L	-	Rsf1	2.686926	3.439434	1.280063
1315	NR_001933	chr3L	+	snRNA:U5:63BC	64.80563	82.94202	1.279858
1318	NM_001273717	chr2L	+	CG9338	5.17506	6.622725	1.279739
1319	NM_140642	chr3L	-	CG42514	1.30939	1.675525	1.279622
1320	NM_136251	chr2L	+	CG9246	2.970585	3.801039	1.279559
1321	NM_137901	chr2R	-	CG9896	11.2149	14.34876	1.279438
1322	NM_206514	chr3R	-	fru	6.741145	8.624753	1.27942
1323	NM_142517	chr3R	+	NP15.6	1.938792	2.479846	1.279067
1324	NM_001014453	chr2L	+	PNUTS	17.90734	22.90379	1.279017

1325	NM_057862	chr2R	-	SdhA	1.638828	2.095789	1.278834
1326	NM_170635	chr3L	+	Lmpt	6.392058	8.174131	1.278795
1327	NR_133104	chr2R	+	CR46064	3.52808	4.510967	1.27859
1328	NM_001298492	chrX	+	CG7378	2.058569	2.631951	1.278534
1329	NM_141778	chr3R	-	CG14696	24.40015	31.19587	1.278512
1333	NM_206426	chr3R	+	Gel	8.921999	11.40217	1.277984
1334	NM_001259179	chr2L	+	Fs(2)Ket	4.623419	5.908054	1.277854
1335	NM_058133	chr3R	-	eIF2D	1.445472	1.846761	1.277618
1336	NM_001042993	chr2R	+	conu	3.066114	3.916778	1.27744
1337	NM_143629	chr3R	+	CG1896	3.817801	4.876999	1.277437
1339	NM_142706	chr3R	-	CG3308	3.149101	4.021923	1.277166
1341	NM_001272656	chrX	-	tay	2.701767	3.449237	1.27666
1342	NM_137505	chr2R	+	CG5335	1.578836	2.015626	1.276653
1343	NM_079444	chr3L	-	cyc	2.497123	3.18503	1.27548
1344	NM_166880	chrX	+	AMPKalpha	1.390078	1.772922	1.275412
1345	NR_124417	chr2L	+	CR43144	3.268668	4.168652	1.275336
1346	NM_001258605	chrX	-	Tre1	1.520097	1.938625	1.27533
1347	NM_001169518	chr2L	-	CG5953	1.560022	1.989537	1.275326
1348	NM_079081	chr2R	-	Tbp	1.921234	2.450121	1.275285
1349	NM_168209	chr3L	-	pst	20.00583	25.51218	1.275237
1350	NM_132216	chrX	+	CG2116	4.639306	5.91596	1.275182
1352	NM_001299194	chr2L	+	CG8677	5.439489	6.934366	1.274819
1354	NM_001258836	chrX	-	CG14231	1.86563	2.377863	1.274563
1356	NM_001298985	chr2L	-	Smg5	2.529941	3.2244	1.274496
1357	NM_134793	chr2L	+	Npc2a	8.766896	11.17227	1.27437
1359	NM_001169611	chr2R	+	lig	1.474946	1.8787	1.273742
1360	NM_001300194	chr3L	-	CG14182	2.9501	3.756451	1.27333
1361	NM_001259558	chr2R	+	snama	2.452808	3.123208	1.27332
1362	NM_138040	chr2R	+	snama	2.452808	3.123208	1.27332
1363	NM_001015359	chr3R	+	CG41099	5.119039	6.517738	1.273235
1364	NM_001015360	chr3R	+	CG41099	5.119039	6.517738	1.273235
1365	NM_001110981	chr3R	+	CG41099	5.119039	6.517738	1.273235
1366	NM_057933	chr2R	+	Alas	7.50182	9.549241	1.272923
1368	NM_132777	chrX	-	RpL37a	6.053631	7.701689	1.272243
1369	NM_137488	chr2R	+	CG12263	1.128158	1.435193	1.272156

1374	NM_141325	chr3R	-	CG2091	2.814437	3.578732	1.271562
1377	NM_142663	chr3R	+	CG15695	5.213523	6.628259	1.271359
1378	NM_001170379	chr3L	+	Set1	2.151589	2.735357	1.271319
1379	NM_079414	chr3L	-	rpr	24.84602	31.5842	1.271198
1380	NM_142145	chr3R	-	CG7265	1.733312	2.203306	1.271154
1381	NM_001275351	chr3R	+	CG1172	4.045021	5.141364	1.271035
1382	NM_170353	chr3R	-	CG12428	1.782017	2.264812	1.270926
1383	NM_170354	chr3R	-	CG12428	1.782017	2.264812	1.270926
1384	NM_001272124	chr4	+	CG32850	2.150753	2.733301	1.270858
1385	NM_166753	chr4	+	CG32850	2.150753	2.733301	1.270858
1387	NM_205948	chr2L	+	Apoltp	10.07148	12.79783	1.270701
1388	NM_139949	chr3L	-	CG7185	4.744032	6.027746	1.270596
1389	NM_001169668	chr2R	-	Kdm4B	4.321574	5.489845	1.270335
1390	NM_176726	chrX	+	Nna1	1.788497	2.271927	1.2703
1391	NM_168830	chr3L	+	CG7668	4.029762	5.117963	1.270041
1393	NM_136377	chr2R	+	CG9410	1.4739	1.871901	1.270032
1394	NM_001299601	chr2R	+	CG14478	9.937696	12.62106	1.270019
1395	NM_166519	chr2R	-	Swim	21.26108	27.00034	1.269942
1396	NM_170453	chr3R	-	Acph-1	1.701121	2.160299	1.269927
1397	NM_001298097	chrX	+	Rbm13	1.591378	2.020844	1.269871
1399	NM_132160	chrX	+	CG2059	1.442336	1.831424	1.269762
1400	NM_142304	chr3R	-	CG14903	2.166431	2.750852	1.269762
1401	NM_167047	chrX	-	IntS6	1.055205	1.33985	1.269754
1402	NM_001201658	chrX	-	jub	2.961179	3.75993	1.269741
1403	NM_001298303	chrX	-	jub	2.961179	3.75993	1.269741
1404	NM_001259382	chr2R	-	shot	18.54238	23.5432	1.269697
1406	NM_001104477	chr3R	+	CG5938	1.636738	2.077606	1.269358
1410	NM_001272733	chrX	-	Socs16D	2.666232	3.382988	1.268827
1412	NM_140394	chr3L	-	CG10133	4.490264	5.696024	1.268528
1415	NM_001298434	chrX	+	CG5010	11.52343	14.61044	1.26789
1416	NM_001298708	chr2L	+	CG11034	8.039456	10.19308	1.267881
1417	NM_130644	chrX	-	Ilp6	2.494614	3.162736	1.267826
1418	NM_080201	chr2L	-	fs(2)ltoPP43	4.550884	5.767175	1.267265
1419	NM_176062	chr2L	-	fs(2)ltoPP43	4.550884	5.767175	1.267265
1420	NM_079113	chr2R	-	gek	4.563844	5.782354	1.266992
1423	NM_141400	chr3R	+	Zif	1.746481	2.21216	1.266639
1424	NM_079483	chr3L	+	CycH	9.869551	12.50042	1.266564

1426	NM_001259849	chr3L	-	CG15715	1.460313	1.849133	1.266258
1427	NM_139967	chr3L	+	Cbl	1.72495	2.184174	1.266224
1428	NM_168276	chr3L	+	Cbl	1.72495	2.184174	1.266224
1429	NM_168720	chr3L	-	CG6512	3.232714	4.092758	1.266044
1430	NM_168722	chr3L	-	CG6512	3.232714	4.092758	1.266044
1431	NM_145193	chr2R	+	AIMP3	1.375445	1.741141	1.265875
1434	NM_001298003	chrX	+	dtn	1.771565	2.242202	1.265662
1435	NM_169519	chr3R	+	Droj2	2.718908	3.440383	1.265355
1436	NM_136092	chr2L	+	CG10470	1.526786	1.93151	1.265082
1437	NM_141480	chr3R	+	CG2641	4.459118	5.640843	1.265013
1438	NM_001299894	chr2R	+	enok	3.891799	4.923168	1.265011
1439	NM_165481	chr2R	+	CG9410	1.806683	2.285367	1.264952
1441	NM_001273302	chr2L	+	PGAP5	1.056041	1.335423	1.264556
1445	NM_001273012	chr2L	+	CG9886	1.259013	1.590934	1.263636
1446	NM_058094	chr3R	+	CSN5	2.667068	3.369706	1.26345
1448	NM_001297855	chrX	+	rush	4.154973	5.248881	1.263277
1449	NM_001299239	chr2R	+	CG1882	4.531235	5.723852	1.263199
1450	NM_168906	chr3L	+	Syx7	3.228325	4.077895	1.263161
1451	NM_001258552	chrX	+	prage	9.049928	11.42984	1.262976
1452	NM_132260	chrX	-	IntS4	2.492106	3.147241	1.262884
1454	NR_073669	chrX	-	CR43656	3.115237	3.932589	1.262372
1457	NM_135497	chr2L	+	Spn31A	3.313402	4.181933	1.262127
1458	NM_001300000	chr3L	+	CG12012	4.004051	5.053611	1.262125
1459	NM_165069	chr2L	-	Smg5	3.136768	3.95852	1.261974
1460	NM_140331	chr3L	-	nst	1.433766	1.809288	1.261913
1461	NM_141114	chr3L	-	DNApol-eta	3.089735	3.897962	1.261585
1462	NM_140500	chr3L	+	CG6878	1.804593	2.276354	1.261423
1464	NM_001258700	chrX	+	CkIIbeta	2.57133	3.242109	1.260869
1465	NM_137709	chr2R	+	Hmg-2	2.533913	3.194833	1.26083
1467	NM_001258659	chrX	-	CG7766	1.514662	1.909374	1.260594
1468	NM_001169343	chrX	-	DIP1	7.967131	10.04192	1.260419
1469	NM_001104163	chr3L	+	CG34250	2.43065	3.063599	1.260403
1470	NM_001300165	chr3L	+	CG34250	2.43065	3.063599	1.260403
1471	NM_165425	chr2R	+	d4	2.042264	2.573449	1.260096
1472	NM_079330	chr3L	+	Syx13	2.76176	3.480069	1.260091
1473	NM_137540	chr2R	-	CG18190	2.354562	2.966834	1.260037

1475	NR_133415	chr3R	+	CR46035	4.58203	5.773184	1.259962
1478	NM_168112	chr3L	-	shep	5.351485	6.739729	1.259413
1480	NM_001299577	chr2R	+	Ef1beta	5.716877	7.198889	1.259235
1481	NM_079891	chr4	-	pho	1.491668	1.878226	1.259144
1482	NM_143298	chr3R	+	CG3368	2.183363	2.748954	1.259046
1485	NM_001272910	chr2L	+	CG13689	1.35057	1.699716	1.258517
1486	NM_134694	chr2L	+	CG13689	1.35057	1.699716	1.258517
1487	NM_137795	chr2R	+	CG6613	2.880283	3.624743	1.258468
1488	NM_136213	chr2L	+	Pomp	2.736467	3.443229	1.258275
1489	NM_136849	chr2R	+	Tret1-1	4.477722	5.634202	1.258274
1490	NM_136205	chr2L	-	Cen	2.763851	3.477381	1.258165
1491	NM_001299153	chr2L	+	CG31793	4.557364	5.733497	1.258073
1493	NM_001275650	chr3R	-	eff	7.676991	9.655335	1.257698
1494	NM_001032037	chr3R	-	Myo95E	1.534102	1.928822	1.257297
1495	NM_137906	chr2R	-	CG9890	2.25318	2.832912	1.257295
1497	NM_001259765	chr3L	+	Hsp23	1.661822	2.088516	1.256763
1498	NM_001273577	chr2L	+	her	1.241036	1.559628	1.256714
1499	NR_125293	chr3R	-	CR44953	30.46674	38.2795	1.256436
1502	NM_130600	chrX	+	CG14806	2.488971	3.125896	1.255899
1503	NM_138204	chr3L	-	CG17129	1.487697	1.868264	1.25581
1504	NM_141566	chr3R	+	CG8159	1.104955	1.387601	1.255798
1506	NM_169963	chr3R	-	CG31176	6.081433	7.635598	1.255559
1507	NM_001258650	chrX	-	lawc	12.36981	15.52876	1.255376
1508	NM_136685	chr2R	+	CG18446	1.279289	1.605955	1.255349
1509	NM_136704	chr2R	+	magu	3.782683	4.747662	1.255104
1512	NM_079613	chr3R	+	ry	3.935487	4.938663	1.254905
1513	NM_165065	chr2L	-	mRpS23	2.111873	2.649976	1.254799
1514	NM_170524	chr3R	-	wts	5.544006	6.956502	1.254779
1515	NM_137063	chr2R	+	CG6357	3.206794	4.023662	1.25473
1517	NM_001259651	chr3L	-	Mrtf	2.456988	3.081782	1.254293
1518	NM_001272308	chrX	-	Fas2	4.20117	5.269277	1.25424
1519	NM_167005	chrX	-	Fas2	4.20117	5.269277	1.25424
1520	NM_001169962	chr3L	-	Atg1	11.24228	14.09752	1.253974
1521	NM_140344	chr3L	-	Atg1	11.24228	14.09752	1.253974
1522	NM_057266	chr2L	+	lace	6.972755	8.742706	1.253838
1523	NM_001298064	chrX	+	snz	1.883189	2.361103	1.253779
1526	NM_167759	chrX	-	GCS2alpha	1.145717	1.435983	1.253349

1528	NM_079581	chr3R	-	TfIIFbeta	1.860823	2.331694	1.253045
1530	NM_140998	chr3L	-	CG11396	3.070713	3.846417	1.252614
1532	NM_132343	chrX	+	Gga	1.165784	1.460016	1.25239
1533	NM_166335	chr2R	+	hppy	8.520026	10.66995	1.252337
1535	NM_205886	chr2L	-	rempA	1.515289	1.897515	1.252246
1536	NM_001104179	chr3L	+	CG32425	4.767653	5.969244	1.25203
1537	NM_001300249	chr3R	-	ksr	3.965379	4.963486	1.251705
1538	NM_001298311	chrX	+	CG14414	1.019251	1.275656	1.251563
1539	NM_176729	chrX	+	CG14414	1.019251	1.275656	1.251563
1540	NM_165454	chr2R	+	Pngl	5.895601	7.378664	1.251554
1541	NM_142637	chr3R	-	CG10877	4.106268	5.138201	1.251307
1544	NM_001201736	chrX	+	CG6762	1.401784	1.753632	1.251001
1546	NM_001299872	chr2R	+	Sox14	8.131641	10.16636	1.250222
1548	NM_166630	chr2R	+	kcc	3.202613	4.00374	1.250148
1549	NM_137481	chr2R	+	GstE3	15.5442	19.42483	1.249651
1550	NM_001272797	chrX	-	CG14229	3.134677	3.917252	1.249651
1551	NM_001032408	chr3R	+	kay	36.81971	46.01044	1.249614
1552	NM_001299910	chr2R	-	SerT	1.751289	2.188285	1.249529
1553	NM_136927	chr2R	+	CG8501	1.126485	1.407523	1.249482
1555	NM_001201856	chr2L	+	Lip4	1.325695	1.656077	1.249214
1556	NM_078691	chrX	+	AP-1-2beta	2.501513	3.124789	1.24916
1557	NM_078508	chrX	-	RpL7A	5.496764	6.865745	1.249052
1558	NM_136621	chr2R	-	CG8046	10.41868	13.01097	1.248811
1560	NM_135798	chr2L	-	ND-B22	1.771774	2.211528	1.2482
1561	NM_206487	chr3R	-	Sp212	2.608747	3.256181	1.248178
1564	NM_176486	chr3R	+	Hsp70Bbb	150.2379	187.47	1.247821
1565	NM_080045	chr2L	-	abo	4.267016	5.323984	1.247707
1566	NM_001273033	chr2L	-	CG3077	3.464742	4.322496	1.247566
1567	NM_134865	chr2L	-	CG3077	3.464742	4.322496	1.247566
1568	NM_001110989	chr3R	+	Alg-2	2.75319	3.434533	1.247474
1570	NM_001273782	chr2R	+	CG1344	3.500905	4.365661	1.247009
1571	NM_166434	chr2R	+	MFS16	2.389052	2.979167	1.247008
1572	NM_136199	chr2L	+	CG2611	4.064043	5.067841	1.246995
1575	NM_079488	chr3L	+	Ddx1	1.864167	2.323472	1.246386
1578	NM_001275011	chr3L	-	roq	4.190718	5.222001	1.246087
1579	NM_001316521	chr3R	+	fray	1.537656	1.915856	1.245959

1580	NM_001170235	chr3R	+	CG33108	1.036392	1.291152	1.245814
1581	NM_176551	chr3R	+	CG33108	1.036392	1.291152	1.245814
1582	NM_167174	chrX	+	CG32708	1.068165	1.330522	1.245615
1583	NM_166973	chrX	-	CG12206	2.633831	3.280689	1.245596
1584	NM_001316627	chrX	-	l(1)G0289	5.862783	7.302295	1.245534
1585	NM_079972	chr2R	+	Hmgs	2.354353	2.932207	1.245441
1586	NM_164995	chr2L	+	ThrRS	1.267375	1.578127	1.245194
1587	NM_001297989	chrX	+	CG12728	12.28097	15.29207	1.245184
1588	NM_206643	chrX	-	l(1)G0193	7.484053	9.318712	1.245142
1589	NM_058162	chrX	+	Jafrac1	2.335748	2.9077	1.244869
1590	NM_057686	chr2R	-	tsr	11.93376	14.85583	1.244857
1591	NM_001298516	chrX	+	RpS10b	1.96743	2.449014	1.244778
1593	NM_134686	chr2L	-	rempA	4.184029	5.207455	1.244603
1594	NM_140672	chr3L	+	CG9951	1.242499	1.546346	1.244545
1596	NM_143182	chr3R	+	CG5913	3.016573	3.753605	1.244328
1597	NM_001299206	chr2R	-	Gprk1	2.811719	3.497778	1.244
1598	NM_001275752	chr3R	-	osa	7.110299	8.842317	1.243593
1601	NM_001298072	chrX	-	Gclc	7.077481	8.797413	1.243015
1602	NM_079305	chr3L	+	Klp68D	2.07362	2.577402	1.242948
1603	NM_001298094	chrX	+	CG11284	3.307758	4.110783	1.24277
1604	NM_001032076	chr2L	+	cana	1.417461	1.761538	1.242742
1605	NM_001272264	chrX	+	sgg	4.52789	5.626929	1.242726
1606	NM_139578	chr3L	-	Ccz1	1.169128	1.452901	1.242722
1607	NM_139942	chr3L	-	cert	4.744241	5.893982	1.242345
1608	NM_001014644	chr3R	+	CG7956	6.023739	7.483177	1.242281
1609	NM_001170204	chr3R	+	CG7956	6.023739	7.483177	1.242281
1610	NM_001170205	chr3R	+	CG7956	6.023739	7.483177	1.242281
1611	NM_139892	chr3L	+	CG12262	13.70219	17.02024	1.242155
1612	NM_079990	chr2R	+	Sara	3.122553	3.878514	1.242097
1613	NM_168789	chr3L	+	Bet1	2.538512	3.151985	1.241666
1616	NM_140544	chr3L	-	comm2	11.70111	14.5238	1.241232
1620	NM_137246	chr2R	-	CG10734	1.135892	1.40863	1.240109
1621	NM_136659	chr2R	+	RpL31	8.619735	10.68813	1.23996
1622	NM_001169585	chr2R	+	vlc	7.060549	8.753774	1.239815
1624	NM_079506	chr3R	-	Ubc6	3.698652	4.585122	1.239674
1626	NM_080525	chrX	+	cv	2.054179	2.546411	1.239625

1627	NM_001275932	chr3R	+	Irk1	3.103949	3.847682	1.239609
1628	NM_166505	chr2R	+	Synj	2.744201	3.401645	1.239576
1630	NM_132150	chrX	-	CG12541	6.762466	8.380785	1.239309
1631	NM_137695	chr2R	+	cpa	3.903087	4.835415	1.238869
1632	NM_001015095	chr2R	-	MFS17	5.551113	6.876339	1.238732
1633	NM_001110895	chr2R	-	MFS17	5.551113	6.876339	1.238732
1634	NM_001276229	chr2R	-	MFS17	5.551113	6.876339	1.238732
1635	NM_166449	chr2R	-	Sdc	13.90015	17.21567	1.238524
1639	NM_135432	chr2L	+	CG13108	1.694431	2.098003	1.238175
1640	NM_001272567	chrX	-	Pde9	6.082269	7.527923	1.237683
1641	NM_135461	chr2L	-	CG4364	2.481445	3.071189	1.237661
1642	NM_176070	chr2L	+	Tif-IA	2.981873	3.69036	1.237598
1643	NM_169933	chr3R	+	RpS30	4.51284	5.584239	1.237411
1645	NM_001297832	chrX	+	CG16989	2.83973	3.512957	1.237074
1646	NM_001103752	chr2R	+	CG34430	2.84621	3.519123	1.236424
1647	NM_169098	chr3R	-	Sec8	2.955535	3.653678	1.236215
1648	NM_001260330	chr3R	-	cnc	8.859916	10.95123	1.236042
1649	NM_001260331	chr3R	-	cnc	8.859916	10.95123	1.236042
1650	NM_001103775	chr2R	-	CG12929	1.298939	1.605164	1.235751
1651	NM_141618	chr3R	+	Ibf1	1.052069	1.300006	1.235666
1652	NM_001169277	chrX	+	rdgB	9.695217	11.97976	1.235636
1653	NM_141532	chr3R	-	Coq2	1.723069	2.128835	1.23549
1654	NM_134771	chr2L	-	Rim2	4.979195	6.151548	1.23545
1656	NM_001274146	chr2R	-	GEFmeso	20.7826	25.67061	1.235197
1657	NM_166265	chr2R	+	pAbp	1.879218	2.320942	1.235058
1658	NM_001258923	chr2L	+	Hydr2	12.74022	15.73478	1.235048
1659	NM_001273064	chr2L	+	Hydr2	12.74022	15.73478	1.235048
1660	NM_139536	chr3L	+	CG11505	2.314009	2.856471	1.234425
1661	NM_001259326	chr2R	+	RanBPM	3.737741	4.613266	1.234239
1662	NM_001297816	chrX	-	CG13366	2.756325	3.401487	1.234066
1663	NM_079372	chr3L	+	CkIIalpha-i1	1.911618	2.358889	1.233975
1664	NM_143064	chr3R	-	Smg6	3.458471	4.267314	1.233873
1665	NM_001299673	chr2R	+	ena	12.44005	15.3482	1.233773
1666	NM_166330	chr2R	+	ena	12.44005	15.3482	1.233773

1669	NM_001273681	chr2L	+	sick	11.52364	14.21437	1.233496
1674	NM_140316	chr3L	-	CG32104	1.622106	2.000131	1.233046
1676	NM_142994	chr3R	-	CG18528	1.36792	1.686434	1.232846
1677	NM_001258957	chr2L	+	cype	3.695307	4.555238	1.232709
1678	NM_167337	chrX	+	CG3812	1.566921	1.931352	1.232578
1679	NM_132429	chrX	+	CG2202	2.050208	2.526964	1.23254
1682	NM_001258807	chrX	-	ari-1	2.196323	2.705631	1.231892
1683	NM_001272743	chrX	-	ari-1	2.196323	2.705631	1.231892
1685	NM_169504	chr3R	+	CG32473	13.06192	16.09038	1.231854
1687	NM_139602	chr3L	+	Ack	2.244191	2.763026	1.23119
1688	NM_001259426	chr2R	-	Mlf	3.087436	3.800565	1.230978
1689	NM_137042	chr2R	+	Roe1	3.315701	4.081532	1.230971
1690	NM_079319	chr3L	-	eIF-2beta	6.40021	7.878143	1.23092
1691	NM_206425	chr3L	+	CG33217	4.829109	5.944104	1.23089
1693	NM_136394	chr2R	-	CG15237	2.257779	2.778838	1.230784
1694	NM_001259551	chr2R	+	Rpi	4.076167	5.016771	1.230757
1695	NM_141442	chr3R	+	CG2656	1.616044	1.988905	1.230725
1698	NM_137943	chr2R	-	Golgin245	2.2814	2.806349	1.2301
1699	NR_133197	chr3L	+	CR45874	2.432113	2.9915	1.23
1700	NM_001259546	chr2R	-	CG30187	7.78318	9.572483	1.229894
1702	NM_169408	chr3R	-	Jupiter	2.733123	3.360536	1.229559
1703	NM_001299765	chr2R	-	HmgZ	8.758952	10.76924	1.229513
1705	NM_079391	chr3L	-	Prosbeta6	4.185283	5.145633	1.229459
1706	NM_143099	chr3R	-	CG10420	1.981435	2.43589	1.229356
1707	NM_001014528	chr2R	-	CG33506	2.69048	3.307094	1.229184
1709	NM_001202069	chr2R	+	ocm	1.456132	1.789682	1.229066
1711	NM_078835	chr2L	-	kek1	26.23359	32.24179	1.229027
1712	NM_001274050	chr2R	-	Spred	6.185114	7.600655	1.228863
1714	NM_135549	chr2L	+	gny	1.468674	1.804703	1.228797
1717	NM_001169302	chrX	+	Fur2	6.049033	7.431948	1.228618
1718	NM_206763	chrX	+	Fur2	6.049033	7.431948	1.228618
1725	NM_001103570	chrX	+	Ntf-2	6.555941	8.049222	1.227775
1726	NM_001272819	chrX	+	Ntf-2	6.555941	8.049222	1.227775
1727	NM_001272821	chrX	+	Ntf-2	6.555941	8.049222	1.227775
1728	NM_001258843	chrX	+	Hers	1.076944	1.322142	1.227679

1731	NM_144474	chr3R	+	Desat1	3.417501	4.195215	1.227568
1732	NM_001042984	chr2R	+	CG17883	1.364994	1.675525	1.227496
1734	NM_143815	chr3R	+	Invadolysin	14.29167	17.53316	1.22681
1735	NM_001259532	chr2R	+	rad50	1.978927	2.427669	1.22676
1736	NM_166533	chr2R	+	rad50	1.978927	2.427669	1.22676
1737	NM_169485	chr3R	-	CG7381	3.759063	4.610578	1.226523
1738	NM_137625	chr2R	-	CG16868	1.497312	1.836484	1.22652
1740	NM_001273740	chr2L	+	CG8671	11.40344	13.98558	1.226435
1741	NM_001273742	chr2L	+	CG8671	11.40344	13.98558	1.226435
1742	NM_001299195	chr2L	+	CG8671	11.40344	13.98558	1.226435
1743	NM_001169693	chr2R	-	Mlf	3.007166	3.687672	1.226295
1744	NM_166123	chr2R	-	Mlf	3.007166	3.687672	1.226295
1749	NM_168448	chr3L	+	IRSp53	7.041736	8.631869	1.225815
1753	NM_135182	chr2L	+	Fic	7.107791	8.710767	1.225524
1754	NM_169663	chr3R	-	CG44014	2.3786	2.914815	1.225433
1755	NR_124143	chr2L	-	CR45371	1.079244	1.3223	1.22521
1756	NM_143151	chr3R	-	Ssadh	1.533893	1.879332	1.225204
1757	NM_078801	chr2L	-	jp	1.202156	1.472824	1.225152
1758	NM_001272611	chrX	+	ben	2.097031	2.56918	1.225151
1760	NM_001169268	chrX	-	CG1998	8.183481	10.02579	1.225126
1761	NM_140693	chr3L	+	beg	1.304583	1.598207	1.225072
1762	NM_057293	chr2R	-	mle	3.666669	4.491361	1.224916
1764	NM_001298016	chrX	-	RpL7A	8.338793	10.2111	1.22453
1765	NM_001103572	chrX	+	CG34334	2.66874	3.266933	1.224148
1766	NM_139621	chr3L	+	CG1265	4.546494	5.565423	1.224113
1767	NM_130495	chrX	+	CG13367	2.98898	3.658737	1.224075
1768	NM_079727	chr3R	+	CSN6	3.100396	3.794556	1.223894
1769	NM_136395	chr2R	-	ubl	2.790189	3.414769	1.223849
1770	NM_142317	chr3R	-	CG14907	8.295941	10.1526	1.223803
1771	NM_001038824	chr2L	-	Pax	10.21968	12.50627	1.223744
1773	NM_079560	chr3R	+	mRpL19	1.632557	1.997285	1.223409
1775	NM_138985	chr3L	+	26-29-p	12.71994	15.55691	1.223033
1776	NM_057753	chr2R	+	SdhB	2.999432	3.668382	1.223026
1777	NM_001272975	chr2L	-	CG4259	7.894596	9.655177	1.223011
1778	NM_001014529	chr2R	-	U3-55K	1.079662	1.320403	1.222978
1780	NM_001298158	chrX	-	Atg8a	1.164739	1.424283	1.222835

1781	NM_168336	chr3L	-	eIF-4E	3.189444	3.899702	1.22269
1782	NM_078655	chrX	+	mRpL22	2.49336	3.048579	1.222679
1785	NM_001042997	chr2R	-	CG17528	2.061705	2.519532	1.222063
1787	NM_139956	chr3L	+	GAPcenA	1.128994	1.379062	1.221497
1788	NM_169577	chr3R	+	PR-Set7	5.094791	6.223174	1.221478
1789	NM_134310	chr3R	+	Rab11	6.541726	7.990087	1.221404
1791	NM_170212	chr3R	-	CG31098	5.883477	7.184343	1.221105
1792	NM_142322	chr3R	-	CG18622	16.31993	19.92778	1.221071
1793	NM_001259756	chr3L	+	dally	19.51962	23.8346	1.221059
1795	NM_001258475	chr4	-	RpS3A	8.623916	10.52511	1.220457
1796	NM_164980	chr2L	+	Ada1-2	3.138231	3.829499	1.220273
1797	NM_078725	chr2L	-	aru	4.312585	5.26153	1.220041
1798	NM_167267	chrX	-	Klp10A	1.970566	2.403793	1.219849
1799	NM_001258817	chrX	+	kek5	11.97369	14.60427	1.219697
1801	NM_170043	chr3R	-	Nha2	7.250352	8.842791	1.219636
1802	NM_078706	chrX	+	Sep-01	9.927036	12.10688	1.219586
1803	NM_079809	chr3R	+	Mtl	1.808146	2.204887	1.219419
1804	NM_001258788	chrX	-	CanA-14F	1.509436	1.84012	1.219078
1809	NM_001202081	chr2R	-	zip	8.284027	10.09536	1.218654
1810	NM_206613	chrX	+	sgg	4.575759	5.574435	1.218254
1812	NM_057892	chr2L	-	dbe	3.650992	4.446773	1.217963
1813	NM_079049	chr2R	+	cyp33	1.988125	2.421186	1.217824
1814	NM_139608	chr3L	+	Ero1L	6.396447	7.789442	1.217776
1815	NM_057225	chr2L	-	hook	3.788745	4.61374	1.217749
1817	NM_001274404	chr3L	-	msn	15.03228	18.30112	1.217455
1818	NM_079940	chr3L	-	msn	15.03228	18.30112	1.217455
1819	NM_001259847	chr3L	-	DCP2	5.704126	6.941323	1.216895
1820	NM_137248	chr2R	-	CG8435	1.304583	1.587456	1.21683
1821	NM_132049	chrX	+	CG12236	2.960761	3.602291	1.216677
1822	NM_167054	chrX	+	CG12236	2.960761	3.602291	1.216677
1823	NM_058083	chr2L	-	esc	1.249398	1.520099	1.216666
1825	NR_001679	chr2L	-	snRNA:U4:39B	73.97638	89.99956	1.216599
1826	NM_001104099	chr3L	+	nudE	3.365242	4.093548	1.21642
1827	NM_001144458	chr3L	+	nudE	3.365242	4.093548	1.21642
1828	NM_001300088	chr3L	+	nudE	3.365242	4.093548	1.21642
1829	NM_137295	chr2R	-	CG8311	1.439828	1.751419	1.216409
1830	NM_135259	chr2L	-	CG4502	4.027672	4.898818	1.21629
1831	NM_164741	chr2L	-	CG4502	4.027672	4.898818	1.21629

1832	NR_133100	chr2L	+	CR46253	3.492753	4.248183	1.216285
1833	NM_001298872	chr2L	-	nmd	4.112957	5.001908	1.216134
1834	NM_001298121	chrX	-	c11.1	2.857289	3.474694	1.216081
1836	NM_132484	chrX	+	Pa1	1.61458	1.963132	1.215878
1837	NM_001300707	chr2R	-	Yeti	8.33524	10.13236	1.215605
1838	NM_057638	chr2L	-	poe	9.620173	11.69389	1.215559
1839	NM_079562	chr3R	-	D1	3.645557	4.430645	1.215355
1841	NM_001104032	chr3L	-	CG15019	3.473313	4.220671	1.215172
1842	NM_168723	chr3L	-	CG6479	1.845772	2.242834	1.21512
1843	NM_001273290	chr2L	-	pes	16.0254	19.46657	1.214732
1845	NM_169063	chr3R	-	Pi4KIIalpha	2.446746	2.971736	1.214567
1846	NM_166372	chr2R	-	hrg	1.247934	1.515356	1.214291
1847	NM_144290	chrX	-	CG12643	10.7799	13.0875	1.214065
1848	NM_137462	chr2R	-	CG5721	2.176882	2.64286	1.214057
1849	NM_001015176	chr2R	+	CG40191	3.247138	3.941285	1.213772
1850	NM_001144167	chr2R	+	CAP	9.774859	11.86417	1.213744
1851	NM_001259189	chr2L	-	Dap160	3.280374	3.981288	1.213669
1852	NM_165126	chr2L	-	ND-B17	2.600804	3.156254	1.213569
1853	NM_136577	chr2R	+	CG30349	3.367332	4.086433	1.213552
1854	NM_135511	chr2L	-	CG5727	2.137375	2.593371	1.213344
1857	NM_001259766	chr3L	-	CG4080	15.22898	18.47583	1.213202
1859	NM_139611	chr3L	-	VhaM9.7-c	1.06921	1.297002	1.213047
1860	NM_001202128	chr3L	-	Sh3beta	7.353197	8.917737	1.21277
1861	NM_001274480	chr3L	-	ImpL2	30.87916	37.44766	1.212716
1862	NM_001276132	chr3R	+	Usp1	2.550636	3.092692	1.212518
1863	NM_143430	chr3R	+	Usp1	2.550636	3.092692	1.212518
1864	NM_001014678	chr3R	+	Doa	17.83731	21.62592	1.212398
1866	NM_057604	chr2R	+	Map60	4.310495	5.223741	1.211866
1867	NR_073708	chr2L	+	snRNA:LU	52.52445	63.65238	1.211862
1869	NM_001275339	chr3R	-	CG14657	2.421662	2.933314	1.211282
1870	NM_001275340	chr3R	-	CG14657	2.421662	2.933314	1.211282
1872	NM_079197	chr3L	-	ImpL2	1.777627	2.15271	1.211002
1873	NM_001274189	chr2R	-	CG30389	3.749447	4.540376	1.210945
1874	NR_133457	chr3R	+	CR46061	1.060849	1.284353	1.210684
1876	NM_167296	chrX	+	PhKgamma	3.016782	3.65178	1.210489

1877	NM_167297	chrX	+	PhKgamma	3.016782	3.65178	1.210489
1879	NM_001298618	chr2L	-	Ets21C	11.03304	13.35518	1.210472
1880	NR_133278	chr3L	-	CR46048	3.033087	3.67107	1.210341
1882	NM_141933	chr3R	+	CG5167	2.930451	3.545528	1.209892
1883	NM_079181	chr3L	+	Scsalpha	3.345175	4.046272	1.209585
1884	NM_168081	chr3L	+	PMP34	2.579482	3.120046	1.209563
1886	NM_169557	chr3R	+	Dip-B	5.805717	7.020538	1.209246
1887	NM_001299636	chr2R	+	CG10915	1.976001	2.389405	1.209213
1888	NM_137833	chr2R	+	CG4610	1.088441	1.316133	1.209191
1889	NM_079373	chr3L	-	Pka-C3	1.313153	1.587772	1.209129
1890	NM_001103667	chr2L	-	CG34159	3.248392	3.927688	1.209118
1891	NM_001276015	chr3R	+	CG11790	5.54087	6.698936	1.209004
1892	NM_170192	chr3R	+	CG11790	5.54087	6.698936	1.209004
1894	NM_166112	chr2R	+	CG30090	1.618552	1.95665	1.208889
1896	NM_142919	chr3R	+	CG10365	7.134547	8.622698	1.208584
1897	NM_001299212	chr2R	-	CG11665	2.978529	3.599603	1.208517
1898	NM_166601	chr2R	+	eIF2B-delta	2.083444	2.517793	1.208476
1899	NM_140844	chr3L	+	CG14085	1.146971	1.385861	1.20828
1900	NM_001298330	chrX	+	ND-B18	1.293713	1.563106	1.208233
1901	NM_143755	chrX	-	deltaCOP	5.240906	6.331639	1.208119
1902	NM_079587	chr3R	+	Sodh-2	4.700762	5.677051	1.207687
1903	NM_001297971	chrX	+	RpL35	3.906014	4.717146	1.207663
1905	NM_001298088	chrX	-	Miga	1.295803	1.564687	1.207504
1906	NM_001299196	chr2L	-	CG2201	5.249477	6.33828	1.207412
1908	NM_001274597	chr3L	+	lqf	8.330641	10.05663	1.207185
1910	NR_133414	chr3R	+	CR46036	2.544574	3.07024	1.206583
1911	NM_001144725	chrX	-	CG14408	1.588869	1.916805	1.206396
1912	NM_001298318	chrX	-	CG14408	1.588869	1.916805	1.206396
1913	NM_136267	chr2L	+	Lamp1	14.503	17.49632	1.206393
1915	NM_141346	chr3R	-	CG2017	4.215384	5.084443	1.206164
1916	NM_132118	chrX	-	RpL17	2.602894	3.139336	1.206094
1918	NM_166102	chr2R	-	Flo1	2.843702	3.429157	1.205878
1919	NM_135532	chr2L	-	l(2)SH0834	5.392874	6.502401	1.205739
1920	NM_141654	chr3R	-	CG16790	1.14509	1.380644	1.205708
1921	NM_001299408	chr2R	+	Cam	3.204913	3.864126	1.205688
1922	NM_001169203	chrX	-	CG32767	1.02594	1.236919	1.205644

1923	NM_001273516	chr2L	-	B4	14.63072	17.63767	1.205523
1924	NM_001201646	chrX	-	nej	7.967967	9.604422	1.205379
1925	NM_079903	chrX	-	nej	7.967967	9.604422	1.205379
1926	NM_143252	chr3R	-	SPARC	12.46116	15.01948	1.205304
1927	NM_137399	chr2R	-	P32	1.880472	2.265919	1.204974
1928	NM_057378	chrX	+	sl	1.318797	1.588879	1.204794
1930	NM_136764	chr2R	-	wde	11.15386	13.43376	1.204405
1931	NM_001275602	chr3R	+	CG11686	11.76549	14.17041	1.204405
1932	NM_137339	chr2R	+	CG9646	4.481067	5.395926	1.204161
1933	NM_143421	chr3R	+	CG11897	14.17231	17.06341	1.203996
1935	NM_057551	chr2R	-	robo1	5.551949	6.684231	1.203943
1938	NM_166118	chr2R	-	Gpo-1	9.920974	11.94165	1.203677
1939	NM_141746	chr3R	+	Cyp12e1	6.547788	7.880989	1.203611
1940	NM_165917	chr2R	-	Sin3A	7.545509	9.080435	1.203423
1941	NM_135978	chr2L	-	CG12288	1.011308	1.216997	1.203389
1942	NR_033163	chr3L	+	Uhg8	7.116361	8.563722	1.203385
1943	NM_079012	chr2R	-	RN-tre	6.662548	8.016967	1.203288
1944	NM_144124	chr2R	-	RN-tre	6.662548	8.016967	1.203288
1945	NM_001104411	chr3R	+	CG7029	4.73797	5.701084	1.203276
1946	NM_164377	chr2L	-	CG3645	2.244191	2.700256	1.20322
1950	NM_166925	chrX	-	CG4199	3.314029	3.986506	1.202918
1951	NM_132906	chrX	+	CG13014	1.630467	1.961235	1.202867
1952	NM_079347	chr3L	+	dlp	26.49404	31.86738	1.202813
1953	NM_136321	chr2R	-	CG10465	1.912663	2.300546	1.202797
1955	NM_141204	chr3R	+	Cont	3.459726	4.160904	1.202669
1956	NR_002496	chr3R	+	snoRNA:Psi28S-291	1.31587	1.582396	1.202547
1959	NM_001202143	chr3L	+	Fhos	24.71913	29.72084	1.202341
1961	NM_001299811	chr2R	+	CG42566	1.58657	1.907476	1.202264
1962	NM_140916	chr3L	-	CG14184	1.771774	2.1301	1.202241
1963	NM_142069	chr3R	-	rdx	14.4336	17.35149	1.202159
1964	NM_140822	chr3L	+	CG6836	2.43713	2.92952	1.202037
1965	NM_135521	chr2L	+	CG4953	1.844309	2.216904	1.202024
1966	NM_164798	chr2L	+	PGAP5	1.394885	1.676631	1.201985
1967	NM_001300002	chr3L	-	CG10866	1.469093	1.765807	1.201971
1969	NM_057319	chr2R	+	pAbp	19.14335	23.00561	1.201755
1970	NM_206295	chr3L	+	Pura	22.0389	26.48521	1.201748
1971	NM_001298384	chrX	-	ND-20	1.731012	2.079978	1.201596
1972	NM_001300425	chr3R	+	Akt1	4.003633	4.810591	1.201557

1974	NM_143295	chr3R	+	CG5934	2.043937	2.455813	1.201511
1975	NM_001103849	chr2R	-	Rpb12	3.574067	4.294194	1.201487
1976	NM_001316436	chr3L	+	Mul1	1.278244	1.535753	1.201455
1978	NM_164428	chr2L	+	chinmo	2.09515	2.516686	1.201196
1979	NM_169953	chr3R	-	Rab1	7.22046	8.671239	1.200926
1981	NM_001276203	chr3R	-	dco	4.219147	5.065786	1.200666
1982	NM_079863	chr3R	-	dco	4.219147	5.065786	1.200666
1983	NM_001258477	chr4	+	pan	3.770768	4.527252	1.200618
1984	NM_080085	chrX	-	ogre	3.864416	4.639671	1.200614
1985	NM_135691	chr2L	-	CG6734	1.072555	1.287673	1.200566
1987	NM_001272970	chr2L	+	Su(dx)	1.765294	2.118874	1.200295
1988	NM_001316528	chr3R	-	Vps24	1.614162	1.93736	1.200226
1990	NM_001042934	chr2L	+	Slmap	3.274103	3.929427	1.200154
1991	NM_167315	chrX	+	regucalcin	5.266826	6.320413	1.200042

Table S4. List of primers used in present study (bold=T7 promoter region)		
No	**Primer Name**	**Primer Sequence**
1	UPF1 RNAi (F)	5'-**TTAATACGACTCACTATAGGGGAGA**GGAGAAGCCAGGCATTGA-3'
2	UPF1 RNA (R)	5'-**TTAATACGACTCACTATAGGGGAGA**GACCGTGGCCCAACAGG-3'
3	Y14 RNAi (F)	5'-**TTAATACGACTCACTATAGGGGAGA**CGATGTGTTGGACATTGACA-3'
4	Y14 RNAi (R)	5'-**TTAATACGACTCACTATAGGGGAGA**GACGCTTTTCGGACTTTTT-3'
5	eIF4AIII RNAi (F)	5'-**TTAATACGACTCACTATAGGGGAGA**GACGAATTGACACTGGAAGG-3'
6	eIF4AIII RNAi (R)	5'-**TTAATACGACTCACTATAGGGGAGA**AGAATATTAGTTTAGATCAAGTCAG-3'
7	snRNPU1 70K RNAi (F)	5'-**TTAATACGACTCACTATAGGGGAGA**AGCACGCCGATGGTAAG-3'
8	snRNPU1 70K RNAi (R)	5'-**TTAATACGACTCACTATAGGGGAGA**TGGAGCGCTTCTTTTTCTT-3'
9	snRNPU1 70K (F)	5'-CTACGGGCCCATCAAGAAGA-3'
10	snRNPU1 70K (R)	5'-CGCTTGCTGTCGATCTTCTT-3'
11	RpL23A s (F)	5'-GGCAATCGAATTTGTGCGAA-3'
12	RpL23A s (R)	5'-GATTGCTCACTCGGTTGCTA-3'
13	RpL23A m (F)	5'-TCGAACAGATCATCAAGGGC-3'
14	RpL23A m (R)	5'-CGATTTCCTGGGGTACTTGG-3'
15	RpL23A e (F)	5'-TAACGTGTGGAATGGGCATC-3'
16	RpL23A e (R)	5'-GAAACGTTCATCCTCGCTCT-3'
17	Xrp1 E1 (F)	5'-AGATCCTACGACGCTCCAAG-3'
18	Xrp1 E1 (R)	5'-TGCTCCTTATCTCCGGTGAC-3'
19	Xrp1 E3 (F)	5'-TCATAATGCTTGTGGGGCCT-3'
20	Xrp1 E3 (R)	5'-AGGGTCCCTCTAAACAAGCT-3'
21	Xrp1 I3 (F)	5'-AACCACGTAACCACCCATCT-3'
22	Xrp1 I3 (R)	5'-TATCTTGGGTTGGCTTGGGT-3'
23	Xrp1 E4 (F)	5'-GCAGCAACAGCAACAACAAC-3'
24	Xrp1 E4 (R)	5'-TTGAGATACGGCACCTCCTC-3'
25	Xrp1 I4 (F)	5'-TTCTAACTTGTTGCGCCGAC-3'
26	Xrp1 I4 (R)	5'-TCAGATTTATCCGCGGACCA-3'
27	Xrp1 E6 (F)	5'-CGTTGAAGAAGTCGAGAAGCA-3'
28	Xrp1 E6 (R)	5'-TAAACACTCCTCGCGCACTA-3'
29	Socs36E (F)	5'-CAGAAAACCGCACACAGACA-3'
30	Socs36E (R)	5'-CACACATCGGACTAACAGCG-3'
31	RpS12 e (F)	5'-AAGATCGACAAGGAGGGCAA-3'
32	RpS12 e (R)	5'-GTTCTGCCTGAGATGGTCCT-3'
33	Intergenic 2R (F)	5'-TCGTATCGCTGGCACTGTAA-3'
34	Intergenic 2R (R)	5'-ATATAGCCCGTGCCAGGAGT-3'
36	18s RNA (F)	5'-ACCGGTGGAGTTCTTATATGTGAT-3'
37	18s RNA (R)	5'-CGGCCCACAATAACACTCGT-3'